ELECTRONIC COOLING USING ERG ALUMINUM FOAM SUBJECTED TO STEADY/PULSATING WATER AND γ-Al_2O_3 –WATER NANOFLUID FLOWS: EXPERIMENTAL AND NUMERICAL APPROACH

by

Ayman Mahmoud Bayomy Mahmoud

Bachelor of Mechanical Power Engineering, Cairo University, 2011

Master of Science, Mechanical Power Engineering, Cairo University, 2013

A dissertation presented to

Ryerson University

in partial fulfillment of the requirement

for the degree of

Doctor of Philosophy

in the program of

Mechanical & Industrial Engineering

Toronto, Ontario, Canada, 2017

Author's Declaration

I hereby declare that I am the sole author of this dissertation.

This is a true copy of the dissertation, including any required final revisions, as accepted by my examiners.

I authorize Ryerson University to lend this dissertation to other institutions or individuals for the purpose of scholarly research.

I further authorize Ryerson University to reproduce this dissertation by photocopying or by other means, in total or in part, at the request of other institutions or individuals for the purpose of scholarly research.

I understand that my dissertation may be made electronically available to the public.

Ayman Bayomy

Abstract

Electronic Cooling Using ERG Aluminum Foam Subjected to Steady/Pulsating Water and γ-Al_2O_3 –Water Nanofluid Flows: Experimental and Numerical Approach

Doctor of Philosophy

Ayman Mahmoud Bayomy Mahmoud

Mechanical & Industrial Engineering

Ryerson University

2017

Rapid developments in the design of chips and electronic devices for high-performance computers have led to a need for new and more effective methods of chip cooling. The first purpose of this study was to investigate the thermal development and heat transfer characteristics of aluminum foam heat sinks for the heater which simulated Intel core i7 processor. Three main features were then added to the aluminum foam heat sink: 1) introducing pulsating water flow through the aluminum foam in order to achieve a uniform surface temperature, 2) the addition of channels in the aluminum foam in order to increase the surface area to volume ratio and 3) using γ-Al_2O_3-water nanofluid as a coolant instead of water. The experimental results revealed that the thermal entry length of the flow through the aluminum foam increases along with increases in the Reynolds number. The results also revealed a convex profile for the local temperature distribution of the pulsating water flow through the aluminum foam due to the reversing flow and development of a boundary layers. The pulsating flow also enhanced the average Nusselt number by 14% and the temperature uniformity by 73% compared to the steady flow. The introduction of channels in the aluminum foam reduced the average Nusselt number by 10% (for two channels) and 25% (for three channels). The results revealed that the aluminum foam with two channels achieved a higher thermal efficiency compared to the block and three channel designs. The results also revealed that the foam filled channel enhanced the average Nusselt number by 20% compared with the empty channel. The maximum heat transfer rate enhancement was achieved at 0.2vol% and there was a sudden drop in the positive effect at 0.3vol% (compared with pure water). The positive effect then showed a slight increase along with increases in nanoparticle concentration up to 0.6vol%. The

average enhancement percentages of the Nusselt number at a 0.2vol% nanofluid concentration were 37% and 28% at Reynolds numbers of 601.3 and 210, respectively. The numerical results were in good agreement with the experimental data with a maximum relative error of 3% in all studies.

Acknowledgments

I would like to express my gratitude and sincere thanks to my father Eng. Mahmoud Bayomy who gave me the chance to learn the mechanical engineering from his huge knowledge and made me confident in myself.

I would like to express my gratitude and deep appreciation to my mother. Thank you for your steadfast love, support, encouragement and patience.

I would also like to thank my brother Mr. Mostafa Mahmoud. Thank you for being my second father and for your support.

I would like to express my gratitude and deep appreciation to my dear wife Shimaa, who has been with me all these years. Thank you for your steadfast love, support, encouragement and patience. You have kept me going through the most difficult times and have made them the best years of my life.

I would like to express my gratitude and sincere thanks to my supervisor Dr. M. Z. Saghir for giving me the opportunity to work under his supervision. Thank you for your patience, guidance, encouragement and friendship during my graduate studies at Ryerson University.

I would also like to thank my doctoral committee members for their encouragement, accessibility, insightful comments and valuable discussions.

I would like to thank my friends and fellow lab mates in the mechanical engineering department at Ryerson for the stimulating discussions and all of the great times we have shared in the last three years.

I gratefully acknowledge Dr. T. Yousefi for his time and valuable feedback on my work. I am deeply thankful to my dear friend Ayman A. Farid for his support and help.

To my dear daughter Malak, thank you for keeping my life full of happiness.

The author acknowledge the full financial support of the National Science and Engineering Research Council (NSERC) from September 2013 to September 2016.

Table of Contents

List of Tables

List of Figures

Nomenclature

q''	Heat flux (W/cm^2)
Re	Reynolds number
Pr	Prandtl number
T_b	Bulk fluid temperature (℃)
T_x	Local surface temperature (℃)
T_i	Inlet fluid temperature (℃)
T^*	Dimensionless surface Temperature
t	Time (s)
d_p	Pore diameter of porous media (m)
d_f	Ligament dimeter of porous media (m)
c_f	Dimensionless form drag constant
c_p	Specific heat (J/kg.K)
p	Pressure (Pa)
U(u,v,w)	Velocity field vector (m/s)
V	Intrinsic velocity (m/s)
K	Permeability (m^2)
k	Thermal conductivity (W/m.K)
h_x	Local heat transfer coefficient ($W/m^2.K$)
f	Fanning friction factor
F	Body force (N)
L	Channel length (m)
H	Channel height (m)
$I_{efficiency}$	Thermal efficiency index
D_e	Hydraulic diameter of the channel (m)
A_o	Pulsating flow amplitude
Re_w	Kinetic Reynolds number
T^*	Dimensionless surface Temperature
$Nu_{,avg}$	Average Nussely number
Nu_x	Local Nusselt number

Greek symbols

μ	Dynamic viscosity (Pa.s)
μ'	Effective viscosity (Pa.s)
ε	Porosity
ρ	Density (kg/m^3)
ρ_r	Relative density of porous media
β	Expansion coefficient (1/K)
β_f	Forchheimer coefficient (kg/m^4)
υ	Kinematic viscosity (m^2/s)
η	Uniformity index

Subscripts

f	Fluid
nf	Nanofluid
p	nanoparticle
s	Solid
steady	Steady flow
pulsating	Pulsating flow
eff	Effective
bf	Base fluid

CHAPTER 1-RESEARCH MOTIVATIONS AND OBJECTIVES

1.1 General Overview of Electronic Cooling

The field of electronics deals with the construction and employment of devices that involve the flow of a current through a vacuum, gas, or semiconductor. The exciting field of science and engineering dates back to 1883, when Thomas Edison invented the vacuum diode, which played an important role in the development of TV, radars, and computers. The invention of the transistor in 1948 represented the beginning of a new era in the electronics industry. Transistor circuits performed the functions of the vacuum tubes with greater reliability while using less power and space.

The next turning point occurred in 1959 with the introduction of integrated circuits (IC), where several components such as diodes, transistors, resistors, and capacitors are placed in a single chip. Since then, the number of components packed in a single chip has steadily increased, as illustrated in Figure 1.1. As we can see in this figure, there have been rapid developments in the number of components per single chip. These days, it is not unusual to see a $3\text{cm} \times 3\text{cm}$ chip with several million components. In addition, the development of the microprocessor in the early 1970s by the Intel Corporation marked yet another beginning in the electronics industry.

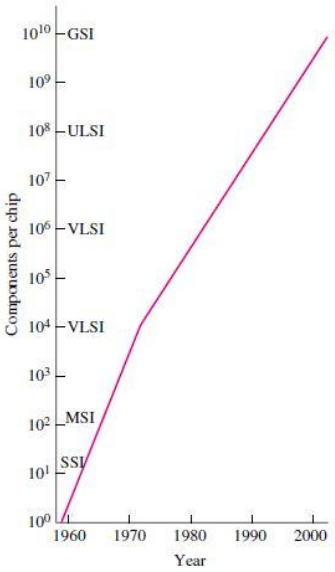

Figure 1.1: The rapid development in the number of components per single chip [1]

Nowadays, electronic devices are part of our everyday lives, from toys and appliances to high speed computers. Heat dissipation always accompanies the flow of a current through resistance. This heat dissipation is represented by $I^2.R$, where I represents the electric current and R represents the resistance. The continuous developments in the design of electronic chips have resulted in an increase in the amount of heat generated per unit of volume. The international technology road map for semiconductors reported that the heat flux from single chips rose from

330W/cm^2 in 2007 to 520W/cm^2 in 2011[2]. In addition, Gochman et al. [3] reported that the heat dissipation of desktop and mobile processors are 100W and 30W, respectively.

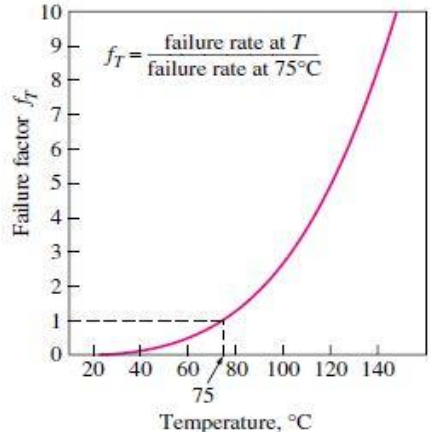

Figure 1.2: Increases in the failure rate of electronic components with increases in temperature [4]

Research has revealed that the performance reliability and lifetime of electronic component are inversely related to the temperature of the component. In silicon semi-conductor devices, reductions in temperature result in an exponential increase in performance reliability and lifetime, as illustrated in Figure 1.2. As we can see in this figure, the failure rate of electronic components increases exponentially with operating temperature. In addition, the high thermal stress on the solder joints of electronic components mounted on circuit boards, resulting from variation in the temperature, is one of the major causes of the failure of electronic components.

This is not the only challenge in the field of electronic cooling. Research has revealed that, for modern high speed computers, the operating speed and reliability of transistors depend on average surface temperatures as well as temperature uniformity over the surface. Hot regions can affect the performance of electronic components due to prolonged gate delay. It is thus imperative to maintain a uniform temperature distribution across the surface of electronics and to keep the temperature below a certain level. The junction temperatures of silicon-based electronic devices are usually limited to 125°C [1]; however, lower temperature reduces the maintenance rate of the electronic component.

Air cooling heat sinks are widely used for the cooling of electronics. Air cooling is usually used for extended surface heat sinks such as single or multiple square, rectangular and circular modules (rods) mounted on the heated surface [5-10], or fin array heat sinks attached to the heated surface [11]. The heat generated from chips flows through the thermal spreader and the thermal interface material into the heat sink which is cooled by forced or free convection. These traditional

free or forced convection cooling methods are only capable of removing small amounts of heat flux, making it imperative to search for new methods of cooling high-speed electronic components with high heat flux (>100W/cm^2) at the chip level.

Air cooling heat sinks have a low heat transfer coefficient because of the low thermal properties and heat capacity of air. As a result, researchers are searching for new cooling techniques that allow for the rapid removal of the heat generated by electronic components. Because of the high thermal properties of liquids, this limitation can be overcome with the introduction of water or other forms of liquid. The most common electronic heat sinks, which use liquid cooling, are microchannel heat sinks, jet impingement cooling heat sinks, and spray cooling heat sinks.

The limitations of microchannel heat sinks include the fact that the temperature of liquid coolants increases with stream wise direction (non-uniform temperature distribution), significantly higher pumping power is required, and they are not suitable for solid-liquid suspension coolant fluids.

Unfortunately, the current thermal management system designs have already stretched this extended surface technology to its limits. With continued miniaturization and increasing heat dissipation in new generations of products, the issue of cooling will intensify in many industries including electronics and photonics, transportation, energy supply, defense, and medicine.

1.2 Introduction of Porous Structured Heat Sinks

Open cell porous structures have recently been used for various applications. Metal foams are a class of porous material with a low density and novel thermal, electrical, mechanical and acoustic properties. Metal foams can be used for low temperature applications such as electronic cooling and high temperature applications such as the transpiration cooling of lean premixed combustors. Metal foam can be used also as a sound absorber (e.g. sandwich acoustic damper) around jet engines in order to reduce engine noise, as a thermal shield for rockets and satellites, and as high temperature filtration material and in impact absorbing parts in vehicles.

Metal foams constructed from materials with high thermal conductivity, such as aluminum or copper, are widely used in thermal management applications [12-15], as illustrated in Figure 1.3. These metal foams provide good heat transfer due to the large surface area to volume ratio (roughly 1000-3000m^2/m^3) [16]. The tortuosity of metal foam also enhances fluid mixing. Because

the flow paths are interconnected throughout the foam, the fluid flow is accessible from anywhere within the material, as illustrated in figure 1.4.

Metal foam cells are normally polyhedrons composed of 12-14 pentagonal or hexagonal shaped faces. The microstructural properties of metal foam include the pore size, ligament diameter, relative density, porosity, and pore density. Pore size represents the size of each window or face in the polyhedron cell. Ligament diameter represents the diameter of the solid filaments. Relative density represents the ratio between the volume of the solid material and the total volume. Porosity represents the ratio between the void volume and the total volume. Pore density represents the number of pores (e.g. window or face) per unit inch (PPI). The pentagonal or hexagonal pores actually are of two or three different characteristic sizes and shapes, but for material designation purposes, they are simplified to an average size and circular shape.

Metal foam is usually described by two independent microstructural properties: relative density and pore density (PPI). The remaining microstructural properties are dependent parameters that can be calculated using different models. The effective thermal conductivity of metal foam filled with a fluid is a key parameter in thermal management applications.

(a) Copper foam heat exchanger (b) Tube heat exchanger (c) Aluminum foam heat exchanger

Figure 1.3: Metal foam applications for heat transportation [12-15]

The majority of researchers apply the effective thermal conductivity model [17] by simply accounting for the volume fraction of each substance:

$$k_{eff} = \varepsilon \cdot k_f + (1-\varepsilon) \cdot k_s \quad (1.1)$$

Where ε represents porosity of the metal foam, k_s represents the thermal conductivity of the solid material, and k_f represents the thermal conductivity of the fluid. This equation does not account for the natural convection between the solid and fluid phases, the thermal resistance between the cells of the porous medium, and the structural features of the porous medium, which all play a significant role in the heat transfer characteristics of porous mediums. An accurate representation of the structural parameters of metal foams is important for the estimation of effective thermal conductivity. A thorough literature review of the different models which evaluate the effective thermal conductivity of fluid filled metal foams is therefore presented in section 2.3.1.

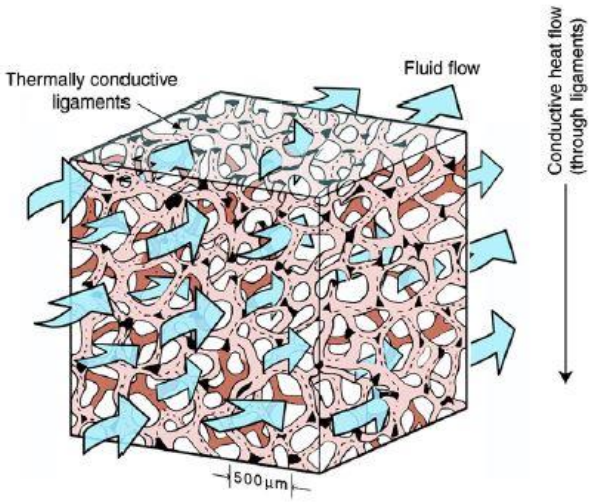

Figure 1.4: Forced convection through metal foam [16]

As previously mentioned, metal foams can be used in advanced compact heat exchangers. Several thermal engineering applications can therefore benefit from a better understanding of convection through porous media.

1.2.1 Seepage Velocity and Continuity Equation

In order to apply usual differential equations which express the conservation laws, one must assume that the porous medium is a continuum medium. When considering volume elements that are sufficiently large when compared with the pore volumes (V_m) (including solid and liquid volumes), we end up with two types of velocities: the seepage or Darcy velocity (U= (u, v, w)), which is the average of the fluid velocity over the total volume of the chosen element, and the intrinsic average velocity (V), which is the average of the fluid velocity over the fluid volume (V_f). Based on these definitions, the continuity equation can be expressed as follows:

$$\varepsilon \frac{\partial \rho_f}{\partial t} + \nabla \cdot (\rho_f U) = 0 \quad (1.2)$$

Where U, ρ_f and ε represent the Darcy velocity vector, fluid density, and porosity, respectively.

1.2.2 Momentum Equation

The first investigation of fluid flow through porous media was conducted by Darcy in the nineteenth century. Darcy [18] was the first to conduct experiments in order to obtain formulas for the flow of fluid through porous media. He observed that the velocity in the column of porous media is proportional to the pressure gradient and inversely related to the viscosity of the fluid. The formula is as follows:

$$u = \frac{K}{\mu_f} \cdot \left(-\frac{dP}{dx}\right) \tag{1.3}$$

Where μ_f, p, and K represent the fluid viscosity, pressure and permeability, respectively. The permeability of a porous medium (K) depends on the geometry of that medium and can be defined as the fluid conductance of the medium.

The Darcy equation describes the seepage velocity as a linear relationship. Darcy neglected several important physical effects such as the surface drag friction as a result of shear stress over the ligaments of porous media and inertial forces (assumed creeping flow). Therefore, the Darcy law is only valid for very small seepage velocities ($Re \ll 1$). As (U) increases, the linearity breaks down due to the form drag caused by the solid ligaments of the porous medium. Forchheimer [19] made some modifications to the Darcy equation:

$$\nabla p = -\frac{\mu_f}{K} U - \beta_f |U| U \tag{1.4}$$

β_f is called the Forchheimer coefficient. Ward [20] discovered the dependence of the Forchheimer coefficient on the permeability and fluid density of the porous medium as follow:

$$\beta_f = c_f \cdot \frac{\rho_f}{\sqrt{K}} \tag{1.5}$$

Where c_f represents the dimensionless form drag constant. Ward believed that (c_f) might be a universal constant with a value of approximately 0.55. It was later discovered that (c_f) varies depending on the nature of the porous medium and can be as small as 0.1 (as is the case for metal foam). Brinkman [21, 22] added a second viscous term to the Darcy equation:

$$\nabla P = -\frac{\mu_f}{K} U + \mu' \nabla^2 U \tag{1.6}$$

Where $\mu'$is the effective viscosity. This term is analogous to the Laplacian term that appears in the Navier–Stokes equation. Brinkman claimed that μ and μ' are equal, however, various studies [23-25] revealed that $\frac{\mu_f}{\mu'}$ depends on the geometry of the porous medium and should exceed unity. Ochoa-Tapia and Whitaker [26] noticed that is greater than unity as $\left(\frac{\mu_f}{\mu'} = \frac{1}{\varepsilon}\right)$. Valdes-Parada et al. [27] also noted that it is common practice for high porosity cases to assume that μ' and μ are equal. Durlofsky and Brady [28] concluded that the Brinkman model is valid for porosity greater than 0.95 while Rubinstein [29] observed that the Brinkman model is valid for porosity as small as 0.8. Several studies added this Laplacian term to Eq. (1.4) to form the Brinkman- Forchheimer equation:

$$\nabla P = -\frac{\mu_f}{K}U + \frac{\mu_f}{\varepsilon}\nabla^2 U - \beta_f |U|U \tag{1.7}$$

Later, Vafai and Tien [30, 31] and Hsu and Cheng [32] obtained a general equation that takes into consideration the inertia and body forces analogous to the Navier–Stokes equation:

$$\rho_f\left[\frac{1}{\varepsilon}\frac{\partial U}{\partial t} + \left(\frac{U}{\varepsilon}\cdot\nabla\right)\left(\frac{U}{\varepsilon}\right)\right] = -\nabla P - \frac{\mu_f}{K}U + \frac{\mu_f}{\varepsilon}\nabla^2 U - \beta_f |U|U + F \tag{1.8}$$

Where F represents the body forces. It is important to note that the Brinkman term is negligible compared to the Darcy term when $\sqrt{K} \ll L$, where L is the appropriate length scale; In other words, when the Darcy number is very small. However, when the Brinkman term is comparable with the Darcy term throughout the medium, K, which appears in Eq. (1.8), can no longer be determined using a simple Darcy-type experiment [33].

Many studies have examined the validity of the Brinkman-Forchheimer model [34-41]. These studies provide some assurance that the model is reliable and can be used with confidence. In addition, Auriault [42] concluded that then Brinkman-Forchheimer equation is valid for media with high porosity, and that the effective viscosity is equal to the viscosity of the fluid.

1.2.3 Energy Equation

The heat transfer inside porous media with the assumption of local thermal equilibrium, where the localized temperatures of solid and fluid phases are equal, can be described using the following energy equation:

$$(\rho c_p)_{eff}.\frac{\partial T}{\partial t} + (\rho c_p)_f U.\nabla T = \nabla.(k_{eff}.\nabla T) \quad (1.9)$$

Where ρ represents the density, c_p represents specific heat, T represents the fluid temperature, k_{eff} represents the effective thermal conductivity of the fluid filled porous media (discussed in chapter 2), and $(\rho c_p)_{eff} = \varepsilon \cdot (\rho c_p)_f + (1-\varepsilon) \cdot (\rho c_p)_s$.

The effect of solid material thermal conductivity of the metal foam as a class of porous media was demonstrated by Zhao et al. [43]. Zhao et al. [43] observed that at Re=2200, the average Nusselt number is independent on the solid material thermal conductivity (K_s), when the solid material thermal conductivity is at level of 200W/m.k or higher. That is why, in the present study the aluminum metal foam was chosen, which has a solid material thermal conductivity of 218W/m.K. Besides that, the aluminum foam has lower cost and lighter weight compared with copper foam.

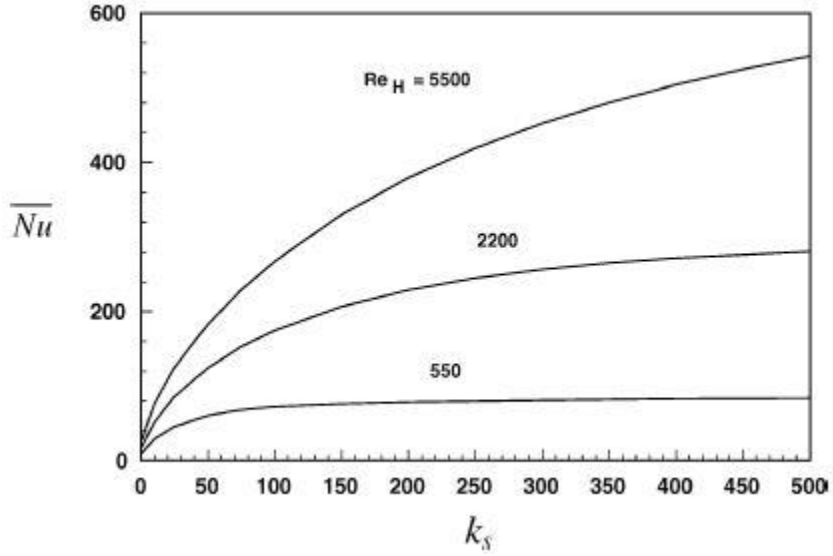

Figure 1.5: The effect of soild thermal conductivity on the average Nusselt number [43]

1.3 Introduction to Nanofluids

Cooling is important in order to maintain the desired performance and reliability of various applications such as computers, power electronics, car engines, and high-powered lasers or x-rays. The electronic industry has created faster computers with smaller sizes and expanded features, leading to increases in heat loads (over 100W/cm^2). This is what has led the manufacturers of electronic components to believe that electronic systems require the use of liquid cooling.

Many efforts have been made to find innovative heat transfer liquids and improve cooling systems in order to allow them to handle continual increases in the heat dissipation of microelectronic devices. One promising technique that offers an enhancement in the thermal properties of heat transfer coolant liquids is the use of solid-liquid suspension coolants such as nanofluids.

Maxwell [44] was the first person to disperse millimeter or micrometer sized particles in liquids. He discovered that dispersing relatively large metallic particles caused the particles to settle down rapidly, achieving low thermal properties at low particle concentrations. Maxwell also observed some increases in the thermal conductivity of these fluids. That being said, many applications have suffered from problems such as abrasion, channel clogging due to the unstable mixing of the particles, and high pressure drop.

Modern technology later allowed for the production of nano-sized metallic particles (less than 100 nm). Compared with micro-particles, nanoparticles have a higher surface area to volume ratio (1000 times larger) and stay suspended for longer periods. Choi [45] was the first to describe a new category of heat transfer fluids: nanofluids. He observed that nanofluids have superior thermal properties when compared to their host fluids or traditional heat transfer coolant fluids. Choi also presented the possibility of increasing the convection heat transfer coefficient by 100% of the nanofluids instead of increasing the pumping power.

Since Choi's description of nanofluids in the spring of 1993, thermal scientists and researcher in the rapidly growing nanofluid community have made many scientific breakthroughs, including the discovery of the unexpected thermal properties of nanofluids and the proposal of new mechanisms behind the enhanced thermal properties of nanofluids. Various studies have examined the enhanced thermal conductivity of nanofluids. These studies will be presented in section 5.1.

The intent behind the use of nanofluids is to achieve the highest possible thermal properties at lower nanoparticle concentrations through the use of the uniform dispersion and stable suspension of nanoparticles in the host fluid.

1.3.1 Nanoparticles Material Types and Dispersion Techniques

Nanoparticles are made from various materials such as oxide ceramics (Al_2O_3, CuO), Nitride ceramics (AlN, SiN), carbide ceramics (SiC, TiC), metals (Cu, Ag, Au), semiconductors

(TiO_2, SiC), carbon nanotubes, and composite materials such as alloyed nanoparticles $Al_{70}Cu_{30}$. Many different liquids have been used to host nanofluids, including water, ethylene glycol and oil.

The stability and dispersion behaviour of nanofluids play a key role in the enhancement of the thermal properties of nanofluids. The stable suspension of nanoparticles in conventional fluids is produced using two common methods: the two step and single step techniques. In the two step technique, the nano-powder is prepared in nano-scale size, mixed in the base fluid, and stabilized using a dispersion technique such as the high shear or ultrasound mixer. In the single step technique, nanoparticles are formed and dispersed in the host fluid in a single process [46, 47]. In this technique, the drying and dispersion of nanoparticles is eliminated, reducing the chance of particle agglomeration. Therefore, the suspension of non-agglomerated or monodispersed nanoparticles is the key parameter in enhancing the thermal properties of nanofluids.

Eastman et al. [48] developed the direct evaporation system as a one-step technique. He observed that the direct evaporation–condensation process yielded the uniform distribution of nanoparticles in a host liquid. Zhu et al. [49] developed a one-step chemical method for the production of stable Cu in ethylene glycol nanofluids by reducing copper sulfate pentahydrate ($CuSO_4 \cdot 5H_2O$) with sodium hypophosphite ($NaH_2PO_2 \cdot H_2O$) under microwave irradiation. They claim that this one-step chemical method is faster and cheaper than the one-step physical method.

1.3.2 Mechanisms and Models for the Enhanced Thermal Properties of Nanofluids

The majority of the thermal properties of nanofluids that have been experimentally measured have exceeded the predicted values obtained using classical macroscopic solid–liquid suspension theories. In other words, these theories are unable to explain why nanofluids with low particle loading achieve higher thermal properties than the predicted values. It would appear that the behaviour of the thermal properties of nanofluids is much more complex than the explanations provided by conventional solid–liquid suspension theories using the diffusive thermal transportation mechanism.

Researchers have recently observed that the enhanced thermal properties of nanofluids can be attributed two primary mechanisms: the structure-based or static mechanism and the dynamic mechanism. The structure-based mechanism described by Yu and Choi [50] is based on the nano-layers acting as a thermal bridge between the solid particles and bulk fluid, the interfacial thermal resistance, and the fractal structure of agglomerates. Xue [51] was the first researcher to show the

nonlinear behaviour of the thermal conductivity of nanofluids. He also developed a structural model for the thermal conductivity of nanofluids based on the liquid layering mechanism and the average polarization theory. Yu and Choi [52] were the first to model the effective thermal conductivity of nanofluids with a cubic arrangement of spherical nanoparticles. They showed the non-linear relationship between the effective thermal conductivity of the nanofluid and the particle loading.

The dynamic mechanism is based on the Brownian motion of the nanoparticles which is defined as the random motion of suspended nanoparticles as a result of collisions with the molecules of the host fluid. Since nanofluids are dynamic systems, the motion of nanoparticles and the interactions between the dancing nanoparticles or between dancing nanoparticles and liquid molecules must be considered. Various studies have examined the dynamic mechanism (presented in chapter 5).

1.4 Research Objectives

This leads us to the two main challenges of high performance electronic cooling. The first challenge is the rapid removal of the heat generated from the electronic surface because the performance reliability and lifetime of silicon semi-conductor devices are inversely related to the temperature of the component. Conventional convective cooling methods, such as plate fins or micro-channel heat sinks, are only capable of removing small amounts of heat flux.

The second challenge is to achieve a uniform temperature distribution over the electronic surface in order to prevent the localized hot spots which can destroy the electronic component or affect the performance of electronic devices as a result of prolonged gate delay. In addition, the operating speed and reliability of transistors depend not only on average surface temperatures, but also on temperature uniformity over the surface.

Generally speaking, the two parameters that play a key role in convention heat transfer augmentation are the surface area to volume ratio of the heat sink and the thermal properties of the coolant fluid.

The research objectives were set based on the challenges outlined above. Since we are dealing with high performance electronic cooling issues, the Intel core i7 processor was chosen for the present research case study of electronic cooling. However, a heater of the same dimensions of Intel core i7 processor has been placed instead of real processor in order to achieve a wider and

controllable range of heat flux. The heater heat flux was ranged from 8.5W/cm^2 to 13.8W/cm^2 based on the estimated heat flux from chips [2, 3, and 53]. The research objectives are outlined below:

- A study of the steady flow of water through an ERG aluminum foam block heat sink for the cooling of electronics (C**hapter 2**). The water flow covered the entire non-Darcy flow regime (297 to 1353 Reynolds numbers). The following things were examined:
    - The thermal development through the aluminum foam (e.g. thermal entry and fully developed regions).
    - The heat transfer characteristic of the aluminum foam heat sink (e.g. local surface temperature and Nusselt number distributions).
    - The development of an empirical equation for the average Nusselt number as a function of the Reynolds number.
    - The evaluation of the thermal performance of an ERG aluminum foam heat sink subjected to a steady water flow (with respect to the heat transfer rate and pumping power required).
    - The evaluation of the uniformity of the surface temperature distributions.
- A study of pulsating water flow through an ERG aluminum foam block heat sink in order to achieve uniform temperature distributions (**Chapter 3**). The following things were examined:
    - The heat transfer characteristic of pulsating water flow (f = 0.04-0.1Hz) through an aluminum foam heat sink.
    - The development of an empirical equation for the average Nusselt number as a function of the pulsating flow amplitude and kinetic Reynolds number.
    - A comparison of the steady and pulsating water flow through an ERG aluminum foam (with respect to the heat transfer rate and surface temperature uniformity).

- The evaluation of the thermal performance of the heat sink subjected to the pulsating water flow and comparison of the pulsating and steady flows thermal performance.

- A study of channeled ERG aluminum foam heat sinks (e.g. two and three channels) subjected to steady water flow (**Chapter 4**). The following things were examined:
  - The heat transfer characteristics of three aluminum foam heat sink models: without channels (A), with two channels (B), and with three channels (C).
  - The development of an empirical equation for the average Nusselt number as a function of the Reynolds number for each model.
  - A comparison of the thermal performance of the three heat sink models in order to find the optimal design (one that achieves the highest heat transfer and lowest pressure drop).
  - The experimental results were complemented by a numerical study using the finite element technique.
- A study of the interaction between nanofluids and porous structured heat sinks, specifically, γ-Al_2O_3-water nanofluid through an ERG aluminum foam heat sink. The γ-Al_2O_3-water nanofluid concentration ranged from 0vol% to 0.6vol% and the nanofluid flow covered the non-Darcy flow regime (210 to 631 Reynolds numbers) **(Chapter 5).** The following things were examined:
  - The heat transfer characteristic of aluminum foam heat sinks subjected to γ-Al_2O_3-water nanofluids at various particle loadings.
  - A comparison between the heat transfer characteristics of empty channels and metal foam filled channels subjected to a water flow.
  - The development of an empirical correlation of the average Nusselt number as a function of the Reynolds number, Prandtl number, and nanoparticle volume fraction.
  - Obtaining the optimal nanoparticle concentration (the one which achieves the highest heat transfer rate).

CHAPTER 2-ELECTRONIC COOLING USING WATER FLOW IN ALUMINUM METAL FOAM HEAT SINK

This chapter is based on the following published paper:

Bayomy, A. M., Saghir, M. Z., and Yousefi, T., "Electronic Cooling Using Water Flow in Aluminum Metal Foam Heat Sink: Experimental and Numerical Approach" Int. J. Thermal Science, vol. 109, pp. 182-200, 2016.

2.1 Introduction

Electronic components depend on electrical currents passing through resistance in order to perform their duties. This is accompanied by heat flux dissipation. The continuous developments in the design of electronic chips have resulted in an increase in the amount of heat generated per unit of volume. Therefore, an effective cooling method of electronics is a major challenge for electronic devises manufacturer. The performance reliability and lifetime of electronic component are inversely related to the temperature of the component. In silicon semi-conductor devices, reductions in temperature increase the performance reliability and lifetime.

Using porous media as a heat sink subjected to forced cooling fluid is a new technique used to enhance the heat transfer from the surface of electronics as mentioned earlier. Metal foam is a porous material with a low density and novel thermal, electrical, mechanical and acoustic properties. The heat transfer characteristics of metal foam are directly affected by microstructure properties such as porosity, relative density, pore density, pore size, ligament diameter, and permeability.

Hwang et al. [54] investigated the convective heat transfer and friction drag of aluminum metal foam. They observed that the heat transfer coefficient increases along with decreases in porosity for a given Reynolds number. In their study, Lu et al. [55] investigated the heat transfer characteristics of a pipe filled with metal foam. They observed that increases in the relative density are accompanied by increases in the overall Nusselt number. Seyf and Layeghi [56] investigated the effect of inserting metal foam in a pin fin heat sink. They observed that the heat transfer coefficient increases as the relative density increases and it decreases as the cell size (pore size) decreases. Mancin et al. [57, 58] analyzed the heat transfer characteristics and pressure drop of different aluminum foam samples (5, 10, 20, 40 PPI). They observed that the heat transfer coefficient increases with pore density (i.e. low pore size).

The effective thermal conductivity of ERG aluminum foams were studied by Boomsma and Poulikakos [59]. They demonstrated that in high porosity foam, the solid phase thermal conductivity controls the overall effective thermal conductivity of the aluminum foam. Boomsma and Poulikakos [59] derived also an expression of effective thermal conductivity. Zhao et al [43] studied the thermal dissipation of high porosity metal foams, both experimentally and analytically. They found that the pore size plays a more significant role in the heat transfer and an optimal porosity was obtained by balancing between the overall heat transfer and pressure drop. Zhao et al. [60, 55] presented analytical studies of forced convection through open cell metal foam. They found that porosity and pore size have a significant effect on overall heat transfer characteristics. In addition, Zhao et al. [60] demonstrated that the metal foam heat exchanger achieves higher heat transfer than the conventional finned tube heat exchanger. Klett et al. [61] observed that foam radiators transfer heat an order of magnitude better than fin radiators.

Bhattachatya and Mahajan [62] introduced high porosity (0.9) aluminum foam with pore densities of 5 and 20PPI into the air gap between two longitudinal fins. They observed an increase in the heat transfer coefficient with increasing fin numbers until they reached six fins. After six fins, a sudden decrease in the heat transfer coefficient was observed. Bhattachatya and Mahajan [62] also observed a higher heat transfer coefficient for the aluminum foam with 20 PPI pore density compared with the 5 PPI pore density at a given air velocity. In their research, Ding et al. [63] and Bai and Chung [64] found that the heat transfer coefficients are enhanced greatly by using copper metal foam. In their study, Tzeng et al. [65] determined the local and average heat transfer characteristics in sintered bronze bead channels subjected to forced air flow and observed that the wall temperatures increase with increasing axial flow direction distance.

Kim et al. [66] conducted an experimental study to analyze the thermal performance of an aluminum metal foam heat sink. They also compared the thermal performance of the aluminum metal foam heat sink with conventional parallel plate heat sink and found that using aluminum metal foam as a heat sink enhances the heat transfer. The researchers also observed that the local Nusselt number for the aluminum foam with low pore density (low surface area to volume ratio) is higher than other heat sinks with larger surface to volume ratios (larger pore density), which is in direct contrast with heat transfer concepts. Sung et al. [67] discovered that this phenomenon is caused by reductions in the flow rate inside the foam as a result of high pore density (higher flow

resistance), however, the heat transfer enhancement due to increase the pore density was only observed when the channel is completely filled with the foam.

Rachedi and Chikh [68] conducted a numerical study of electronic cooling using foam materials and analyzed the effects of the Reynolds number, Darcy number, thermal conductivity and properties such as porosity and permeability. They found that the insertion of foam reduces the temperature by 50% in comparison with the fluid condition. Fu et al. [69] conducted an experimental study of forced convection air flow through an ERG aluminum metal foam channel. They observed an increase in local surface temperature along with increases in the dimensionless axial flow direction distance until it reached a near constant value when the flow became fully thermally developed. The researchers also presented the local Nusselt number and length average Nusselt number.

Hooman and Ejlali [70] and Hooman and Haji-Sheikh [71] conducted analytical studies of heat development in rectangular porous channels using the Brinkman flow model. They studied the effect of viscous dissipation on the Nusselt number under the assumption of local thermal equilibrium between the fluid and the solid phases of the porous media. They observed that viscous dissipation reduces the Nusselt number in both the thermally developing and fully developed regions. Nield et al. [72] conducted an analytical study of the thermal entry region length in circle porous tubes or parallel plate channels subjected to a constant heat flux under the assumption of local thermal equilibrium. The researchers determined a correlation between the Nusselt number as a function of dimensionless axial coordinate and the Darcy number.

A small number of studies have used water as a working coolant fluid through metal foams. Boomsma et al. [73] conducted an experimental comparison of the thermal resistance of a compressed metal foam heat exchanger and commercially available heat exchangers using water as a coolant. They found that the thermal resistance of the compressed foam heat exchanger is two to three times lower than that of other heat exchangers. The pressure drop and friction factor of different foam porosities were also presented. Noh et al. [74] conducted an experimental study of non-Darcy water flow in annulus filled with high porosity aluminum foam and presented the correlations of the average Nusselt number and friction factor. Hetsroni et al. [75] conducted an experimental study of the transmission window cooling technique of an accelerator using on aluminum foam. Dukhan et al. [76] conducted an experimental study of thermal development in open cell metal foam subjected to constant heat flux. The flow rates used covered both the Darcy

and non- Darcy regimes. They found that the wall temperature and local Nusselt number showed two main behaviours related to the thermally developing and fully developed conditions.

As one can see from the literature review above, there have been many numerical and experimental studies using metal foam (porous medium) as a heat sink subjected to forced air flow under the assumption of local thermal equilibrium. Only a few studies have used water instead of air as a coolant through a porous medium and all of them ignored the heat transfer development and thermal entry length except for Dukhan et al. [76], who focused experimentally on the heat transfer development in the aluminum foam tube subjected to the water flow. There is therefore a need for more research regarding the heat transfer development and characteristics of aluminum foam subjected to water flow, especially for the cooling of electronics.

This chapter presents an experimental and numerical study of aluminum foam as a heat sink in the cooling of a heater which simulate an Intel core i7 processor. The heat flux was ranged from 8.5W/cm^2 to 13.8W/cm^2 [2, 3, and 53]. The aluminum foam was subjected to a water flow covering the non-Darcy flow regime. The thermal entry length was obtained for different Reynolds numbers and the heat transfer development of the aluminum foam is presented. Local temperature distributions were measured for different heat fluxes and Reynolds numbers and the local Nusselt number was calculated based on the local surface temperature and bulk water temperature for the entry and fully developed regions. The average Nusselt number was obtained for the entire range of Reynolds numbers. An empirical correlation of the average Nusselt number was developed based on the Reynolds number. The pressure drop across the foam was also measured and the thermal performance of the aluminum foam heat sink was evaluated based on the average Nusselt number and the pumping power required. The results of the experiment were then compared with those obtained in previous experimental studies. Lastly, a numerical approach was used (finite element method) [77] and the results were compared with those obtained experimentally. Section 2 presents the experimental setup while section 3 presents the numerical approach. Section 4 presents the results of the experimental and numerical approaches and a comparison between them. Section 5 highlights the findings obtained in the study and provides conclusions.

2.2 Experimental Apparatus and Procedures

An experimental setup was developed to examine the heat transfer development and characteristics of aluminum foam as a heat sink in the cooling of electronic component.

2.2.1 Test Section and Experimental Facility

The experimental setup consisted of a pump with a control valve, a tank, flow meter and pressure transducer (see Figure 2.1). The flow meter range was from 0 to 3gpm with corresponding output signals between 4 and 20mA. The pressure differential transducer range was from 0 to 30psi with corresponding output signals between 0 and 10Vdc. The test section consisted of high temperature Teflon insulation attached to a 37.5mm ×37.5mm heater (corresponding to the size of an Intel core i7 processor). The heater contained an adjustable current input in order to control the heat flux, as shown in Figure 2.2. Eight type (T) thermocouples were attached to the surface of the heater to measure the surface temperature and two thermocouples were used to measure the inlet and outlet water temperatures. The positioning of the thermocouples can be seen in Figure 2.3(a). Because of their large head connections, the thermocouples were inserted through the Teflon insulation in a staggered arrangement, as shown in Figure 2.3(b).

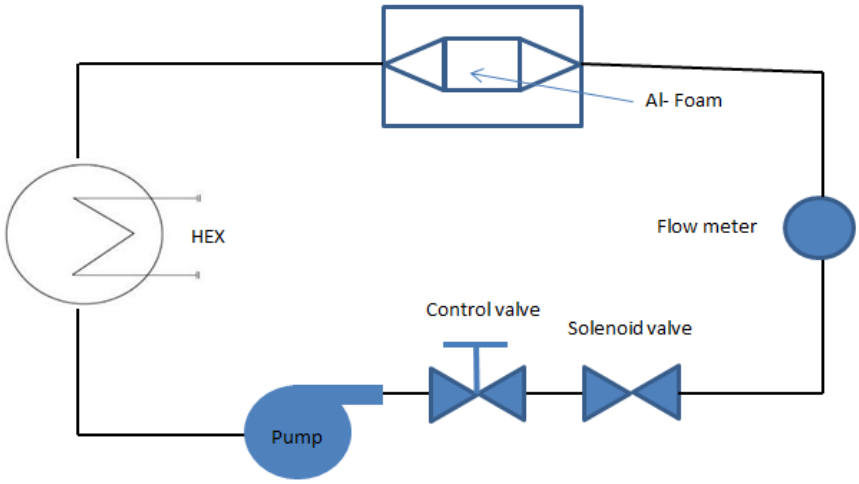

Figure 2.1: Experimental schematic diagram [78]

All of the signals from the thermocouples, the flow meter and the pressure transducer were connected to a data acquisition system in order to monitor and save the experimental data. The ERG aluminum metal foam (alloy 6101-T6) was cut to match the size of the heater (37.5mm×37.5mm), as shown in Figure 2.4. The physical and geometric properties of the ERG test section foam are as follows: relative density (ρ_r) of 9%, pore density of 40PPI, permeability (K) of 3.38e-8m^2, and thermal conductivity of solid material (K_s) of 218W/m.K. It is important to note that these properties are not all independent of one another. The relationships between them are presented by Calmidi and Mahajan [79]. They developed the following formula to describe the

relationship between the ratio of the ligament and pore diameter of ERG foams as a function of porosity;

$$\frac{d_f}{d_p} = 1.18\sqrt{\frac{1-\varepsilon}{3\pi}} \cdot \left(\frac{1}{1-\exp\{\frac{\varepsilon-1}{0.04}\}}\right) \tag{2.1}$$

Where d_p and d_f represent the pore diameter and ligament diameter, respectively. The simple relationship between the porosity and relative density of ERG foams is obtained using the following equation:

$$\rho_r = 1 - \varepsilon \tag{2.2}$$

Calmidi [80] developed the following formula to obtain the permeability of ERG foams:

$$\frac{K}{d_p^2} = 0.00073 \cdot (1-\varepsilon)^{-0.224} \left(\frac{d_f}{d_p}\right)^{-1.11} \tag{2.3}$$

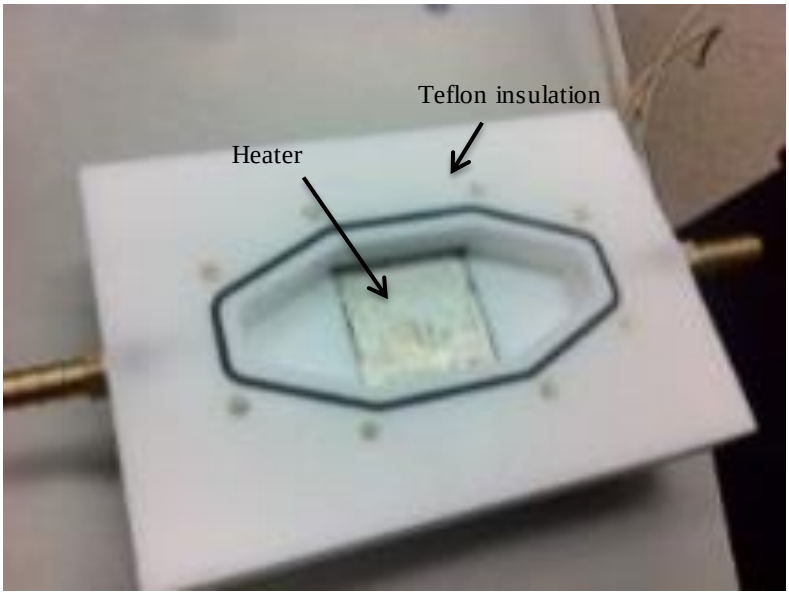

Figure 2.2: Test section heater [78]

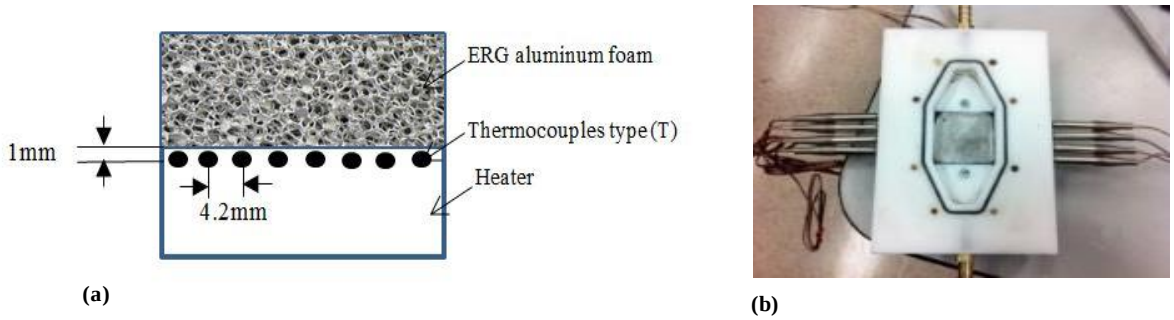

Figure 2.3: Thermocouples positions and arrangements [78]

The aluminum foam was attached to the heater surface using the Arctic MX-2 compound. The Arctic MX-2 is a carbon micro particle compound which causes extremely high thermal conductivity. A Plexiglas cover was placed on top of the test section using bolts to affix the foam to the heater and prevent water leakage. The Plexiglas cover has two openings, just before and after the aluminum foam, to allow for connections to the pressure differential transducer ports, as shown in Figure 2.5. In order to obtain experimental steady state conditions, the surface temperature, inlet and outlet temperatures, pressure drop across the foam, and water flow rate were monitored using the data acquisition system.

Figure 2.4: ERG aluminum foam heat sink [78]

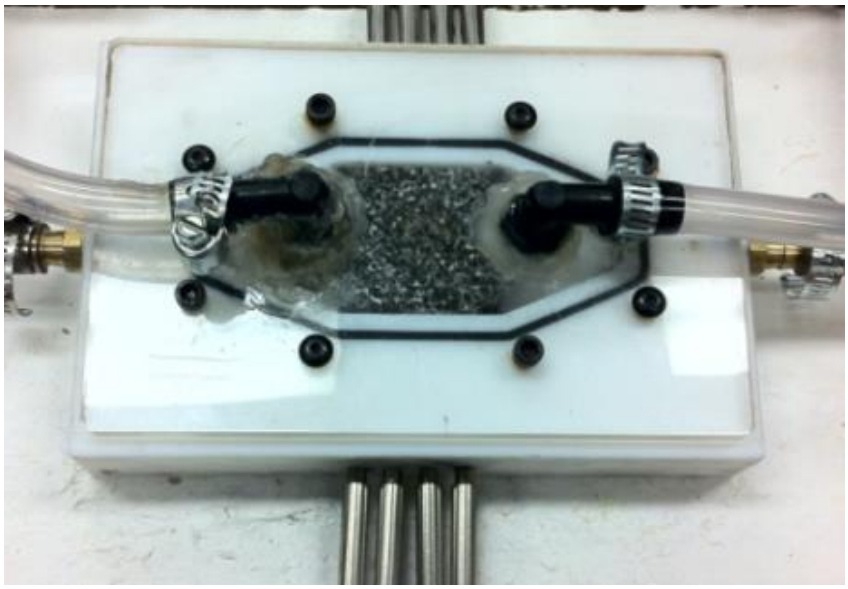

Figure 2.5: Test section [78]

2.2.2 Uncertainty Analysis

In order to calculate the uncertainties of parameters such as the local Nusselt number (Nu_x) and the Reynolds number (Re), the uncertainties of measuring data must be known. The uncertainties of the temperature, flow rate and pressure drop were 0.75% (°C), 0.44% (gpm) and 0.03% (psi), respectively. These uncertainty values were obtained from the calibration process for each instrument based on standard and random errors. The uncertainties of (Nu_x) and (Re) were obtained using the Taylor method [81]. If x, y, z are measurement quantities such as temperature, flow rate and pressure difference, and those measurement quantities have uncertainties of $\delta x, \delta y$ and δz and are used to calculate parameters such as the local Nusselt number $Nu_x(x, y, z)$, then the uncertainty of the local Nusselt number is:

$$\delta Nu_x = \sqrt{\left(\frac{\partial Nu_x}{\partial x}\cdot \delta x\right)^2 + \cdots + \left(\frac{\partial Nu_x}{\partial y}\cdot \delta y\right)^2 + \cdots \left(\frac{\partial Nu_x}{\partial z}\cdot \delta z\right)^2} \quad (2.4)$$

The local Nusselt number and the Reynolds number are calculated as follows:

$$h_x = \frac{q''}{(T_x - T_b)} \quad (2.5)$$

$$Nu_x = \frac{h_x \cdot D_e}{k_{eff}} \quad (2.6)$$

$$Re = \frac{U \cdot D_e}{\upsilon_f} \tag{2.7}$$

Where h_x represents the local heat transfer coefficient over the heater surface, T_x represents the local surface temperature, T_b represents the bulk water temperature, D_e represents the hydraulic diameter of the channel, U represents the water velocity throughout the test section, υ_f represents the kinematic viscosity of the fluid, and k_{eff} represents the effective thermal conductivity of the metal foam filled with water.

As one can see in Eq. (2.5 and 2.6), the uncertainty of the local Nusselt number is a function of the uncertainty of the difference between the surface temperature and bulk water temperature which varies along the surface (0.75% of the reading). This means that the uncertainty of the local Nusselt number will vary depending on the measurement position. The uncertainties of the local Nusselt number are used to evaluate the error bars for each local Nusselt number data point in section 2.4. The maximum value of the uncertainty of the local Nusselt number was $\pm 2.4\%$ and the uncertainty of the Reynolds number was $\pm 0.44\%$. The energy balance was checked by comparing the quantity of heat absorbed by the water with the actual heat input of the heater. The heat loss was obtained by subtracting the actual heat input from the quantity of heat absorbed by the water and the heat loss was found to be 0.2%.

2.3 Numerical Model Description

Numerical results were obtained using the finite element technique [77] in order to allow for a comparison with the experimental results.

2.3.1 Governing Equations

It is important to state the assumptions upon which the equations are based prior to the formulation of the model. Those assumptions are:

1. The fluid passing through the channel is Newtonian and incompressible.
2. The porous medium is homogenous and has uniform porosity.
3. Local thermal equilibrium between the fluid and the solid phase of metal foam.
4. No heat generation occurs inside the porous medium.
5. Variation in the thermo-physical properties of the solid phase can be neglected.

The first investigation of fluid flow through porous media was conducted by Darcy in the nineteenth century. Darcy [18] was the first to conduct experiments in order to obtain formulas of

fluid flow through porous media. He observed that the velocity through the column of porous media is proportional to the pressure gradient and inversely related to the viscosity of the fluid. The formula is as follows:

$$u = \frac{K}{\mu_f} \cdot \left(-\frac{dP}{dx}\right) \tag{2.8}$$

Where K represents the permeability of the porous material and μ represents the viscosity of the fluid. Darcy neglected several important physical effects such as the friction as a result of shear stress over the ligaments of porous media and inertial forces (assumed creeping flow). The Darcy law is therefore only valid for a very small flow rate ($Re < 1$). Forchheimer extended the Darcy law by taking into consideration the friction effect. Brinkman then formulated a general equation based on the Darcy and Forchheimer models to describe fluid flow through porous media. When finite element modeling assumptions are taken into consideration, the Brinkman- Forchheimer equation and energy equation which describe the fluid flow and heat transfer inside porous media are solved using the following formula:

$$\frac{\rho_f}{\varepsilon}\left(\frac{\partial U}{\partial t} + (U \cdot \nabla)\frac{U}{\varepsilon}\right) = \nabla.\left(-pI + \frac{\mu_f}{\varepsilon}(\nabla U + (\nabla U)^T)\right) - \left(\frac{\mu_f}{K} + \beta_f|U|\right)U + F \tag{2.9}$$

$$\nabla \cdot (\rho_f U) = 0 \tag{2.10}$$

$$(\rho c_p)_{eff} \cdot \frac{\partial T}{\partial t} + (\rho c_p)_f \, U \cdot \nabla T = \nabla.(k_{eff}.\nabla T) \tag{2.11}$$

Where ρ_f represents the water density, c_p represents the water specific heat, ε represents the porosity of the aluminum metal foam, p represents the pressure, U represents the velocity field vector, β_f represents the Forchheimer coefficient, T represents the temperature, μ_f represents the water dynamic viscosity, K represents the permeability of the aluminum foam and k_{eff} represents the effective thermal conductivity of the aluminum metal foam when filled with water. As mentioned in chapter 1, an accurate representation of the structural parameters of the metal foam is important for the estimation of effective thermal conductivity. Hsu et al. [82] developed a model based on phase symmetry for sponge like porous media where each phase is connected to each other. Hsu et al. [82] evaluated the ratio between the effective thermal conductivity of porous media to the fluid phase thermal conductivity at different porosities. It was found that the effective thermal conductivity based on Hsu et al. study [82] is about 12.62 W/m.K at porosity 0.9.

Calmidi and Mahajan [83] obtained experimentally the effective thermal conductivity of ERG aluminum foam based on one dimensional heat conduction through two dimensional foam structures. It was found that the effective thermal conductivity of ERG aluminum foam is about 7.65 W/m.K at porosity 0.905. Boomsma and Pouliakos [59] extended the previous research by investigating a three dimensional analytical model of effective thermal conductivity of ERG foams. They treaded the aluminum foam as tetradecahedron cells with cubic nodes at the intersection between cylindrical ligaments. It was observed from Boomsma and Pouliakos [59] plotted data that the effective thermal conductivity at porosity 0.9 was between 7-9 W/m.K depending on the value of (e), where (e) is the ratio between the length of the cubic node at the intersection of two ligaments to the ligament's length.

Later, Bhattacharya et al. [84] presented an analytical and experimental studies on estimating the effective thermal conductivity for high porosity metal foams. They observed that metal foams form a complex array of interconnected ligaments with irregular lump of metal at the intersections. They traded analytically the metal foam by assuming two dimensional array of hexagonal cells with circular nodes at the intersections. They found that at given porosity the experimentally determined values of the effective thermal conductivity are almost 50% of analytical values which evaluated under condition of minimum metal lump at the intersection. This means that the presence of metal lump at the intersections (large metal node) introduce more thermal resistance (lower effective thermal conductivity). Later, Bai et al. [85] found that Boomsma and Pouliakos [57] model has geometric and algebraic errors.

They fully corrected Boomsma and Pouliakos [59] model and observed that the corrected model has a deviation when it was compared with the experimental data. In addition, Bai et al. [85] extend Boomsma and Pouliakos [57] model by taking into consideration the effect of the inclination of the ligaments. It was found that the extended model was in good agreement with the experimental data with 12.2% relative error.

Finally, Yang et al. [86] presented an analytical and experiment model of effective thermal conductivity of fluid saturated metal foam with more realistic node size. They observed that the analytical values of the effective thermal conductivity were in good agreement with their experimental data and the experimental data presented by Calmidi and Mahajan [83]. In addition, the effective thermal conductivity was found to be 8.5 W/m.K at porosity 0.9 and e=0.3. They observed also that the pore density (PPI) has little influence upon the effective conductivity. As

seen previously, it was observed that there is a little deviation in the effective thermal conductivity between the analytical model presented by Yang et al. [86] at e=0.3 and the plotted data presented by Boomsma and Poulikakos [59] at e= 0.336.

The effect of the effective thermal conductivity deviation of the ERG aluminum foam on the average Nusselt number is evaluated numerically. It was found that the effective thermal conductivity variation based on [59, 86] has not significant effect on the average Nusselt number (less than 5% relative error). Therefore, Boomsma and Poulikakos [59] model was used to evaluated the effective thermal conductivity in the present work. In addition, it was found that using Boomsma and Poulikakos [59] effective thermal conductivity achieved good agreement between experimental data and numerical results.

2.3.2 Boundary Conditions

Boundary conditions can be divided into two categories: thermal boundary conditions and velocity boundary conditions. The thermal boundary conditions included a heat flux from the bottom portion of the heater (q") which represents the heat dissipation from electronic devices, inlet water temperature (T_i) at the inlet portion, the outflow surface at the outlet portion, and adiabatic boundary condition at the remainder of the surface. The velocity boundary conditions included the velocity field (U) at the inlet portion (assuming a flat profile), the open boundary surface at the outlet portion, and walls (u_x=0) at the remainder of the surface, (see Figure 2.6).

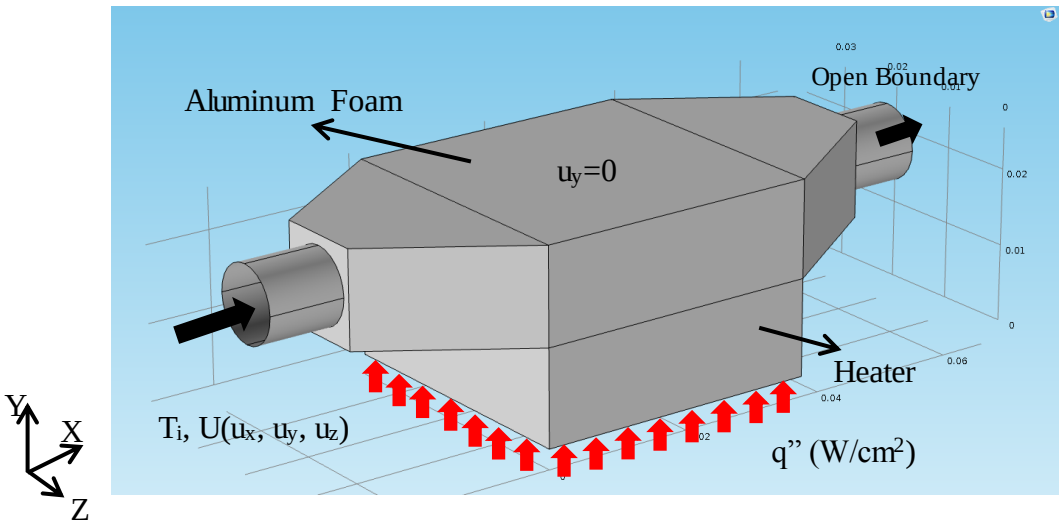

Figure 2.6: Boundary conditions [78]

2.3.3 Mesh Sensitivity Analysis

In the present finite element study, a tetrahedral element was used to describe the numerical model. In order to examine the grid dependency, the calculation of maximum temperature and local Nusselt number on the surface for steady flow through the metal foam channel was performed for different numbers of domain elements, as shown in Figure 2.7(a). The number of elements used was 212493 and the variation was less than 0.001.

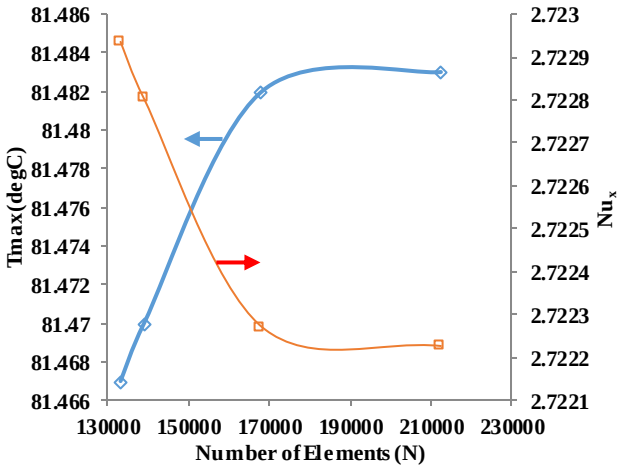

(a) Mesh independent

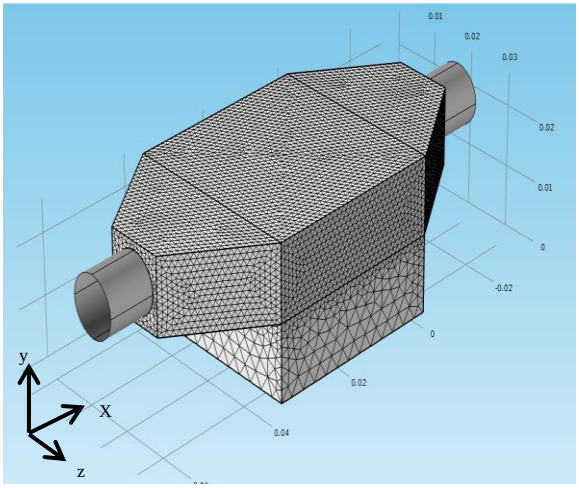

(b) Finite element model

Figure 2.7: Mesh sensitivity and finite element model [78]

2.4 Results and Discussion

In this experimental study, an aluminum foam heat sink was subjected to a uniform heat flux ranging from 13.8 to 8.5W/cm^2 [2, 3, and 53]. The water flow covered the Forchheimer regime (non-Dracy regime). In addition, a numerical model was developed using the finite element technique [77] and the numerical results were compared to the experimental results.

2.4.1 Surface Temperature and Thermal Development of Aluminum Foam

Figures 2.8(a) and 2.8(b) illustrate the surface temperature distributions along the dimensionless flow direction axis (x/D_e), where D_e is the hydraulic diameter of the channel, at q''= 13.8 and 8.5W/cm^2, respectively. As we can see, the surface temperature shows an increase in the flow direction. This trend has been observed in previous experimental studies [67, 74]. We can also see that the surface temperature increases along with decreases in the Reynolds number.

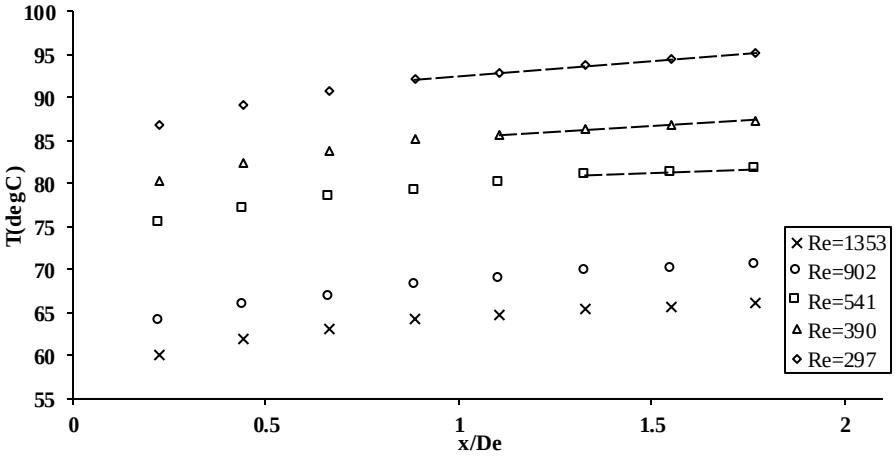

(a) Experimental temperature distributions at q"=13.8W/cm^2

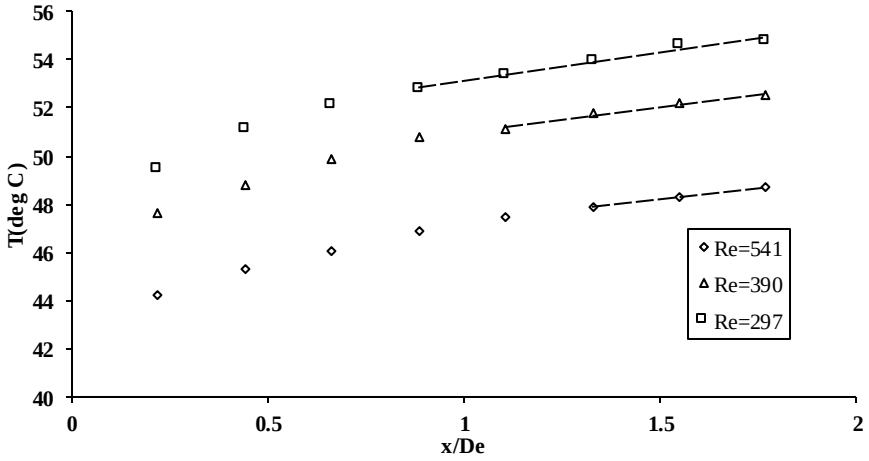

(b) Experimental temperature distributions at q"=8.5W/cm^2

Figure 2.8: Surface temperature along flow direction axis at different Reynolds number

A closer look at the temperature distributions revealed that the surface temperature slopes of Reynolds numbers 541, 390 and 297 show initial changes and become constant when the flow and temperatures reach the fully developed region. In order to estimate the thermal entry length, straight lines of best fit with a curve fit factor (R^2) greater than 0.95 were drawn for each Reynolds number. The beginning of each straight line represents the end of the thermal entry region, as shown in Figure 2.8.

The thermal entry length was found to be longer for higher Reynolds numbers and decreases as the Reynolds numbers decrease. It is for this reason that the thermal entry region covers the entire length of the channel and that the fully developed region could not be captured for Re= 1353 and 902, as shown in Figure 2.8(a). This phenomenon is in contrast with the results obtained by Dukhan et al. [76], who claimed that the thermal entry length is constant for the

Forchheimer flow regime and independent of the Reynolds number. Leong and Jin [87], who studied oscillating air flow through metal foam heat sink, observed that thermal entry length is longer at higher oscillating flow amplitudes.

Based on the current experimental data, the thermal entry length of the fluid flow through ERG aluminum foam is evaluated as follow:

$$\left[\frac{L_{laminar,thermal}}{D_e}\right]_{Porous\ media} = 0.0004.\mathrm{Re}.\mathrm{Pr} \tag{2.12}$$

Where D_e is the hydraulic dimeter of the channel. In order to complement the experimental results, a numerical model was developed using the finite element technique [77]. Figures 2.9(a, b) and 2.10(a, b) show the experimental and numerical surface temperature results for different heat flux and Reynolds numbers (Re=1353, 541, 390 and 297). It was observed that surface temperatures increase along with increases in the heat flux. The numerical results are in good agreement with the experimental results, with a maximum relative error of 0.43% (see figures 2.9 and 2.10).

2.4.2 Local Nusselt Number Distributions and Thermal Development of Aluminum Foam

In order to calculate the local Nusselt number using Eq. (2.6), the bulk temperature of the water must be measured. It is very difficult to obtain an accurate experimental measurement of the bulk water temperature inside of aluminum foam. It is for this reason that the bulk water temperature is estimated using the formula below and assuming linear variation between the inlet and outlet water temperature measured.

$$T_b = C_1 x + C_2 \tag{2.13}$$

Where C_1 and C_2 are constants provided in Table 2.1. This assumption is very accurate for thermally fully developed region and depends on the fact of a constant surface temperature slope as follows:

$$\frac{dT}{dx} = \frac{dT_b}{dx} = \text{constant} \tag{2.14}$$

Where T and T_b represent the surface and bulk water temperatures, respectively. Although the bulk water temperature obtained in Eq. (2.13) contains a few approximations, especially in the thermal entry region.

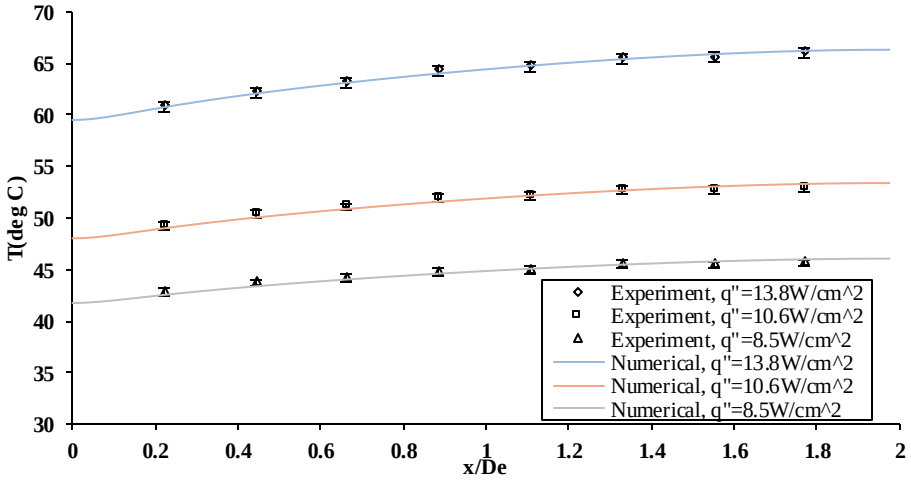

(a) Surface temperature distributions at Re=1353

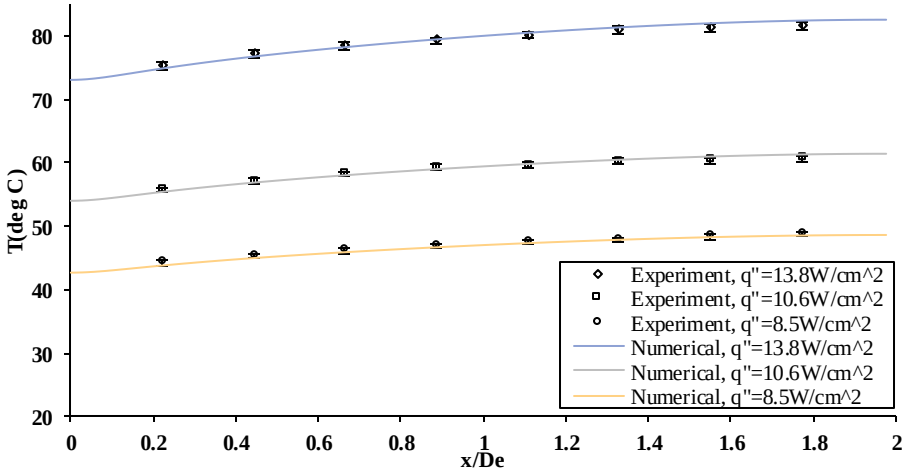

(b) Surface temperature distributions at Re=541

Figure 2.9: Surface temperature distributions at Re= 1353 and 541

It is preferable to use such previous bulk temperature to calculate the local Nusselt number instead of the inlet temperature or average temperature, which are constant and do not capture the thermal development of the aluminum foam. Figure 2.11 shows the calculated local Nusselt number variation with the dimensionless flow direction axis for heat flux q"= 13.8W/cm^2. As we can see, the local Nusselt number is high in the entry region and begins to decrease until a constant value is reached when the flow and temperatures become thermally fully developed.

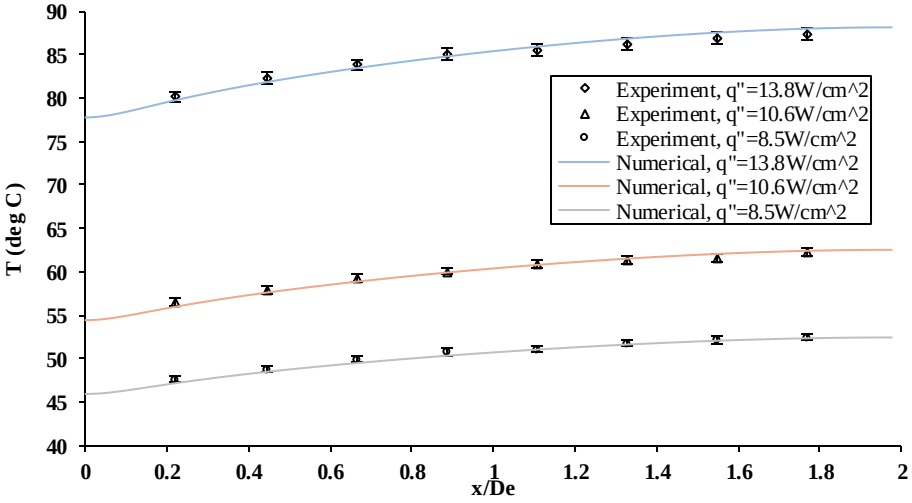

(a) Surface Temperature distributions at Re=390

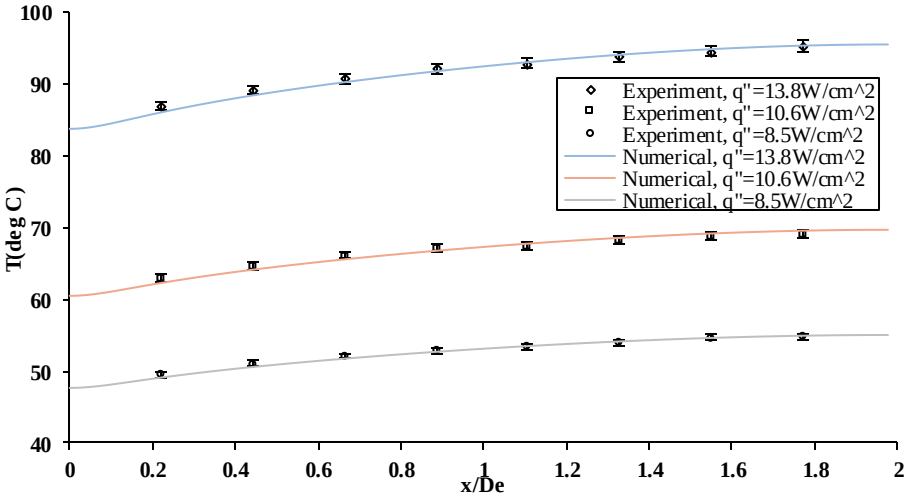

(b) Surface temperature distributions at Re=297

Figure 2.10: Surface temperature distributions at Re=390 and 297

This means that, in the entry regions, the local Nusselt number is inversely proportional to the boundary layer thickness. It is clear from these results that the local Nusselt number is higher in entry regions than in fully developed regions. This implies that the heat transfer rate is higher in the entry regions. This is due to the boundary layer effect of highest temperature gradient. It was also observed that the fully developed local Nusselt number value is significantly enhanced by increases in the Reynolds number. This implies that the local Nusselt number is strongly dependent on the Reynolds number for the non- Darcy flow regime (Forchheimer regime). This finding was also obtained by Dukhan et al. [76].

Table 2.1: Water bulk temperature constant

Re	q"=13.8W/cm^2		q"=10.6W/cm^2		q"=8.5W/cm^2	
	C_1(℃/mm)	C_2(℃)	C_1(℃/mm)	C_2(℃)	C_1(℃/mm)	C_2(℃)
1353	0.03509	26.4	0.0274	26.8	0.0219	26.8
902	0.052635	20.5	0.041121	27	0.0328	27
541	0.087725	20	0.068535	20	0.054828	20
390	0.121465	20	0.094894	20	0.075916	20
297	0.169972	20	0.132791	20	0.106	20

Figures 2.12(a, b) and 2.13(a, b) show the experimental and numerical results of the local Nusselt number distributions for different heat flux and Reynolds numbers (Re=1353, 541, 902 and 297). It was observed that the local Nusselt number increases with decreases in the heat flux for the given Reynolds number. The numerical results are in good agreement with the experimental results, with a maximum relative error of 0.83%.

Figure 2.14 illustrates the velocity contours, temperature contours, and iso-stream lines with temperatures as a colour expression. As we can see in this figure, there are some wakes and eddies in front of the aluminum foam block due to the entrance effect. The flow stabilizes afterward as the aluminum foam creates a high damping effect on the flow. This phenomenon was also observed by Al- Sumaily and Thompson [88]. We can also see a temperature increase on the heater in the flow direction axis and the growth of thermal and hydrodynamic boundary layers.

2.4.3 Heat Transfer Performance of Aluminum Foam as Heat Sink

In order to determine the heat transfer performance of aluminum foam as a heat sink, the average Nusselt number was obtained using the following equation:

$$Nu_{,avg} = \frac{1}{L}\int_0^L Nu_x \cdot dx \qquad (2.15)$$

Where L represents the channel length and Nu_x represents the local Nusselt number. Figure 2.15 shows the relationship between the average Nusselt number and the Reynolds number.

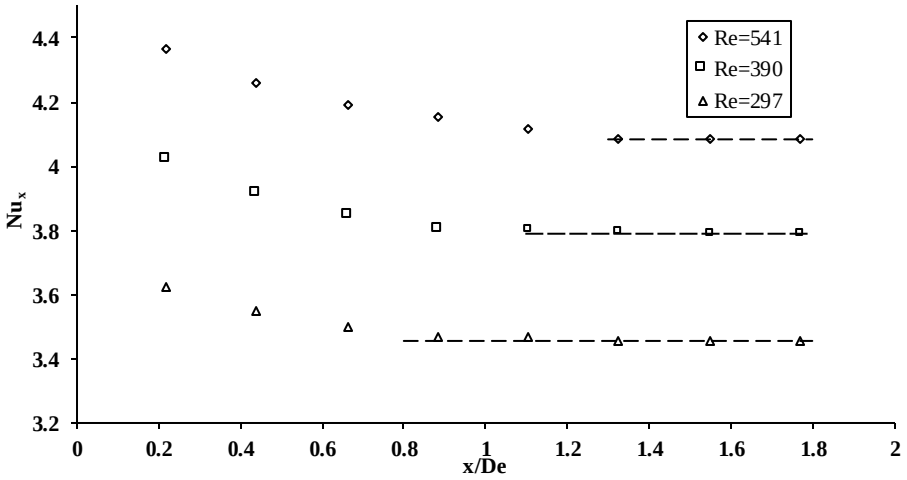

(a) Experimental Nusselt number distributions for entry and developed regions at q"=13.8W/cm^2

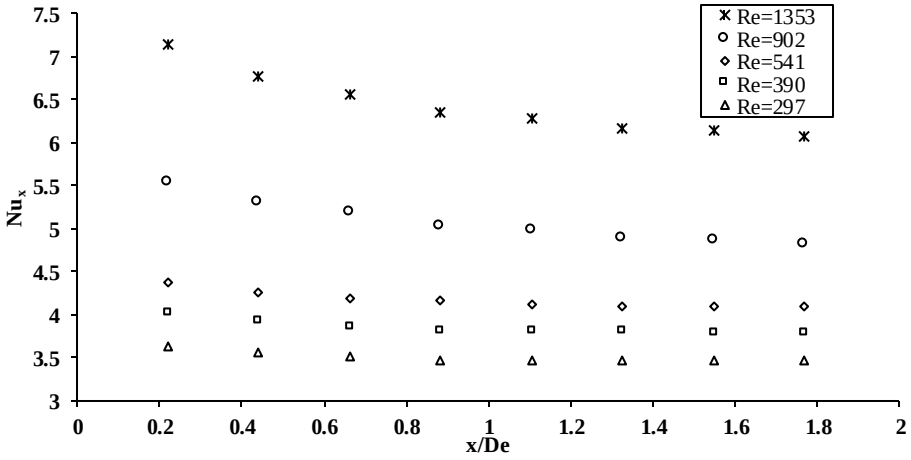

(b) Experimental Nusselt number distribution at q"=13.8W/cm^2

Figure 2.11: Aluminum foam thermal development

One can observe from this figure that the average Nusselt number increases when there are increases in the Reynolds number. The relationship between the average Nusselt number and the Reynolds number was obtained using the following equation:

$$Nu_{,avg} = C \cdot Re^{m} \tag{2.16}$$

Where C=0.41 and m=0.38. It is important also to note that the deviation between this developed empirical equation and the experimental data was 2.5%. As mentioned in section 2.1, only a few studies have used water as a working fluid through aluminum foam. Table 2.2 provides a summary of those studies.

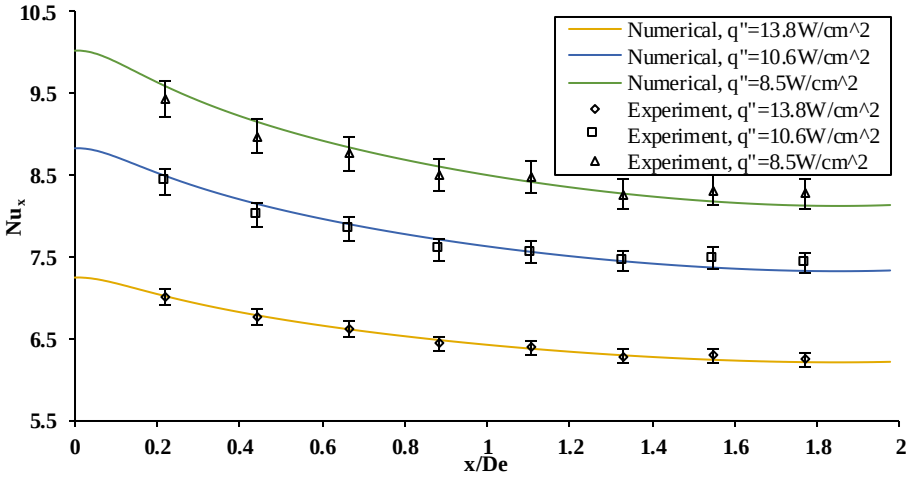

(a) Nusselt number distributions at Re=1353

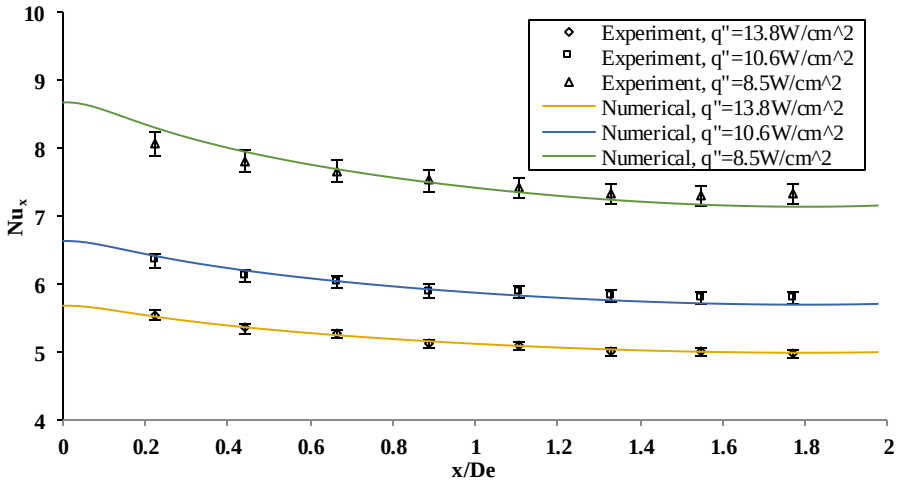

(b) Nusselt number distributions at Re=902

Figure 2.12: Experimental and numerical results of local Nusselt number at Re=1353 and 902

In order to calibrate the empirical correlations of the average Nusselt number for the current study, the average Nusselt numbers of the previous studies (see table 2.2) were compared to those from the present investigation. The results are presented in Figure 2.16. In those experiments [74, 75, and 76], the Nusselt number was calculated based on the fluid thermal conductivity. In order to compare the results of the current study with those from previous experimental studies, the Nusselt number of the previous studies had to be modified to:

$$Nu_{,avg} = Nu_{previous\ work} \cdot \frac{k_f}{k_{eff}} \qquad (2.17)$$

Where k_f and k_{eff} represent the effective thermal conductivities of fluid and foam, respectively.

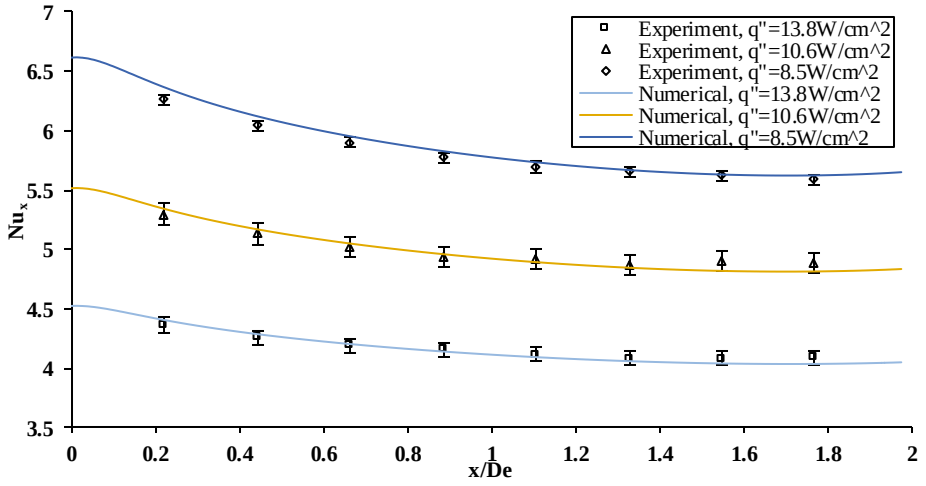

(a) Nusselt number distributions at Re=541

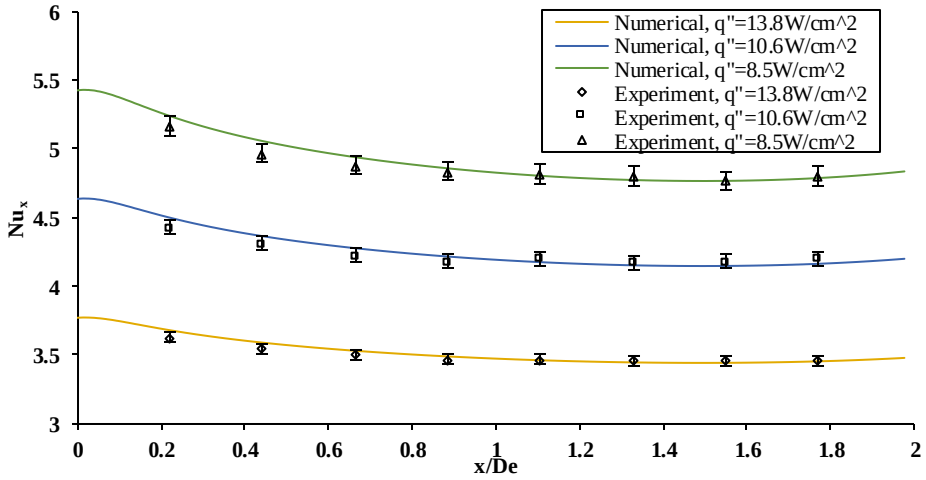

(b) Nusselt number distribution at Re=297

Figure 2.13: Experimental and numerical results of local Nusselt number at Re=541 and 297

The pressure drop across the aluminum foam is presented in figure 2.17 in order to complement the heat transfer performance analysis of the aluminum foam as a heat sink. As we can see, the pressure drop increases as the fluid velocity increases. This trend was also observed by Boomsma et al. [73]. There was good agreement between the numerical and experimental pressure drop results. The Fanning friction factor (f) is commonly used to provide information regarding the required pressure drop of the heat exchanger. This is done to ensure that the pressure drop across the foam is non-dimensional. The friction factor of aluminum foam is obtained using the following equation:

$$f = \frac{\Delta p}{4\left(\frac{L}{De}\right)\cdot\left(\frac{\rho_f U^2}{2}\right)} \tag{2.18}$$

Where L represents the channel length, D_e represents the hydraulic diameter of the channel, ρ_f represents the water density, and U represents the velocity of the fluid. The friction factor of aluminum foam verses Reynolds number is presented in Figure 2.18.

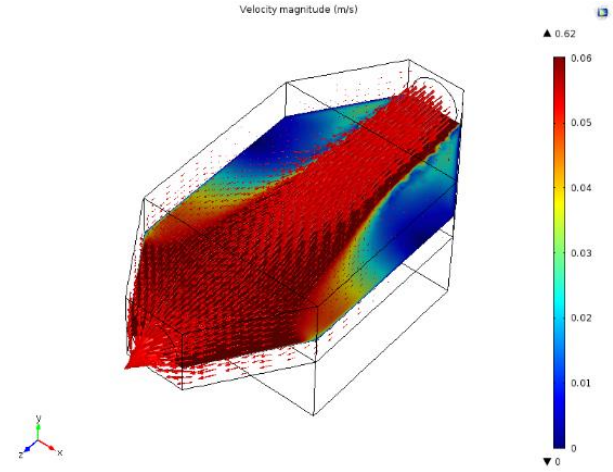

(a) Velocity contours and arrows at q"=13.8W/cm^2, Re=1353

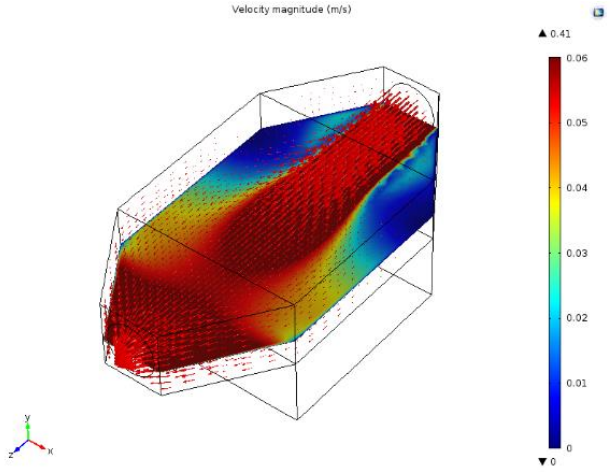

(b) Velocity contours and arrows at q"=13.8W/cm^2, Re=902

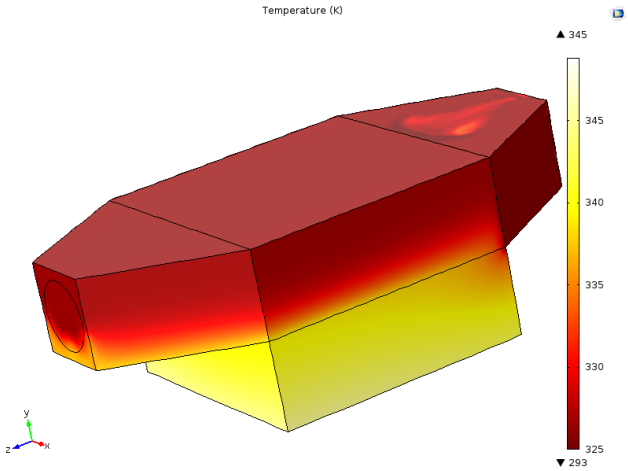

(c) Temperature contours at q"=13.8W/cm2, Re=1353

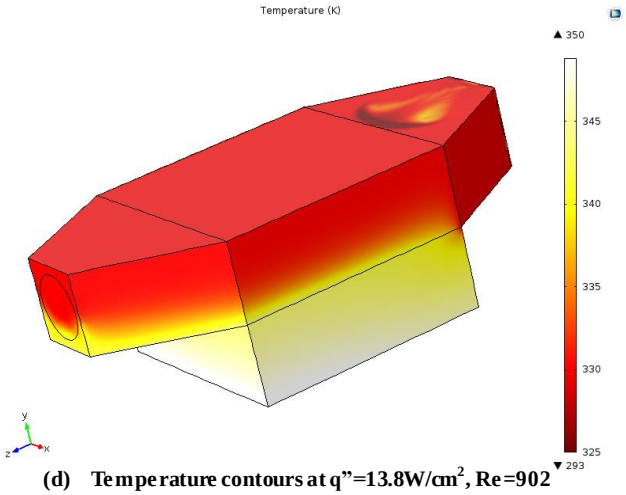

(d) Temperature contours at q"=13.8W/cm^2, Re=902

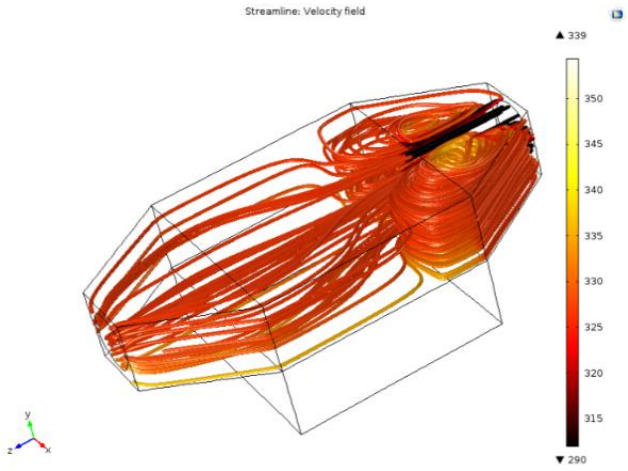

(e) Iso- stream lines at q"=13.8W/cm^2, Re=1353

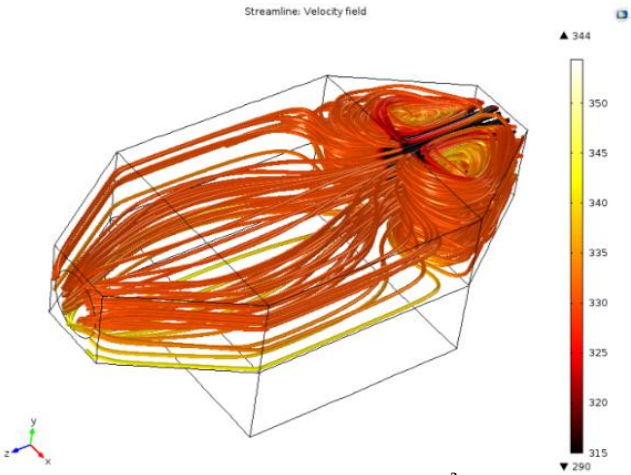

(f) Iso- stream lines at q"=13.8W/cm^2, Re=902

Figure 2.14: Velocity contours, temperature contours, and iso-stream lines

As we can see, the heat transfer rate of the aluminum foam heat sink increases along with increases in the Reynolds number. This increase is accompanied by an increase in the required pumping power which results from an increase in the pressure drop across the aluminum foam. In order to combine the heat transfer rate with the pressure drop, the thermal efficiency index is defined as:

$$I_{efficiency}=\frac{Nu_{,avg}\cdot L}{f\cdot H} \tag{2.19}$$

Where f represents the Fanning friction factor of the aluminum foam, L represents the channel length, H represents the channel height, and $Nu_{,avg}$ represents the average Nusselt number.

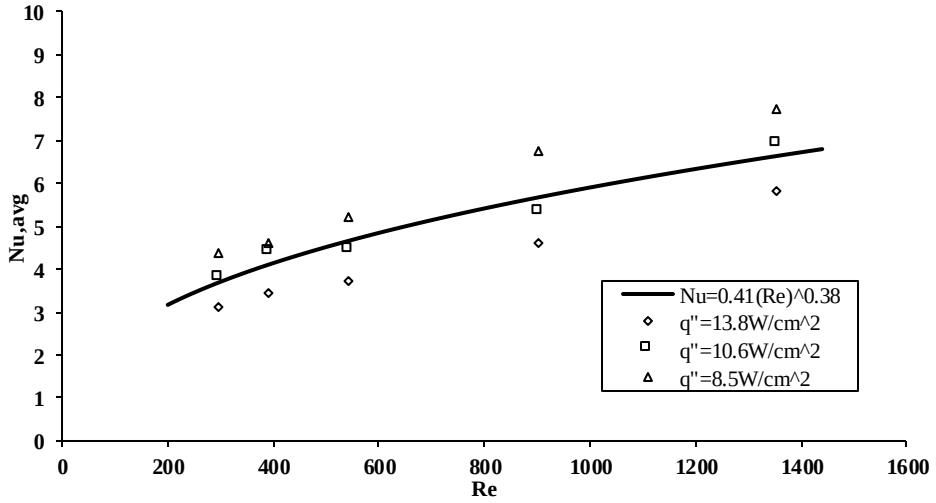

Figure 2.15: Average Nusselt number verses Reynolds number

The thermal efficiency index combines the heat transfer with the pressure drop across the aluminum foam in order to evaluate the performance of the present heat sink with respect to how much it transfers heat and required pumping power. The thermal efficiency index verses Reynolds number is presented in Figure 2.19. As one can notice, the aluminum foam heat sink subjected to steady water flow achieves a thermal efficiency index of 2.5 at Re =1353.

Table 2.1: Summary of studies in forced convection through metal foam using water

Investigator	Porous material	PPI	Geometry
Duckan et al. [76]	Al foam	20	Cylindrical aluminum foam
Boomsma et al. [73]	Al foam	40	Rectangular channel
Noh et al. [74]	Al foam	10	Annulus filled with foam
Hetsroni et al. [75]	Al foam	40	Rectangular channel

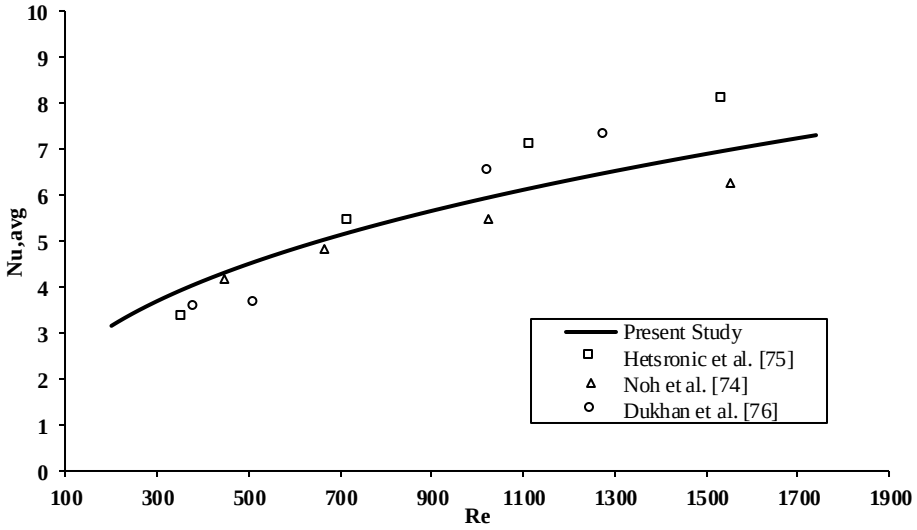

Figure 2.16: Comparison between the present empirical equation of average Nusselt number and previous experimental data

Few studies have used water as a coolant through metal foam as a porous medium; therefore, there are limited comparisons between the heat transfer characteristics of air and water through the aluminum foam.

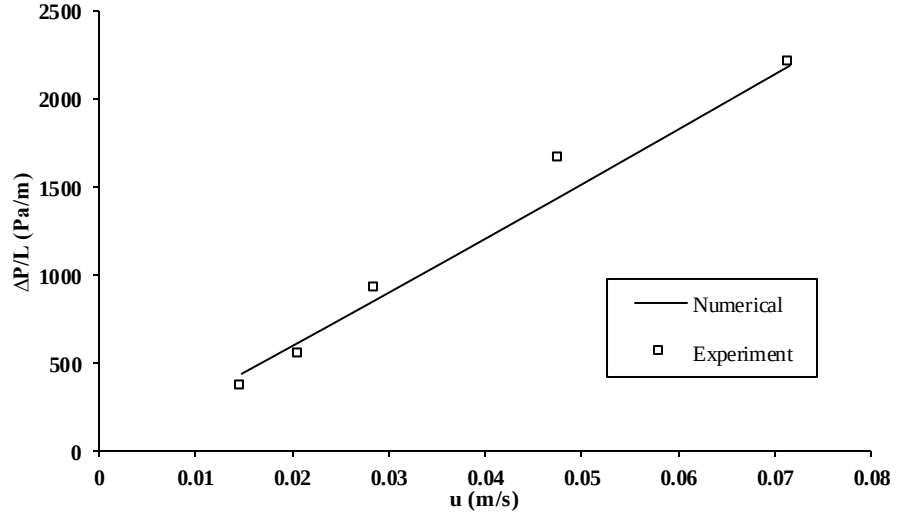

Figure 2.17: Pressure drop verses water inlet velocity

Figure 2.20 illustrates the temperature distributions verses the dimensionless flow direction axis from the current study as well as previous research conducted by Fu et al. [69] who used air as a coolant through the aluminum foam heat sink. The results indicate that, in comparison with air, the use of water as a coolant leads to lower average surface temperatures.

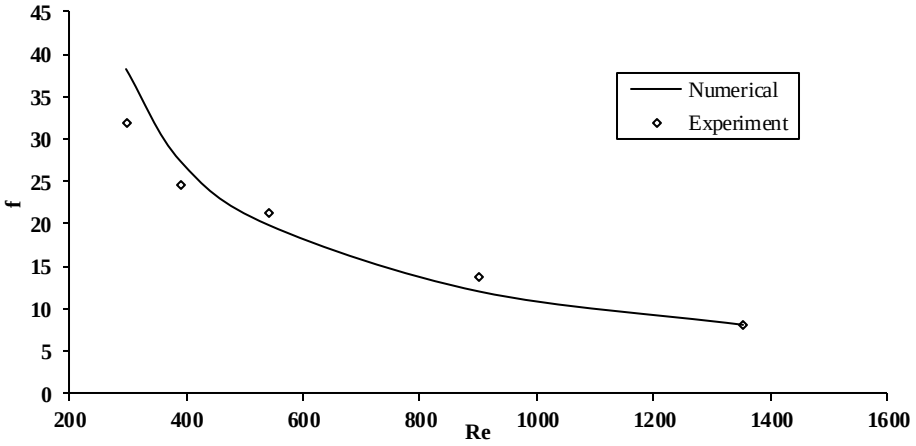

Figure 2.18: Fanning friction factor of aluminum foam verses Reynolds number

That being said, local surface temperature is more important than average surface temperature from an electronic cooling point of view. This means that the temperature uniformity of electronic surfaces is an important parameter which controls the overall efficiency of electronic devices. In order to quantify the temperature uniformity, a uniformity index is calculated as follows:

$$\eta = \frac{T_{max} - T_{min}}{T_{max}} \tag{2.20}$$

Where T_{max} and T_{min} represent the maximum and minimum surface temperature in Kelvin units. The uniformity index represents the temperature lift on the surface, where the temperature lift is defined as the difference between maximum and minimum surface temperature.

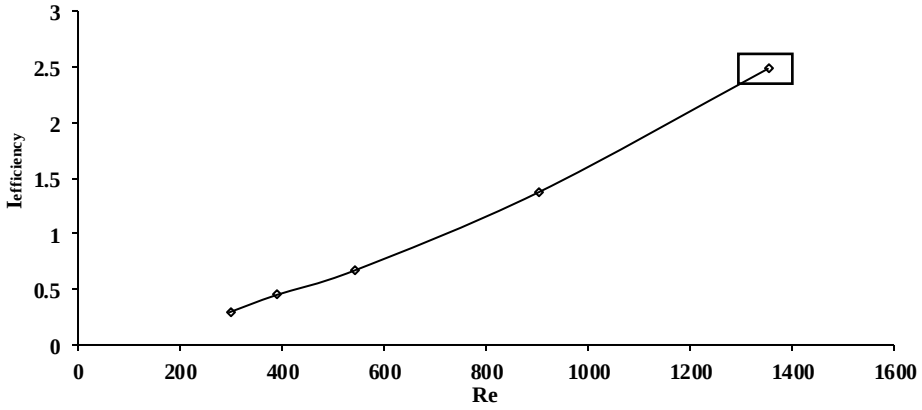

Figure 2.19: Thermal efficiency index ($I_{efficiency}$) verses Reynolds number

It is important to note that when the surface temperature profile is perfectly uniform, the uniformity index approaches zero. Figure 2.21 provides a comparison of the uniformity index of water and air as coolants. As we can see, the uniformity index is 68% lower when using water instead of air as a coolant.

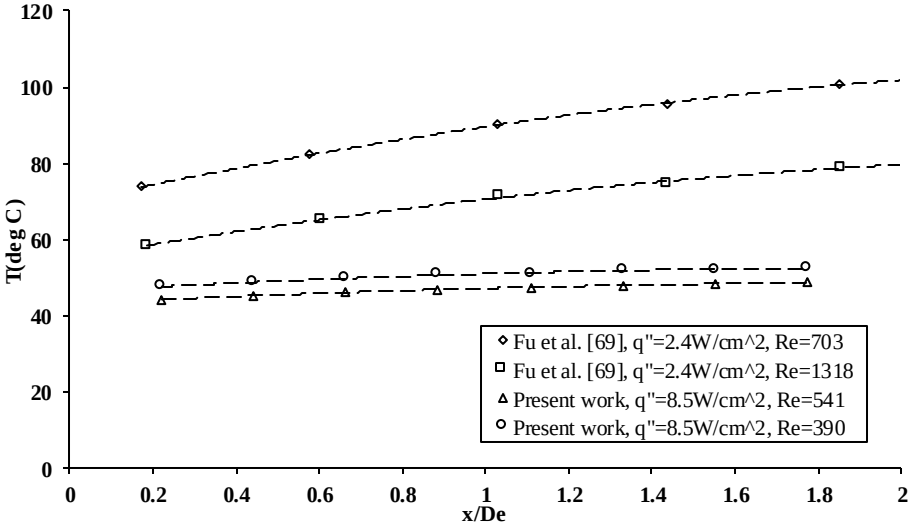

Figure 2.20: Surface temperature distributions of air [69] and water as a coolants through aluminum foam heat sink

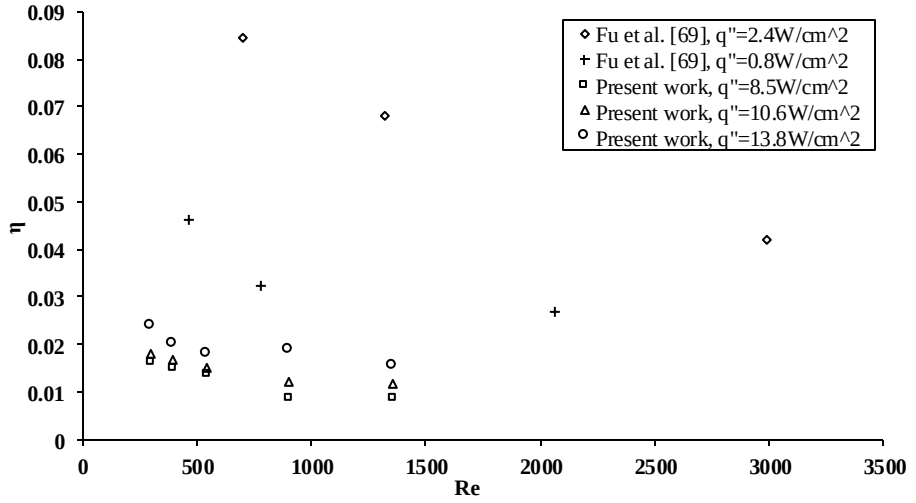

Figure 2.21: Temperature uniformity index of using water and air as a coolant

This finding is of great importance in electronic cooling since the reliability of transistors and operating speed depend on temperature uniformity along the surface. High temperature in one region spot can affect the performance level of the electronic component due to prolonged gate delay.

2.5 Conclusions

This chapter presented an experimental and numerical study of the heat development and heat transfer characteristics of aluminum foam as a heat sink. The aluminum foam was subjected to a water flow covering the non-Darcy flow regime (ranging from 297 to 1353 Reynolds numbers). The following conclusions were drawn based on the findings of the study:

- The thermal entry length of the fully developed region is determined by looking at the temperature distributions for each Reynolds number. The thermal entry length is found to be longer for higher Reynolds numbers and decreases as the Reynolds numbers decrease.
- The temperature distributions for steady flow increase along with increases in the dimensionless flow direction axis, decreasing the Reynolds number and increasing the heat flux.
- The numerical results of local surface temperature were in good agreement with the experimental results, with a maximum relative error of 0.43%
- At any given Reynolds number, the local Nusselt number is inversely proportional to the boundary layer thickness and reaches a constant value at the fully developed region.
- The local Nusselt number in the fully developed region is highly dependent on the Reynolds number.
- The local Nusselt number increases with decreases in the heat flux for the given Reynolds number.
- The numerical results of the local Nusselt number were in good agreement with the experimental results, with a maximum relative error of 0.83%.
- The heat transfer performance of the aluminum foam heat sink is obtained by evaluating the average Nusselt number. The results indicate that the average Nusselt number is strongly affected by increases in the Reynolds number.
- Based on the results of the present experiment and the given range of Reynolds numbers, the relationship between the average Nusselt number and the Reynolds number is $Nu_{,avg} = CRe^{m}$ (where C=0.41 and m=0.38).
- In order to calibrate the empirical correlations of the average Nusselt number for the current study, the average Nusselt numbers of the previous studies were compared with those from the present study.

- In order to find the optimal design condition of aluminum heat sinks, the pressure drop across the foam was measured. The results revealed that the pressure drop increases as the Reynolds number increases.
- The thermal efficiency index combines the heat transfer with the pressure drop across the aluminum foam in order to find the optimal design condition that achieve higher heat transfer with lower pumping power. The optimal design condition was found to be at Re=1353 (highest heat transfer and lowest pumping power).
- Lastly, the results indicate that, in comparison with air, the use of water as a coolant through aluminum foam leads to lower average surface temperatures and more uniform temperature profiles. The uniformity index was 68% lower when water is used instead of air as a coolant.

CHAPTER 3-HEAT TRANSFER CHARACTERISTICS OF A PULSATING/STEADY WATER FLOW THROUGH ALUMINUM FOAM HEAT SINK

This chapter is based on the following published paper:

Bayomy, A. M., Saghir, M. Z., "Heat Transfer Characteristics of Aluminum Metal Foam Subjected to a Pulsating/Steady Water Flow: Experimental and Numerical Approach" Int. J. Heat Mass Transfer, vol. 97, pp. 318-336, 2016.

3.1 Introduction

Electronic devices are part of our everyday lives. The overall efficiency of electronics is controlled primarily by the efficiency of particular electronic components. The recent acceleration in the design of modern high speed computers has led to a demand for new and more effective methods of electronic cooling.

In order to enhance the heat transfer rate of modern high speed electronic devices, researchers have conducted extensive investigations using different shapes and arrangements (single or multiple square, rectangular and circular modules (rods)) mounted on the heated surface in order to attempt to increase the surface to volume ratio of heat sinks. Buller and Kilburn [5] investigated the convective heat transfer using a single rectangular module (rectangular rod). Sparrow et al. [6, 7] used different arrangements of square modules and studied the effect of missing modules. They found that the heat transfer coefficient increased by 40% when the missing module located upstream. Sparrow et al. [8] then investigated the heat transfer characteristic using different module heights. Jubran et al. [9] conducted an experimental investigation of the effect of module size and the presence of cylindrical modules or missing modules on heat transfer and pressure drop across the array.

Igarashi et al. [10] used circle modules mounted on the walls of parallel channels. They found that the separation of the flow caused a 10% reduction in the Nusselt number in the first row compared to the second to fifth rows. Iwasaki and Ishizuka [11] calculated the optimum value of fin spacing or the fin thickness of plate fins for a notebook personal computer heat sink and developed an empirical equation for the average Nusselt number. As one can see, many studies have been conducted using various types of heat sinks for electronic cooling, either extending the

surface area or increasing the fluid flow. Despite this research, there still exists a demand for more effective electronic cooling methods.

The use of metal foam as a heat sink is a new technique used to enhance the heat transfer rate of the surface of electronics. Many studies have investigated the effect of microstructure properties such as porosity, relative density, pore density, pore size, ligament diameter, and permeability on the heat transfer characteristics of metal foams as was mentioned in section 2.1 [52-56]. Boomsma and Poulikakos [59] studied the effective thermal conductivity of ERG aluminum foams. Klett et al. [61] compared the heat transfer characteristics of the foam radiator with the fin radiator. They found that foam radiators transfer heat better than fin radiators. Kim et al. [66] compared the aluminum metal foam heat sink with the conventional parallel plate heat sink. They observed an increase in the heat transfer when using the aluminum metal foam heat sink.

There are various studies have been conducted in using different types of metal foams [62-65, 69]. They found that the use of metal foam as a heat sink greatly increases the heat transfer coefficient. In addition, Boomsma et al. [73] observed that the thermal resistance of the compressed foam heat exchanger is two to three times lower than that of other heat exchangers using water flow through metal foam. Noh et al. [74] conducted an experimental study of non-Darcy water flow in an annulus filled with high porosity aluminum foam and presented the correlations for the average Nusselt number and friction factor. Hetsroni et al. [75] conducted an experimental study of the transmission window cooling technique of an accelerator using aluminum foam.

The local temperature over the surface is more important than the average temperature for electronic cooling applications. Fu et al. [69] observed a 60°C surface temperature difference when steady air flow is used through ERG aluminum foam. This indicates that a steady flow through metal foam yields a high local surface temperature. For modern high speed computers, the operating speed and reliability of transistors depend not only on average surface temperatures, but also on temperature uniformity over the surface. Localized high temperature spots can affect the performance of electronics due to prolonged gate delay.

It is conceivable that the pulsating flow will produce a more uniform surface temperature than the steady flow due to the reversing flow (there are two entry regions). Leong and Jin [87, 89] and Fu et al. [69] conducted an experimental investigation of the heat transfer characteristics of

aluminum metal foam subjected to pulsating air flow. The researchers measured the surface temperature distributions, pressure drop across the metal foam, and flow velocity inside of the foam. They also analyzed the effects of the dimensionless amplitude and frequency. They observed a higher average Nusselt number for pulsating flow when compared to the steady flow. The results also revealed that the heat transfer enhancement of the pulsating flow increases as the dimensionless amplitude and dimensionless frequency increase.

Paek et al. [90] conducted an experimental study of pulsating flow through packed spherical beads. They observed a small effect of pulsating flow on heat transfer enhancement at small amplitudes. The results also revealed that frequency has a positive effect on the heat transfer between the fluid and the beads. Cooper et al. [91] conducted an experimental study to analyze the heat transfer characteristics of heated rectangular ducts. They observed increases in the heat transfer enhancement with increases in the pulsating frequencies, increasing tidal displacement (amplitude of pulsating flow). Sumaily and Thompson [88] conducted a numerical study of a heated circular cylinder placed either in an empty or porous medium filled channel subjected to both steady and oscillating flows. The results revealed that the pulsating flow enhances the heat transfer rate. As observed, the literature on the heat transfer characteristics of metal foams subjected to pulsating flows is very scarce and incomplete, especially when water is used as a coolant (for electronic cooling purposes). In addition, most of exiting studies of air pulsating flow through metal foam are depending on creating the pulsating flow by piston and cylinder arrangement driven by DC electrical motor, which mix the effect of pulsating flow amplitude and frequency. In that case, increases in the frequency of the motor (rpm) causes increasing in both pulsating flow amplitude and frequency. That is why the exiting studies of air pulsating flow through the porous media failed to evaluate the true effect of pulsating flow amplitude and frequency separately.

This chapter presents an experimental and numerical study of pulsating water flow through an ERG aluminum metal foam as a heat sink in the cooling of electronic surfaces. The aluminum foam was subjected to a pulsating water flow. The investigation was performed using a pulsating flow frequency range between 0.04 and 0.1 Hz, a pulsating flow amplitude range between 297 and 1353 (non-Darcy flow regime), and a heat flux range between 8.5 and 13.8W/cm^2[2, 3, and 53]. The cycle average local temperature distributions along the heater surface (electronic surface) were measured and the local Nusselt number distributions along the surface were calculated. The effects

of the amplitude and frequency of the pulsating flow on the heat transfer characteristics were also analyzed and an empirical correlation of the average Nusselt number of the pulsating flow was developed as a function of dimensionless pulsating flow frequency and amplitude. A comparison between the pulsating and steady flow through the aluminum foam was conducted. The thermal performance of the aluminum foam heat sink was evaluated based on the average Nusselt number and pumping power required. Lastly, the experimental approach was complimented with a numerical approach [77] as mentioned previously and a comparison of the results from the two approaches was conducted.

3.2 Experimental Apparatus and Procedures

An experimental setup was developed to examine the heat transfer characteristics of a pulsating water flow through an aluminum foam as a heat sink.

3.2.1 Test Section and Experimental Facility

The experimental setup consisted of a pump with a control valve, a tank, flow meter and pressure transducer (see Figure 3.1). In order to create the pulsating water flow, a system of solenoid valves was added to the water flow loop (see Figure 3.1). When valve #1and valve #2 are opened, the water flows in one direction for half of the complete cycle time. Valve #1 and valve #2 are then closed and valve #3 and valve #4 are opened. At this time, the water begins to flow in the opposite direction for the second half of the complete cycle time. The solenoid valves were controlled by the data acquisition system (digital output module) to obtain the pulsating flow frequency range.

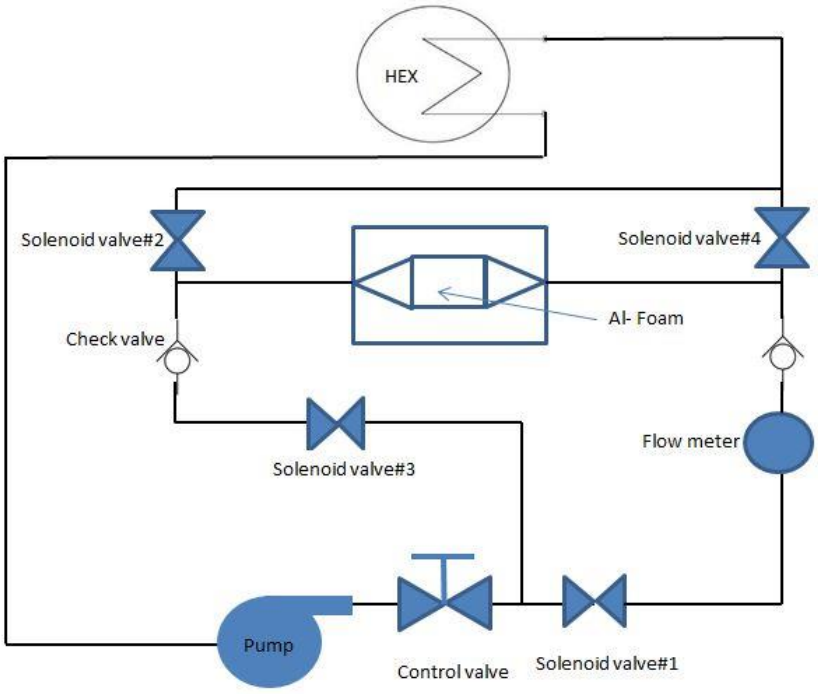

Figure 3.1: Experimental schematic diagram [92]

The test section facility was previously mentioned in section 2.2.1. The data acquisition system consists of three main modules: digital output modules to control the solenoid valves, analog input modules to monitor the flow meter reading and pressure differential across the foam, and thermocouple modules to monitor the surface temperature. The ERG aluminum metal foam heat sink was cut to match the size of the heater (37.5mm×37.5mm×12.7mm).

The physical and geometric properties of the ERG aluminum foam (alloy 6101-T6) were mentioned in section 2.2.1. It is important to note that these properties are not all independent of one another.

3.2.2 Data Reduction and Uncertainty Analysis

From the electronics point of view, time averaged heat transfer characteristics are more important and practical than instantaneous quantities due to the instantaneous high temperature spot may not damage the electronic component. In the present study, the experimental data of the pulsating flow were reduced by time averaged over 50 complete cycles. This type of time averaging is called a cycle average. In addition, the surface temperatures, flow rate and pressure drop were monitored in order to achieve the cyclic steady state condition.

Temperatures, flow amplitudes, and pressure drop were directly measured. The uncertainties of the temperature, flow amplitudes and pressure drop were mentioned in section 2.2.2. The propagation of error was obtained using Taylor method [81] as follow:

$$Nu_x = \sqrt{\left(\frac{\partial Nu_x}{\partial x}.\delta x\right)^2 + \cdots + \left(\frac{\partial Nu_x}{\partial y}.\delta y\right)^2 + \cdots \left(\frac{\partial Nu_x}{\partial z}.\delta z\right)^2} \quad (3.1)$$

The local Nusselt number and the pulsating flow amplitude are calculated as follows:

$$h_x = \frac{q^{"}}{(T_x - T_{i)}} \quad (3.2)$$

$$Nu_x = \frac{h_x D_e}{k_{eff}} \quad (3.3)$$

$$A_o = \frac{U.D_e}{\upsilon_f} \quad (3.4)$$

Where h_x represents the local heat transfer coefficient over the heater surface, T_x represents the local surface temperature, T_{in} represents the water inlet temperature, D_e represents the hydraulic diameter of the channel, U represents the pulsating water velocity throughout the test section, υ_f represents the kinematic viscosity of the fluid, and k_{eff} represents the effective thermal conductivity of the metal foam filled with water. The maximum value of the uncertainty of the local Nusselt number was 2.6% and the uncertainty of the pulsating flow amplitude was 0.44%.

3.3 Numerical Model Description

Numerical model was created and compared with the experimental data of pulsating water flow through porous media using finite element method [77].

3.3.1 Governing Equations

When finite element modeling assumptions are taken into consideration (section 2.3.1), the Brinkman-Forchheimer equation and energy equation which describe the fluid flow and heat transfer inside porous media are solved using the following formula [77]:

$$\frac{\rho_f}{\varepsilon}\left(\frac{\partial U}{\partial t} + (U.\nabla)\frac{U}{\varepsilon}\right) = \nabla.(-pI + \frac{\mu_f}{\varepsilon}(\nabla U + (\nabla U)^T)) - (\frac{\mu_f}{K} + \beta_f|U|)U + F \quad (3.5)$$

$$\nabla.(\rho_f U) = 0 \quad (3.6)$$

$$(\rho c_p)_{eff}.\frac{\partial T}{\partial t} + (\rho c_p)_f\, U.\nabla T = \nabla.(k_{eff}.\nabla T) \tag{3.7}$$

Where ρ_f represents the water density, c_p represents the fluid specific heat, ε represents the porosity of the aluminum metal foam, p represents the pressure, U represents the velocity field vector, β_f represents the Forchheimer coefficient, T represents the temperature, μ_f represents the dynamic viscosity of the fluid, K_b represents the permeability of the aluminum foam, k_{eff} represents the effective thermal conductivity of the aluminum metal foam filled with water, and F represents the body force. An accurate representation of the structural parameters of the metal foam is important for the estimation of the effective thermal conductivity. Calmidi and Mahajan [83] determined the effective thermal conductivity of ERG aluminum foam based on one dimensional heat conduction through two dimensional foam structures. Boomsma and Pouliakos [59] extended the previous research by investigating a three dimensional analytical model of effective thermal conductivity of ERG foams as follows:

$$k_{eff} = \frac{\sqrt{2}}{2(R_A+R_B+R_C+R_D)} \tag{3.8}$$

$$R_A = \frac{4d}{(2e^2+\pi d(1-e))k_s+(4-2e^2-\pi d(1-e))k_f} \tag{3.9}$$

$$R_B = \frac{(e-2d)^2}{(e-2d)e^2 k_s+(2e-4d-(e-2d)e^2)k_f} \tag{3.10}$$

$$R_C = \frac{(\sqrt{2}-2e)^2}{2\pi d^2(1-2e\sqrt{2})k_s+2(\sqrt{2}-2e-\pi d^2(1-2e\sqrt{2}))k_f} \tag{3.11}$$

$$R_D = \frac{2e}{e^2 k_s+(4-e^2)k_f} \tag{3.12}$$

Where $d=\sqrt{\frac{\sqrt{2}(2-\left(\frac{5}{8}\right)e^3\sqrt{2}-2\varepsilon)}{\pi(3-4e\sqrt{2}-e)}}$,$e=\frac{r}{L}$, r represents the length of the cubic node of the foam, and L represents the length between two nodes. Eq. (3.8) was used to evaluate the effective thermal conductivity of the ERG aluminum foam (alloy 6101-T6) used in the present study.

3.3.2 Boundary Conditions

As illustrated in Figure 3.2, the boundary conditions of the numerical model consist of the heat flux (q") from the bottom portion, the adiabatic surface at the top portion of the model ($\nabla.T =$

0), the inlet water temperature at the left side portion and the open boundary at the right side portion ($-p + \frac{\mu}{\varepsilon}(\nabla U + (\nabla U)^T = 0$). In order to create the pulsating flow at different frequencies through the aluminum foam, the square sine form of inlet velocity (flat profile) is applied to the left side portion. Figure 3.3(a, b) shows the typical variation of inlet water velocity and pulsating flow amplitude at a frequency of 0.1Hz.

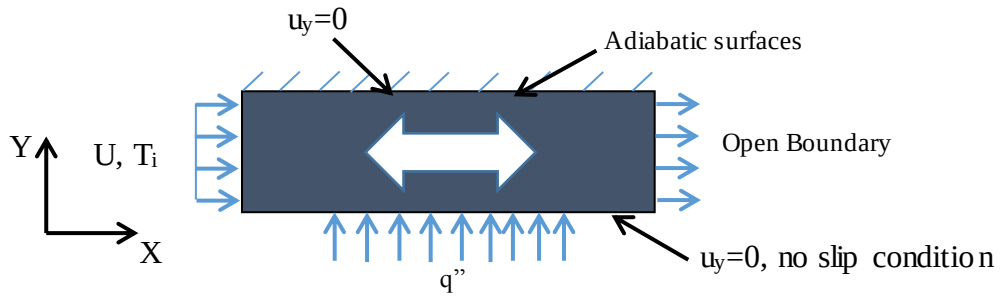

Figure 3.2: Boundary conditions [92]

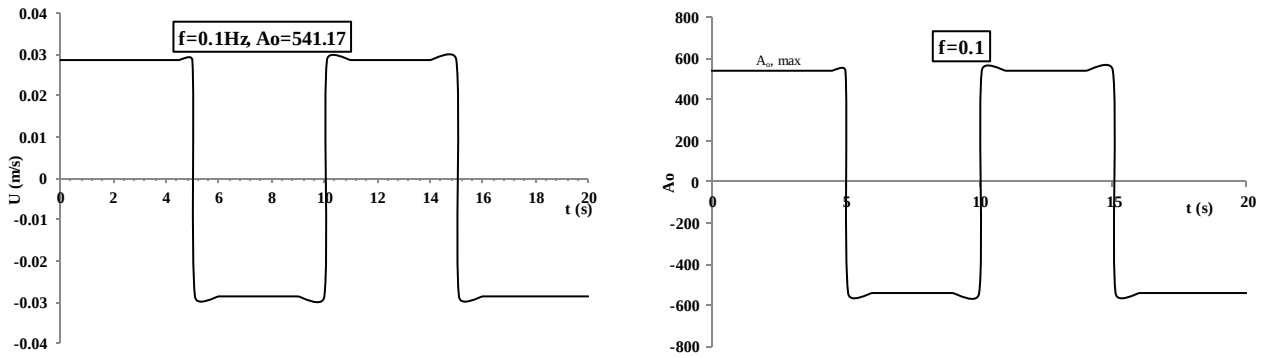

(a) Velocity variation at f= 0.1Hz

(b) Pulsating flow amplitude variation at f= 0.1Hz

Figure 3.3: Characteristics of pulsating flow through aluminum foam[92]

3.3.3 Mesh Sensitivity Analysis

A mesh independence analysis was conducted in order to find the optimum number of domain elements. The maximum temperature and local Nusselt number were evaluated at different numbers of triangular domain elements. The solution reached grid independence for 19403 elements (see Figure 3.4(a)). The number of elements used was 19403 and the variation was less than 0.001. Figure 3.4(b) shows the shape and size of the grid used in the present study. At every

time step, the finite element technique evaluated the errors in all independent parameters such as U, P, and T as follows:

$$R = \frac{1}{n \,.\, m} \sum_{i=1}^{i=m} \sum_{j=1}^{j=n} \left| \frac{(F_{i,j}^{s+1} - F_{i,j}^{s})}{F_{i,j}^{s+1}} \right| \tag{3.13}$$

Where F represents one of the independent parameters, s represents the number of iterations, and (i, j) represent the x and y coordinates. The solution reached convergence when R was below 1e-6 for each independent parameter, as mentioned in Ref. [93].

3.4 Results and Discussion

The present chapter examined the heat transfer characteristics and thermal performance of aluminum foam. The aluminum foam was subjected to a pulsating water flow. The amplitude of the pulsating water flow covered the Forchheimer flow regime (non-Darcy regime). In addition, a numerical model was developed using the finite element technique [77] and compared to the experimental data.

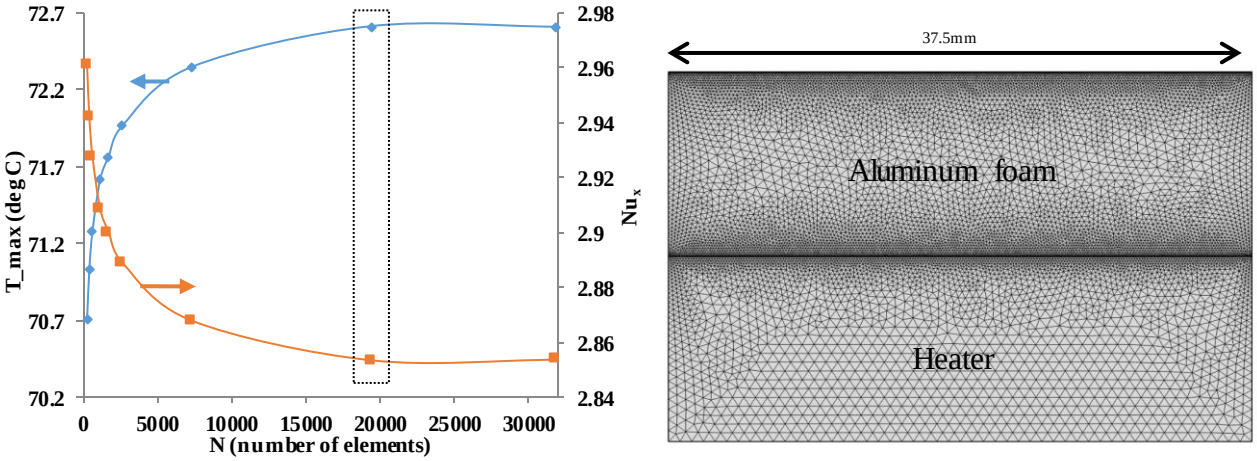

(a) Mesh independent (b) Finite element model

Figure 3.4: Mesh sensitivity and finite element model [92]

3.4.1 Heat Transfer Characteristics of Pulsating Flow Through Aluminum Foam

Figure 3.5(a) illustrates the cycle average dimensionless surface temperature distributions $\left[T^* = \frac{T - T_i}{q''^* \frac{D_e}{K_{eff}}}\right]$ at pulsating flow amplitude (A_o=1353) and heat flux of 13.8 W/cm^2, 10.6 W/cm^2 and 8.5 W/cm^2, respectively. Due to the two flow directions (or reversing flow), there are two entry regions (thermal and hydrodynamic) where the thermal and hydrodynamic layer effects take

place. Inside the boundary layer, there is high velocity and temperature gradient due to the viscous effect. This means that the heat transfer rate is higher in the entry region than in the fully developed region.

As we can see from Figure 3.5(a), the cycle average local temperature is lower at both entrances of the channel than at the center due to the development of the boundary layer. The maximum temperature occurs at the center (approximately) of the test section. The temperature distribution curves show a convex profile with the center as the symmetric point. The results also revealed that the cycle average temperature distribution increases along with increases in the heat flux. The same trend of cycle average dimensionless surface temperature distributions was observed for A_o = 902, 390 and 297, as seen in Figures 3.5(b) and 3.6(a, b). The numerical results of the local temperature distribution were in good agreement with the experimental data, within a maximum relative error of 0.75% (see Figures 3.5 and 3.6).

Figure 3.7(a) illustrates the cycle average local Nusselt number over the surface at pulsating flow amplitude (A_o) of 1353 and a heat flux of 13.8 W/cm^2, 10.6 W/cm^2, and 8.5 W/cm^2, respectively. The results revealed that the local Nusselt number is higher at both channel entrances and begins to decrease until it reaches a minimum point at the center of the test section. The cycle average local Nusselt number distribution shows a concave curve with the center as symmetric point.

The results also revealed that the curvature of the local Nusselt number decreases as the heat flux increases. The same trend of cycle average Nusselt number distributions was observed for A_o = 902, 390 and 297, as seen in Figures 3.7(b) and 3.8(a, b). The numerical results of the local Nusselt number were in good agreement with the experimental data, with a maximum relative error of 1.8% (see Figures 3.7 and 3.8).

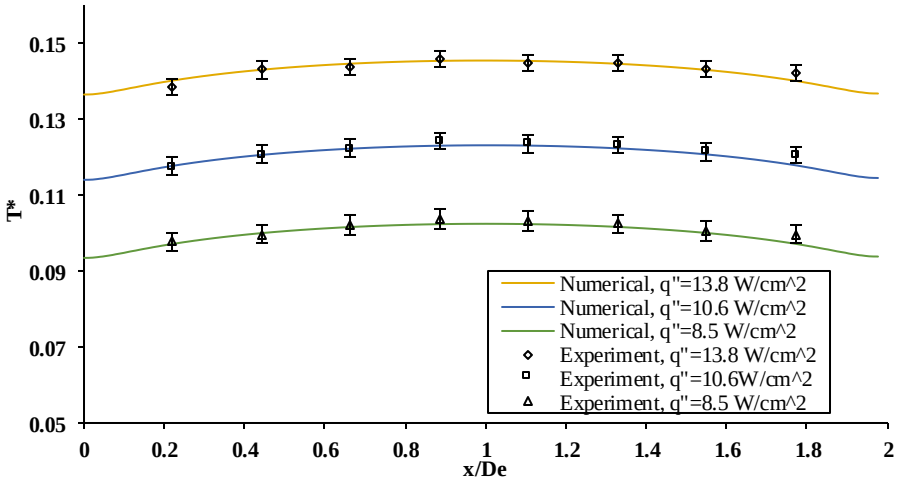

(a) Cycle average local temperature distributions at A_o=1353

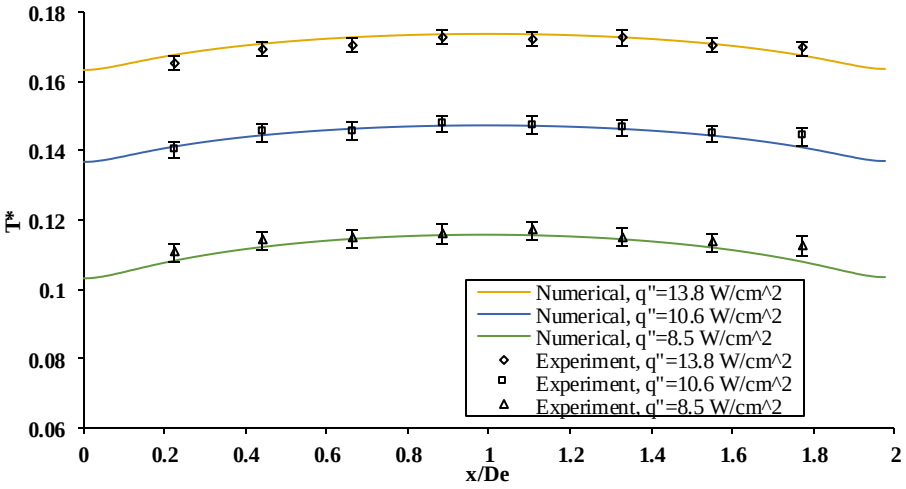

(b) Cycle average local temperature distributions at A_o=902

Figure 3.5: Cycle average local temperature distributions at f=0.1Hz

Figure 3.9(a, b) illustrates the cycle average local Nusselt number distributions versus pulsating flow amplitudes at a heat flux of 13.8 W/cm^2 and 8.5 W/cm^2, respectively. The results revealed that the local Nusselt number increases as the pulsating flow amplitude increases. A closer look at the local Nusselt number distributions revealed that the variation of the local Nusselt number along the flow direction axis is much greater for larger amplitudes than that for small amplitudes.

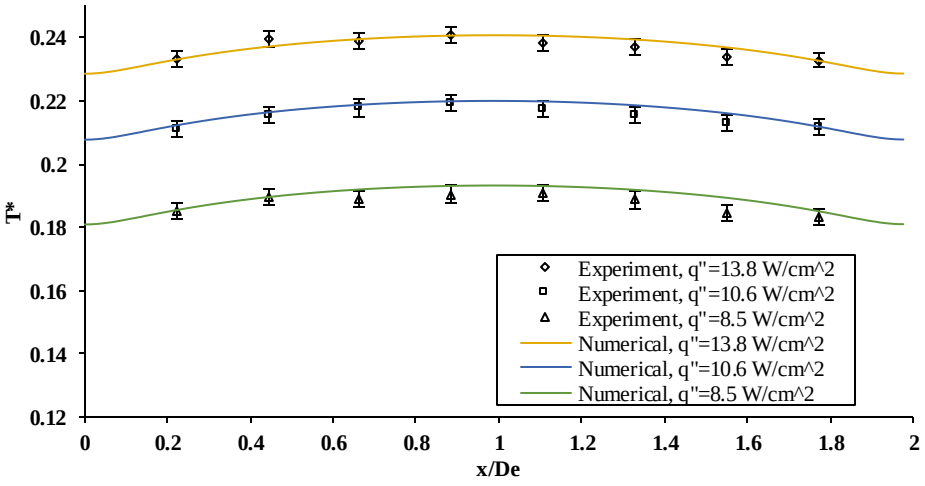

(a) Cycle average local temperature distributions at A_o=390

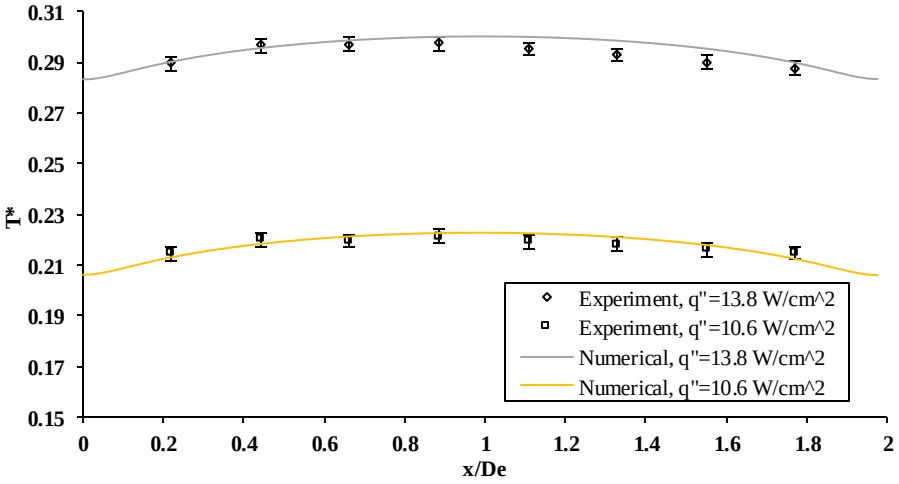

(b) Cycle average local temperature distributions at A_o=297

Figure 3.6: Cycle average local temperature distributions at f=0.1Hz

This means that the curvature of the local Nusselt number distribution is greater at high amplitudes than at lower amplitudes and implies that the thermal entry length of water flow through aluminum foam is shorter for smaller amplitudes than for large amplitudes. The same trend was observed by Leong and Jin [89].

Figure 3.10 illustrates the velocity and temperature contours over one complete cycle of pulsating flow. The results revealed that the velocity and temperature both changed from the positive direction in the first half cycle to the negative direction in the second half cycle according to the velocity profile boundary condition of the pulsating flow. The contours also reveal the growth of the thermal and hydrodynamic boundary layers.

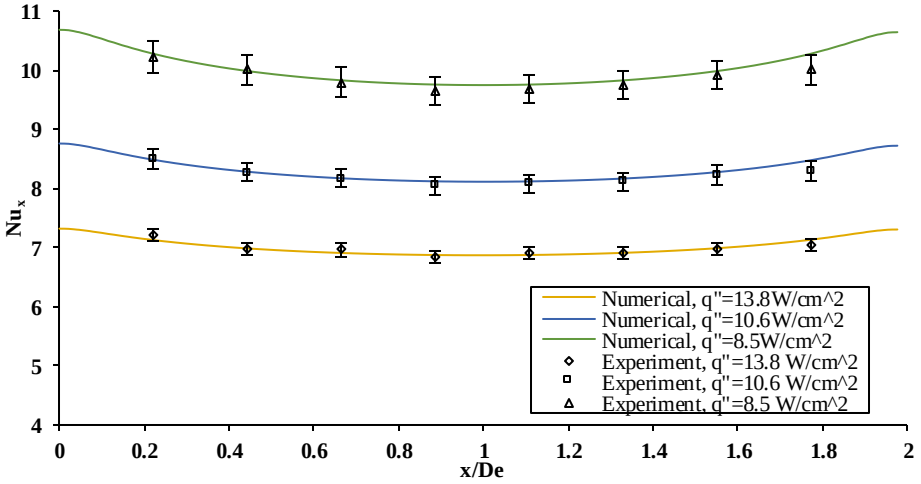

(a) Cycle average local Nusselt number distributions at A_o=1353

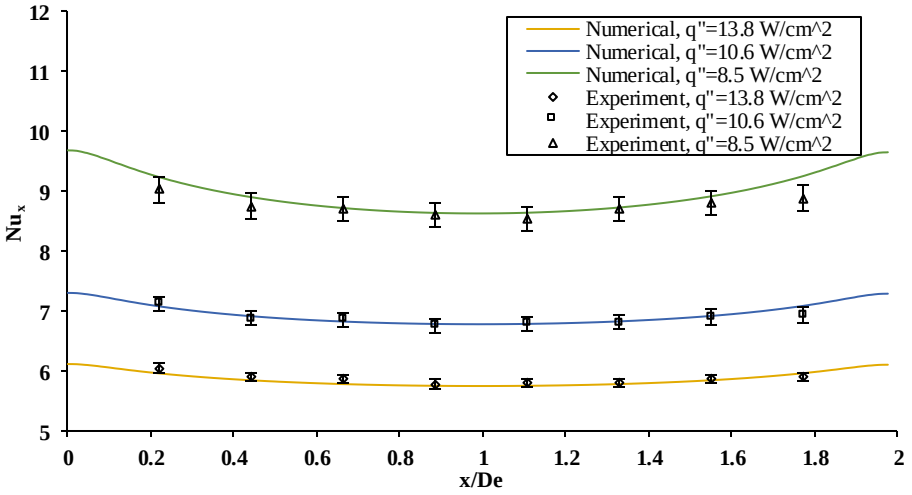

(b) Cycle average local Nusselt number distributions at A_o=902

Figure 3.7: Cycle average local Nusselt number distributions at f=0.1Hz

The average Nusselt number over the surface ($Nu_{,avg}$) was obtained using the following equation:

$$Nu_{,avg} = \frac{1}{L}\int_0^L Nu_x \, dx \tag{3.14}$$

Where L represents the channel length and Nu_x represents the local Nusselt number. Figure 3.11 presents the relationship between the average Nusselt number and the pulsating flow amplitude. As we can see, the average Nusselt number increases as the pulsating flow amplitude increases. An empirical correlation can be obtained as follows:

$$Nu_{,avg} = 0.2732*(A_o)^{0.46} \tag{3.15}$$

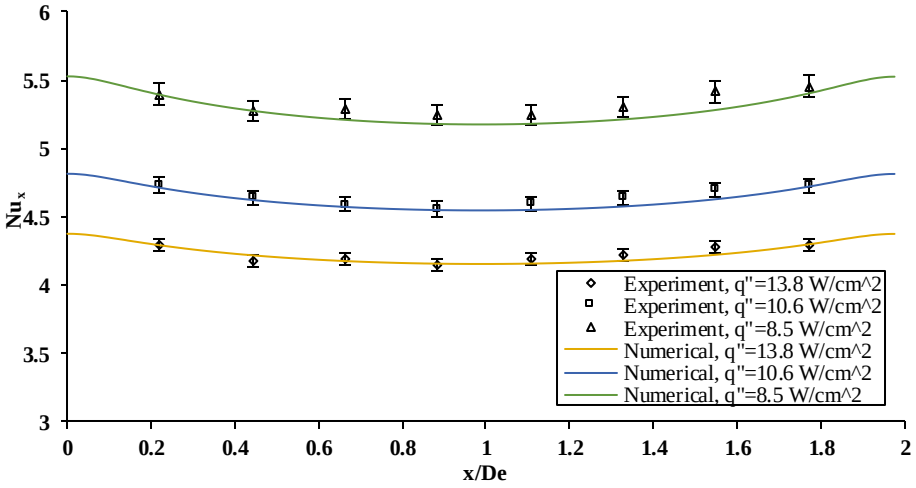

(a) Cycle average local Nusselt number at A_o=390

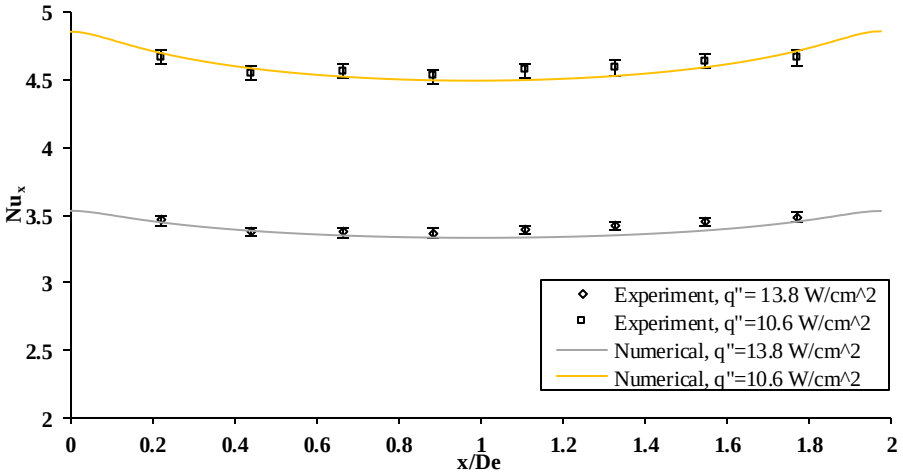

(b) Cycle average local Nusselt number at A_o=297

Figure 3.8: Cycle average local temperature distributions at f=0.1Hz

This empirical relationship is based on the present experimental data of a pulsating water flow through the aluminum foam heat sink and the given range of pulsating flow amplitude.

3.4.2 Effect of Pulsating Flow Frequency on Heat Transfer Characteristics

Figure 3.12(a, b) illustrates the effect of the kinetic Reynolds number on the cycle average local temperature at pulsating flow amplitudes (A_o) of 1353 and 902, respectively. The definition of the kinetic Reynolds number is based on the pulsating flow frequency as follows:

$$Re_w = \frac{2\pi \cdot f \cdot D_e^2}{\upsilon_f} \qquad (3.16)$$

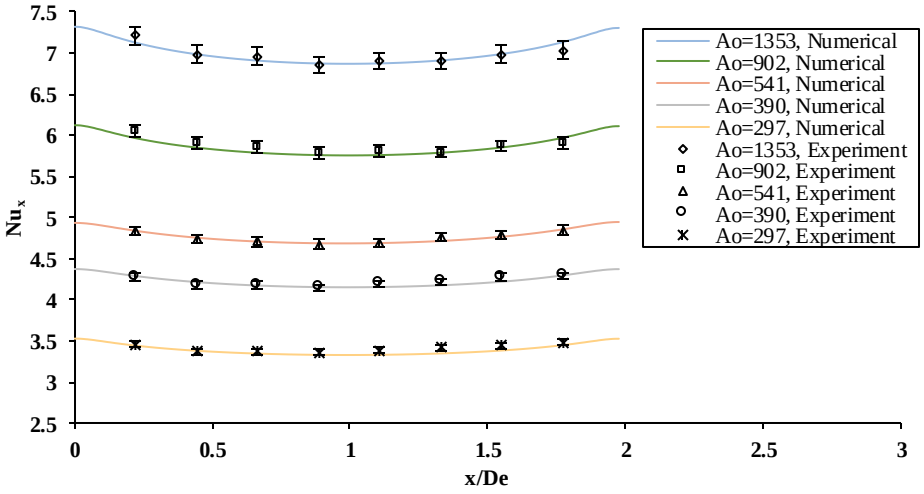

(a) Cycle average local Nusselt number at q"=13.8 W/cm^2

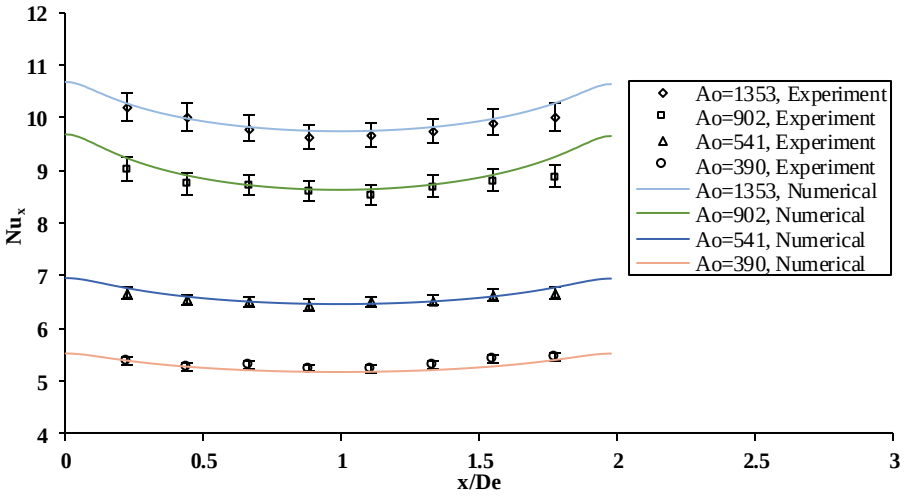

(b) Cycle average local Nusselt number at q"=8.5 W/cm^2

Figure 3.9: Cycle average local Nusselt number distributions at f=0.1Hz

Where f, D_e and ν_f represent the pulsating flow frequency, the hydraulic diameter of the channel, and the fluid kinematic viscosity, respectively. As we can see from Figure 3.14, the cycle average dimensionless local temperature decreases with increases in the kinetic Reynolds number. This means that the heat transfer rate over the heated surface is larger at high pulsating flow frequencies

and implies that the average Nusselt number over the surface is affected by changes in the kinetic Reynolds number (pulsating flow frequency).

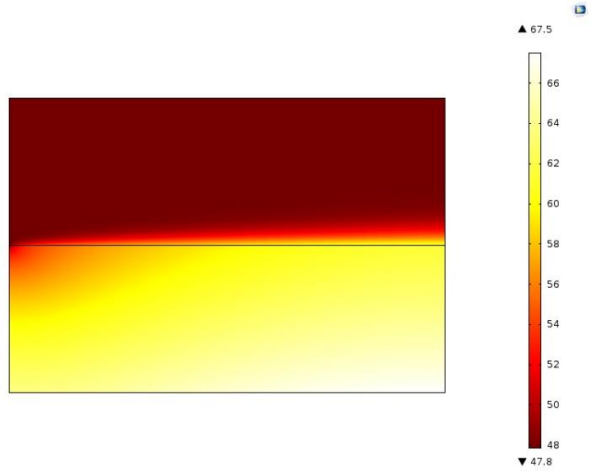

(a) Temperature contours in first half cycle

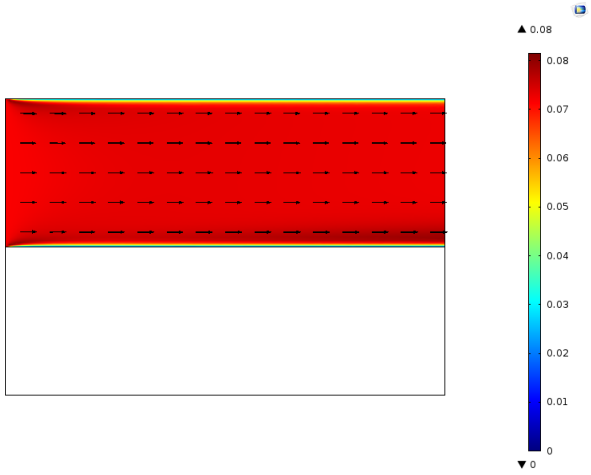

(b) Velocity contours in first half cycle

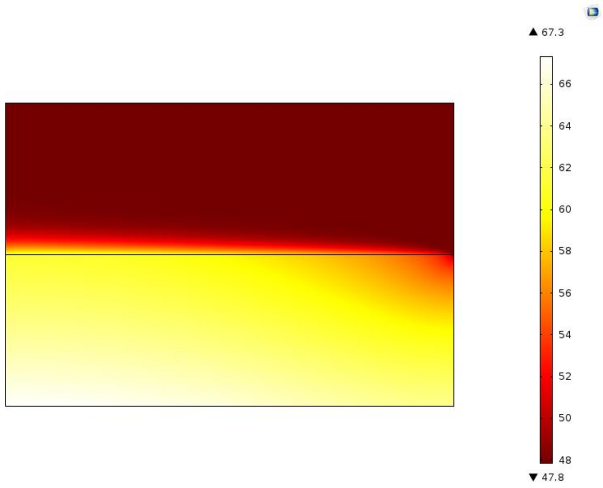

(c) Temperature contours in second half cycle

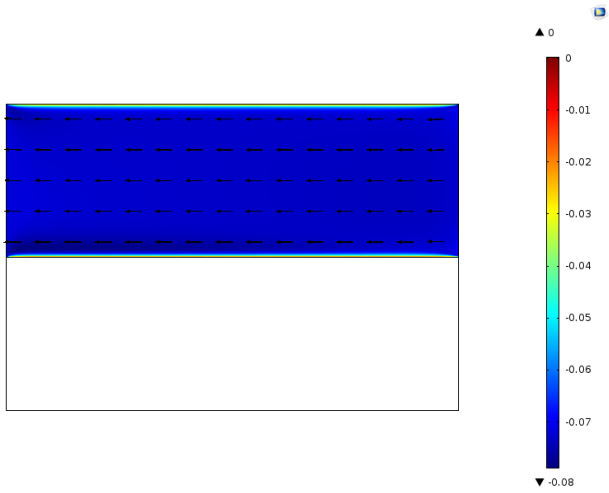

(d) Velocity contours in second half cycle

Figure 3.10: Temperature and velocity contours over a complete cycle of pulsating flow at Ao=1353 and f=0.1

This phenomena can be explained that for high frequency pulsating flow, the surface temperature doesn't get a chance to increase in the fully developed region during the first half cycle and rapidly the flow converts its direction. On the other hand, at low frequency pulsating flow the surface temperature has a longer chance to increase over first half cycle. Figure 3.13(a) illustrates the effect of the kinetic Reynolds number on the average Nusselt number over the surface at pulsating flow amplitudes of (A_o) 1353 and 902.

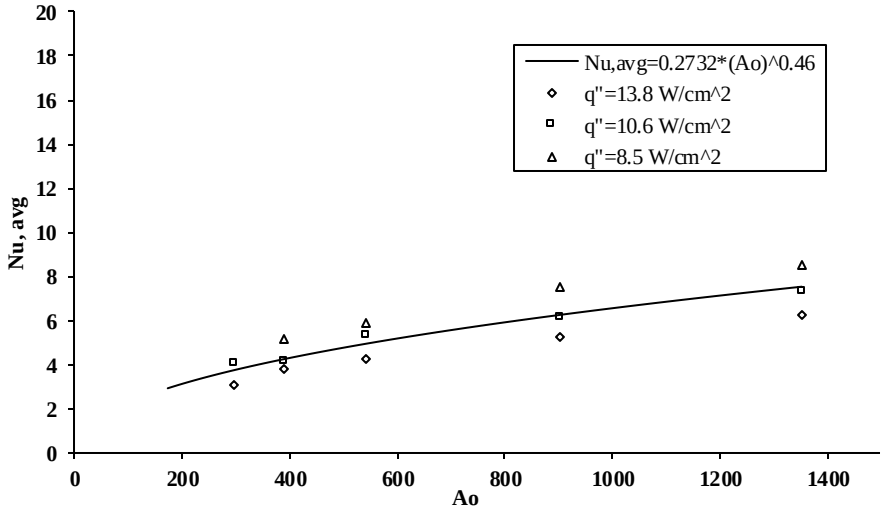

Figure 3.11: Pulsating flow average Nusselt number verses flow amplitude

As we can see, the average Nusselt number increases along with increases in the kinetic Reynolds number. In order to develop an empirical correlation of the average Nusselt number of pulsating flow as a function of the pulsating flow amplitude (A_o) and the kinetic Reynolds number (Re_w), the experimental data of figures 3.11 and 3.13(a) were collapsed. The empirical correlation of the average Nusselt number of the pulsating water flow through the aluminum foam sink was obtained as follows:

$$Nu_{,avg} = 0.2A_o^{0.46} e^{0.000025\,Re_w} \tag{3.17}$$

Where A_o and Re_w represent the pulsating flow amplitude and the kinetic Reynolds number, respectively. This empirical equation is based on the present experimental data and the given range of kinetic Reynolds numbers and pulsating flow amplitude with deviation of 3%. Figure 3.13(b) illustrates the average Nusselt number as a function of the kinetic Reynolds number and pulsating flow amplitude.

3.4.3 Comparison Between Steady and Pulsating Flow Through Aluminum Foam

Figure 3.14(a, b) illustrates the comparison between the local Nusselt number of the steady and pulsating flows at a kinetic Reynolds number (Re_w) of 12905 (f=0.1 Hz) and flow amplitudes of 1353 and 902, respectively. The results revealed that the pulsating flow achieves a higher local Nusselt number along the surface than the steady flow.

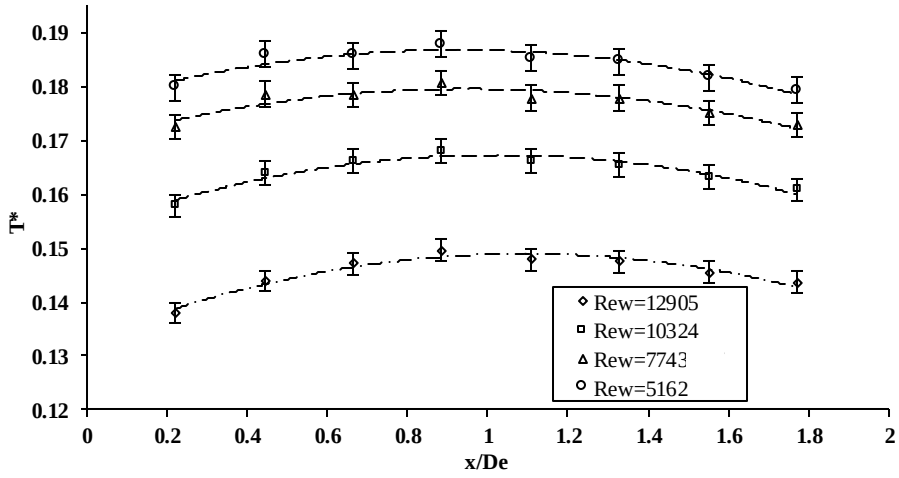

(a) Cycle average local temperature distributions at A_o=1353

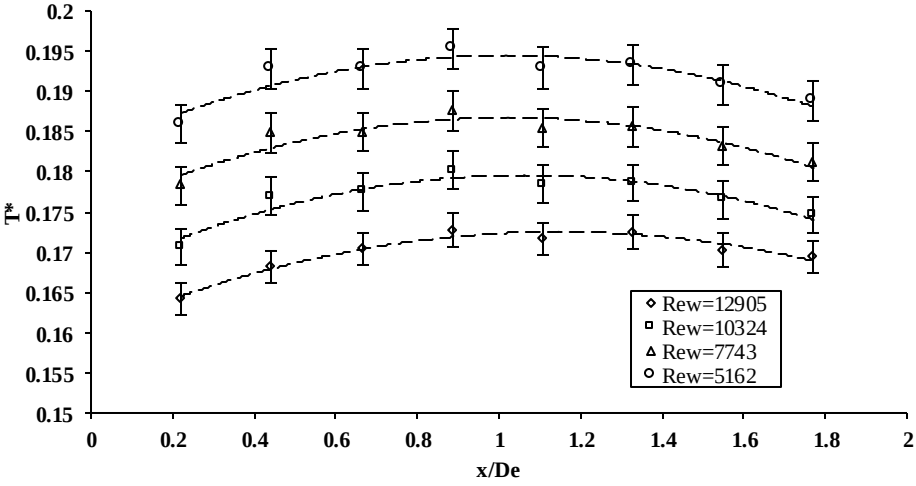

(b) Cycle average local temperature distributions at A_o=902

Figure 3.12: The effect of kinetic Reynolds number on the local temperature distributions

The results also revealed that the local Nusselt number of the steady flow is higher at the beginning of the channel (thermal entry region) and starts to decrease in the flow direction axis.

This is why the local Nusselt number enhancement between the pulsating and steady flow is larger at the end of the channel (x/D_e=2) than at the entrance (x/D_e=0). As we can see in Figure 3.15(a), the enhancement percentage of the local Nusselt number of the pulsating flow compared with steady flow (based on relative difference) is 7-16% at the entrance and 20-31% at the end of the channel.

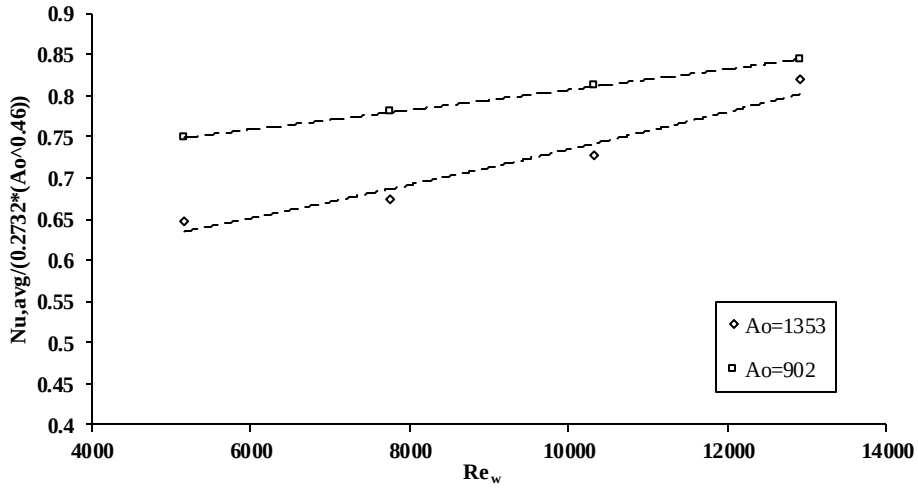

(a) **Average Nusselt number verses kinetic Reynolds number**

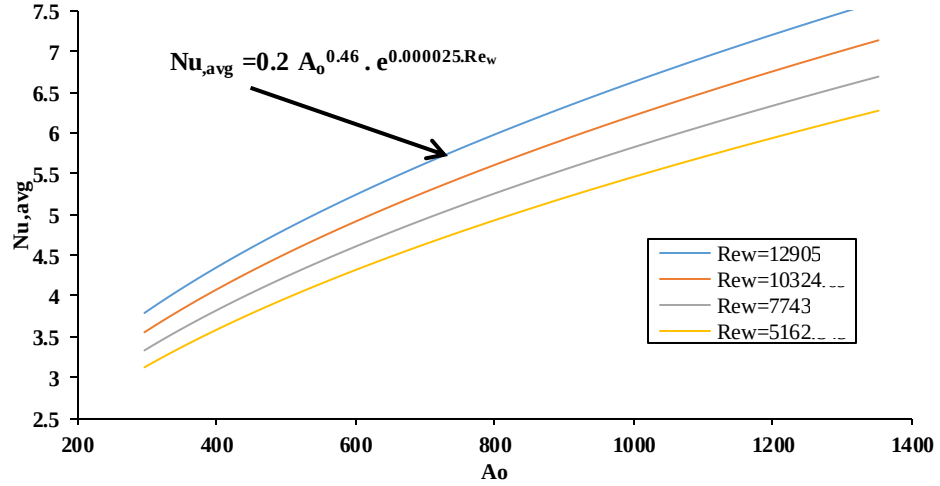

(b) **Average Nusselt number as a function of pulsating flow amplitude and kinetic Reynolds number**

Figure 3.13: Average Nusselt number of pulsating flow

In order to perform a comparison between the average Nusselt number of the pulsating and steady flows, an empirical correlation of the average Nusselt number of the steady water flow as a function of the steady flow amplitude (A_o) was obtained and compared to the correlation obtained for the pulsating water flow Eq. (3.17).

The empirical correlation of the average Nusselt number of steady water flow through the aluminum foam heat sink was obtained as follows:

$$Nu_{,avg,steady} = 0.342 * A_o^{0.41} \quad (3.18)$$

Where $Nu_{,avg,steady}$ represents the average Nusselt number of steady water flow through the aluminum foam.

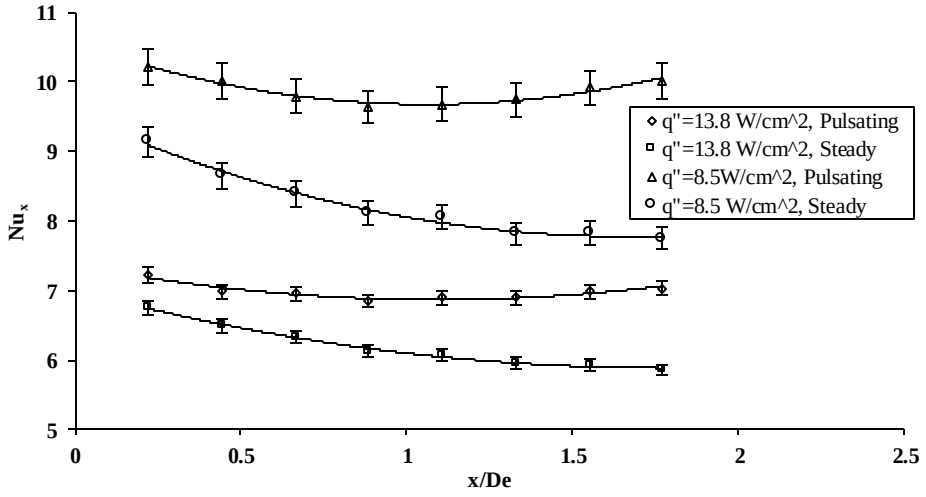

(a) Local Nusselt number distributions of pulsating and steady flow at A_o=1353

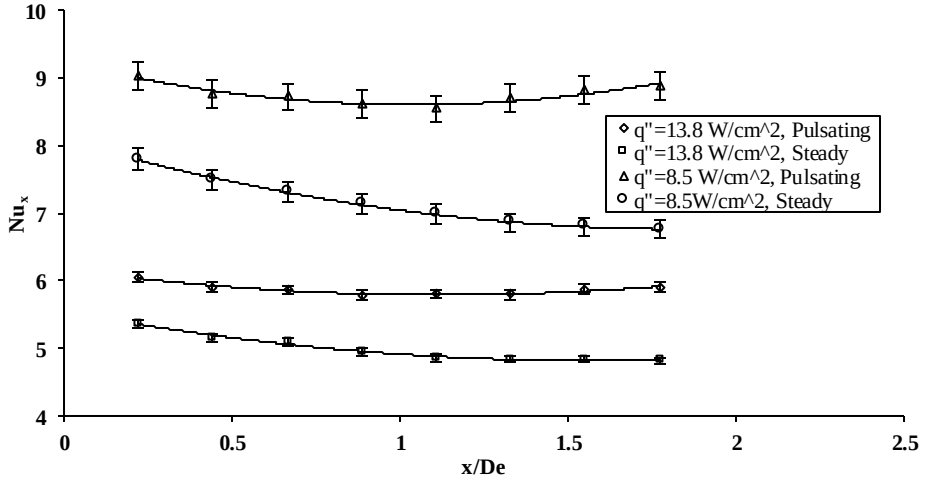

(b) Local Nusselt number distributions of pulsating and steady flow at A_o=902

Figure 3.14: Comparison between steady and pulsating flow's local Nusselt number distributions

Figure 3.15(b) illustrates the comparison between the empirical correlations of the average Nusselt number of the steady and pulsating water flows through the aluminum foam. It is clear from this figure that the pulsating flow achieves higher average Nusselt numbers than the steady flow. Figure 3.16 presents the ratio between the average Nusselt number of the pulsating flow ($Nu_{,avg}$) at Re_w=12905 and the average Nusselt number of the steady flow ($Nu_{,avg,steady}$). The average enhancement percentage in the average Nusselt number was 14%.

3.4.4 Thermal Performance of the Aluminum Foam Heat Sink and Temperature Uniformity

In order to evaluate the thermal performance of the aluminum foam heat sink subjected to the pulsating water flow, the pressure drop across the aluminum foam was measured. Figure 3.17(a) illustrates the pressure drop verses the pulsating flow absolute velocity (U).

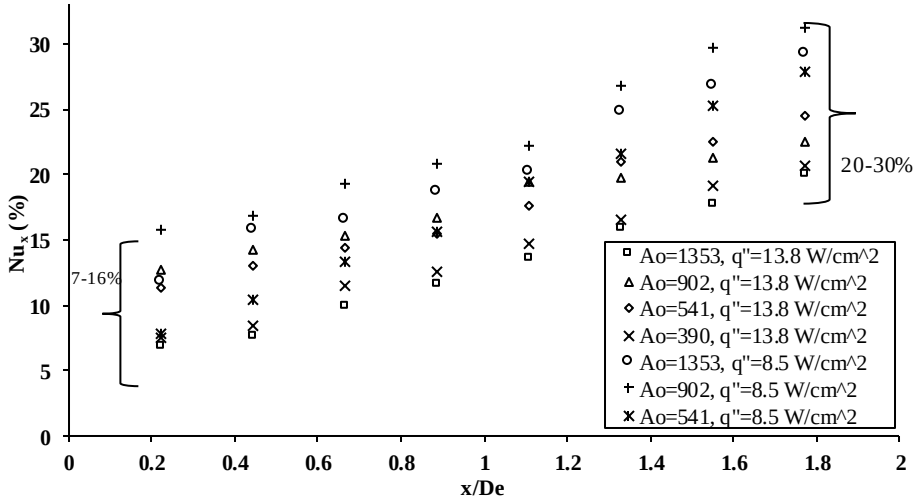

(a) Enhancement percentage of local Nusselt number of pulsating flow

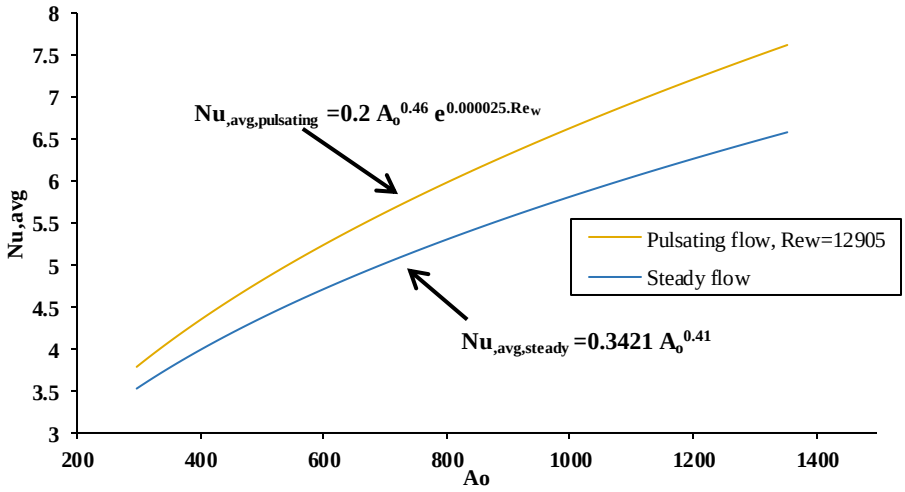

(b) Comparison between average Nusselt number of pulsating and steady flow

Figure 3.15: Local and average Nusselt number improvement of pulsating flow

As one may notice from this figure, the pressure drop increases along with increases in the pulsating flow amplitude. A good agreement between the numerical and experimental pressure drop results is obtained. The Fanning friction factor (f) is commonly used to provide information regarding the required pressure drop of the heat exchanger. This is done to ensure that the pressure drop across the foam is non-dimensional. The friction factor of aluminum foam is obtained using the following equation:

$$f = \frac{\Delta p}{4\left(\frac{L}{De}\right)\left(\frac{\rho_f U^2}{2}\right)} \tag{3.19}$$

Where L represents the channel length, De represents the hydraulic diameter of the channel, ρ represents the water density, and U represents the velocity of the fluid. Figure 3.17(b) illustrates the friction factor of the foam verses the flow amplitude.

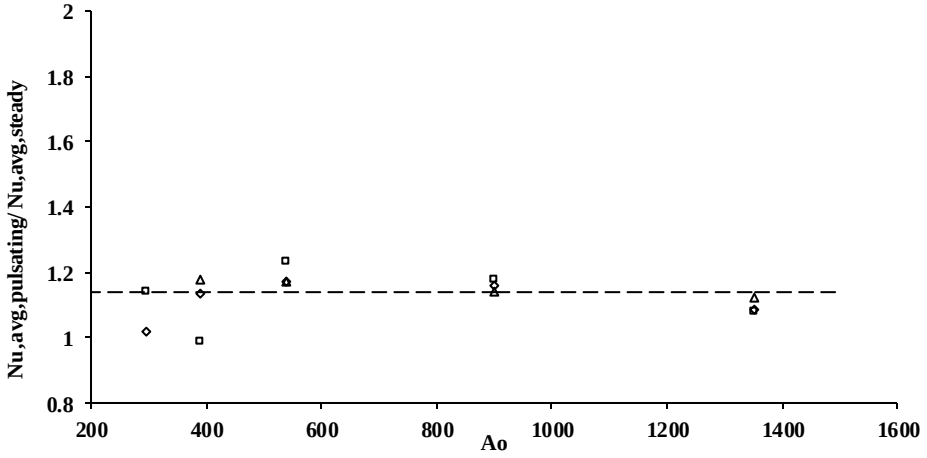

Figure 3.16: Ratio between pulsating and steady water flow's average Nusselt number

As we can see from the analysis of the heat transfer characteristics of the pulsating water flow through the aluminum foam, the average Nusselt number increases along with increases in the flow amplitude. This increase is accompanied by an increase in the required pumping power which results from an increase in the pressure drop across the aluminum foam. In order to combine the heat transfer rate with the pressure drop, the thermal efficiency index is calculated using the following equation;

$$I_{efficiency}=\frac{Nu_{,avg}\cdot L}{f\cdot H} \tag{3.20}$$

Where f represents the Fanning friction factor of the aluminum foam, L represents the channel length, H represents the channel height, and $Nu_{,avg}$ represents the average Nusselt number. The thermal efficiency index combines the heat transfer with the pressure drop across the aluminum foam in order to find the optimal design condition that achieves higher heat transfer with lower pumping power. Figure 3.18 shows the thermal efficiency index verses the pulsating flow amplitude. As one may observe from this figure, that the optimal design condition is obtained at A_o=1353 at which a thermal efficiency index of 2.7 was achieved.

As previously mentioned, the average Nusselt number of the pulsating flow is affected by the kinetic Reynolds number. The empirical correlation of the average Nusselt number for the pulsating water flow through the aluminum foam heat sink (Eq. (3.17)) was used to evaluate the

thermal efficiency index verses the kinetic Reynolds number (Re_w) over a wide range of pulsating flow frequencies, as shown in Figure 3.19(a). As we can see, the thermal efficiency index is greatly enhanced by increases in the pulsating flow frequency.

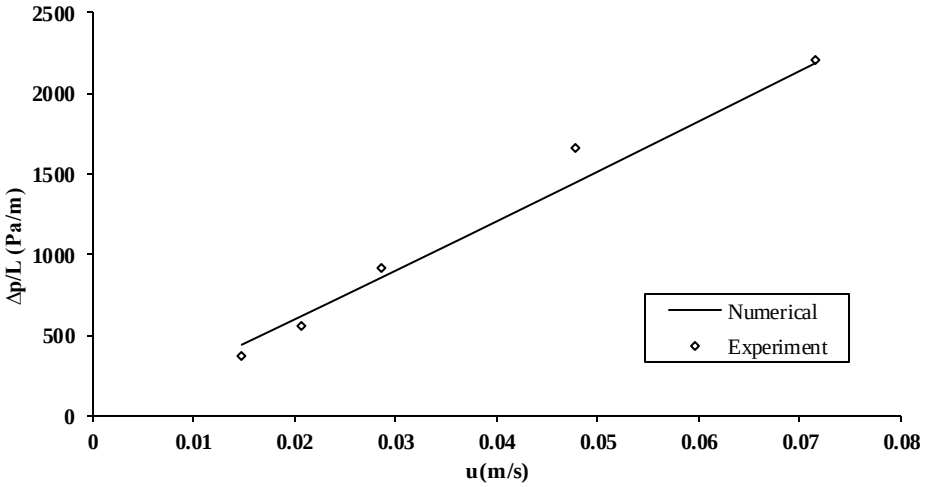

(a) Pressure drop across Aluminum foam

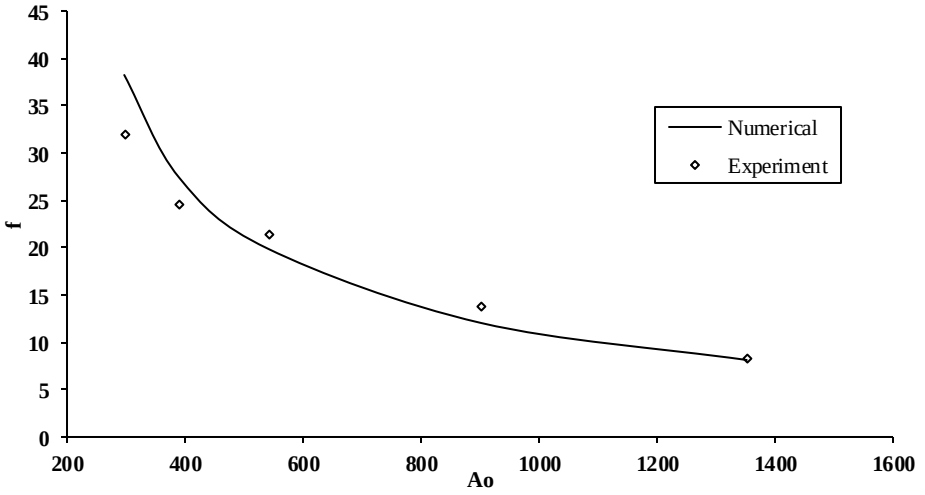

(b) Fanning friction factor of aluminum foam

Figure 3.17: Pressure drop and Fanning friction factor of aluminum foam

In order to quantify the temperature distribution uniformity, an index is obtained using:

$$\eta = \frac{T_{max} - T_{min}}{T_{max}} \tag{3.21}$$

Where T_{max} and T_{min} represent the maximum and minimum temperatures on the heated surface in Kelvin units. The uniformity index approaches zero when the temperature distribution is perfectly uniform.

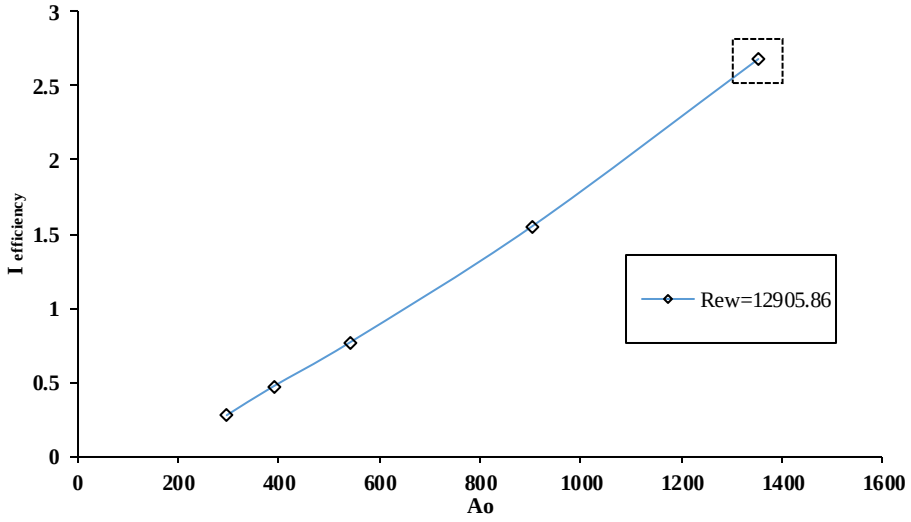

Figure 3.18: Thermal efficiency index verses pulsating flow amplitude

Figure 3.19(b) illustrates the uniformity index of pulsating and steady flows through aluminum foam and the uniformity index of a steady air flow through ERG aluminum foam presented by Fu et al. [69]. The uniformity index of the pulsating flow is 73% lower than the steady water flow and 91% lower than the steady air flow [69]. This implies that the pulsating flow achieves a more uniform temperature distribution over the surface than the steady flow. This finding is of great importance in electronic cooling since the reliability of transistors and operating speed depend on temperature uniformity along the surface. Non-uniformity of temperature may cause electronic gate delay which reduces the overall efficiency of the device.

3.5 Conclusions

This chapter presented an experimental and numerical study in using pulsating water flow through aluminum foam as a heat sink. The pulsating water flow covering the non-Darcy flow regime. The following conclusions were drawn based on the findings of the study:

- The temperature distributions of the pulsating water flow show a convex profile with the maximum temperature at the center of the test section.

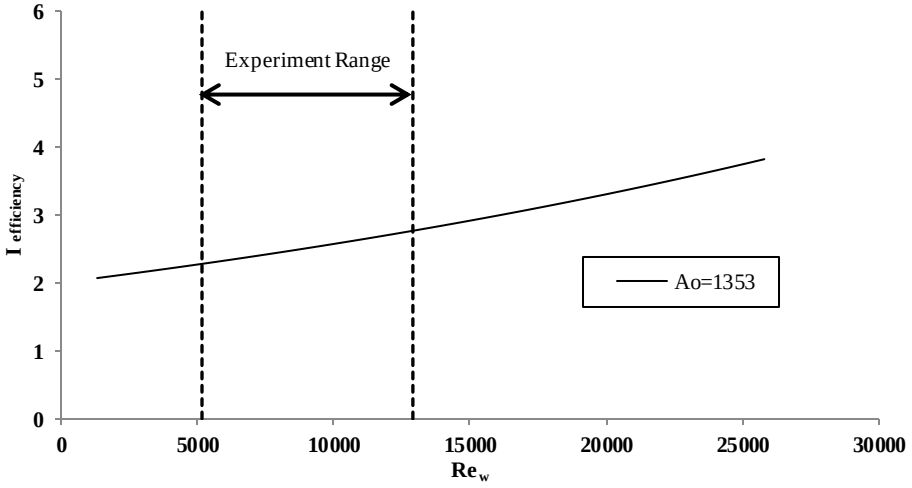

(a) Thermal efficiency index verses kinetic Reynolds number

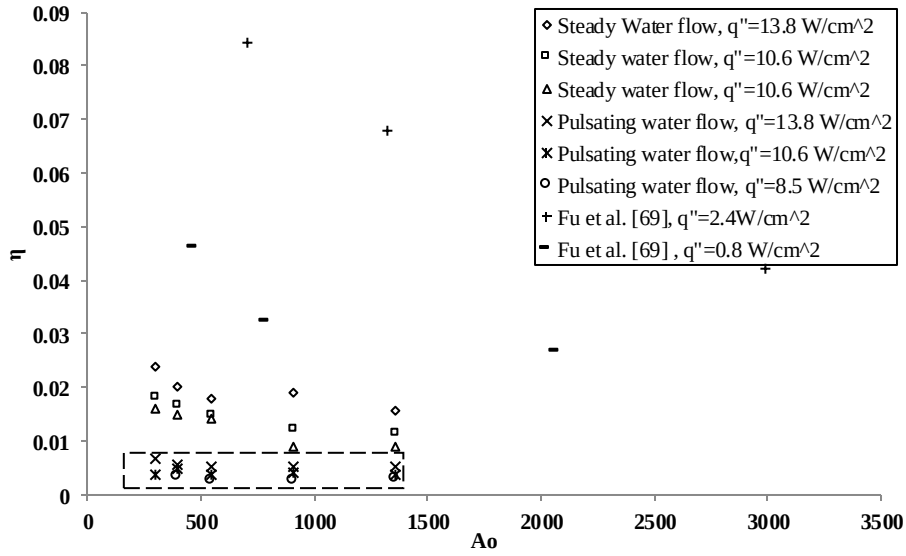

(b) Comparison of uniformity index of water pulsating and steady flow and air steady flow through aluminum foam

Figure 3.19: Thermal efficiency index as a function of kinetic Reynolds number and the uniformity index of water pulsating flow

- The cycle average local temperature increases along with increases in the heat flux and decreases in the flow amplitude.
- The local Nusselt number of the pulsating flow is higher at both channel entrances and begins to decrease until it reaches a minimum point at the center of the test section.
- The local Nusselt number distribution curves show a concave profile with the center as the symmetric point.

- The thermal entry length of the pulsating water flow through aluminum foam is shorter for smaller amplitudes than for larger amplitudes.
- The average Nusselt number of the pulsating water flow increases along with increases in the pulsating flow amplitude and the kinetic Reynolds number. The relationship between the average Nusselt number as a function of pulsating flow amplitude and kinetic Reynolds number was $Nu_{,avg} = 0.2A_o^{0.46}e^{0.000025\,Re_w}$, based on the experimental data.
- The enhancement percentage of the local Nusselt number of the pulsating flow compared with the steady flow was 7-16% at the entrance and 20-31% at the end of the channel.
- The enhancement percentage of the average Nusselt number of the pulsating flow compared with the steady flow was 14%.
- The temperature uniformity index of the pulsating flow was 73% lower than the temperature uniformity index of the steady flow.
- The numerical results were in good agreement with the experimental data for different flow amplitudes and heat flux with a maximum relative error of 0.75% for the local temperature and 1.8% for the local Nusselt number.

CHAPTER 4-HEAT TRANSFER CHARACTERISTICS OF A CHANNELED ALUMINUM FOAM HEAT SINK

This chapter is based on the following accepted paper:

Bayomy, A. M., Saghir, M. Z., "Experimental and Numerical Study of the Heat Transfer Characteristics of Aluminum Metal Foam (with/without channels) Subjected to Steady Water Flow" accepted and procced to publish in J. of Science and Technology, Pertanika Journal, vol. 00, pp. 00-00, 2016.

4.1 Introduction

In order to enhance the heat transfer rate of modern high speed electronic devices, researchers have conducted extensive investigations using different shapes and arrangements in order to increase the surface to volume ratio of heat sinks [5-11]. Although this existing research, there still exists a demand for more effective electronic cooling methods.

The use of porous media as a heat sink subjected to forced cooling fluid is a new technique used to enhance the heat transfer from the surface of electronics. The heat transfer characteristics of metal foam are function of its microstructural properties such as porosity, relative density, pore density, pore size, ligament diameter, and permeability [43, 54-59].

In addition, Zhao et al. [60] and Klett et al. [61] observed that the metal foam heat exchanger achieves higher heat transfer than the conventional finned tube heat exchanger. Moreover, there are some studied have conducted in the effect of using metal foam [62-72] and they demonstrated the positive effect caused by employing the metal foam. On the other hand, there are a small number of studies have used water as a working coolant fluid through metal foams [73-76] as mentioned in section 2.1.

This chapter presents an experimental and numerical study of different configurations of the aluminum foam used as heat sinks. Three aluminum foam heat sink models were used in the study: without channels (A), with two channels (B), and with three channels (C). The aluminum foam was subjected to a water flow covering the non-Darcy flow regime. Local temperature distributions were measured for different heat fluxes and Reynolds numbers and the local Nusselt number was calculated based on the local surface temperature of each heat sink model. The average Nusselt number was obtained for the entire range of Reynolds numbers. An empirical correlation of the average Nusselt number was developed based on the Reynolds number of each model. The

pressure drop across each heat sink model was also measured and the thermal performance of the aluminum foam heat sink was evaluated based on the average Nusselt number and the pumping power required for each model. The thermal efficiency index was defined in order to obtain the optimum design condition for the use of aluminum foam as a heat sink. As mentioned previously, a numerical model has been developed and compared with experimental data.

4.1 Experimental Apparatus and Procedures

The experimental setup was used in order to examine the heat transfer characteristics of different aluminum foam models (with and without channels) as a heat sink in the cooling of electronics.

4.1.1 Test Section and Experimental Facility

The experimental setup was mentioned previously in section 2.2.1. The test section consisted of high temperature Teflon insulation attached to a 37.5mm×37.5mm heater.

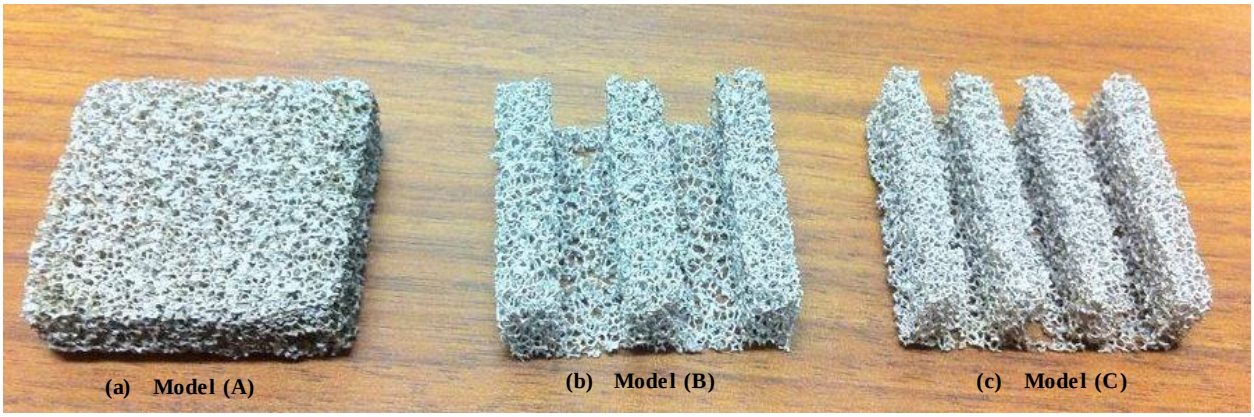

Figure 4.1: ERG aluminum foam models

Test section facilities were presented in section 2.2.1. Three aluminum foam heat sink models were used in the study: one without channels (A), one with two channels (B) and one with three channels (C), as shown in Figure 4.1. The dimensions of the channels for models (B) and (C) are shown in Figure 4.2. The physical and geometric properties of the ERG test section foam were mentioned in section 2.2.1. It is important to note that these properties are not all independent of one another. The relationships between them are presented by Calmidi and Mahajan [79]

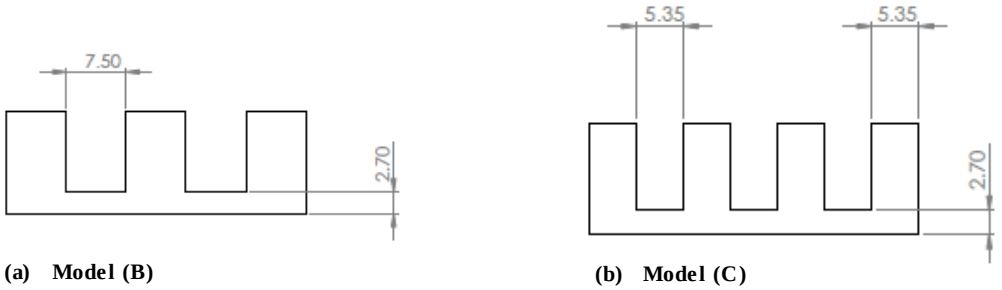

(a) Model (B) (b) Model (C)

Figure 4.2: Models (B) and (C) dimensions

In order to obtain experimental steady state conditions, the surface temperature, inlet and outlet temperatures, pressure drop across the foam, and water flow rate were monitored using the data acquisition system.

4.1.2 Uncertainty Analysis

The uncertainties of the temperature, flow rate and pressure drop were presented in section 2.2.2. These uncertainty values were obtained based on standard and random errors. The uncertainties of (Nu_x) and (Re) were obtained using the Taylor method [81]. The local Nusselt number and the Reynolds number are calculated as follows:

$$h_x = \frac{q''}{(T_x - T_i)} \tag{4.1}$$

$$Nu_x = \frac{h_x D_e}{k_{eff}} \tag{4.2}$$

$$Re = \frac{U.D_e}{\upsilon_f} \tag{4.3}$$

Where h_x represents the local heat transfer coefficient over the heater surface, T_x represents the local surface temperature, T_i represents the inlet water temperature, D_e represents the hydraulic diameter of the channel, U represents the water velocity throughout the test section, υ_f represents the kinematic viscosity of the fluid, and k_{eff} represents the effective thermal conductivity of the metal foam filled with water.

The maximum uncertainty of the local Nusselt number was $\pm$ 2.4 % and the uncertainty of the Reynolds number was $\pm$ 0.44%.

4.2 Numerical Model Description

Numerical model were conducted using the finite element technique [77] in order to compare with the experimental results.

4.2.1 Governing Equations

The set of governing equation were solved based on the numerical model assumptions as mentioned in section 2.3.1. These governing equation consist of the Brinkman- Forchheimer equation and energy equation as follow:

$$\frac{\rho_f}{\varepsilon}\left(\frac{\partial U}{\partial t}+(U\cdot\nabla)\frac{U}{\varepsilon}\right)=\nabla.\left(-pI+\frac{\mu_f}{\varepsilon}(\nabla U+(\nabla U)^T)\right)-\left(\frac{\mu_f}{K}+\beta_f|U|\right)U+F \tag{4.4}$$

$$\nabla\cdot(\rho_f U)=0 \tag{4.5}$$

$$(\rho c_p)_{eff}\cdot\frac{\partial T}{\partial t}+(\rho c_p)_f\,U\cdot\nabla T=\nabla.(k_{eff}.\nabla T) \tag{4.6}$$

Where ρ_f represents the water density, c_p represents the fluid specific heat, ε represents the porosity of the aluminum metal foam, p represents the pressure, U represents the velocity field vector, β_f represents the Forchheimer coefficient, T represents the temperature, μ_f represents the dynamic viscosity of the fluid, K_b represents the permeability of the aluminum foam, F represents the body force, and k_{eff} represents the effective thermal conductivity of the aluminum metal foam filled with water (mentioned in section 2.3.1).

4.2.2 Boundary Conditions

A shown in Figure 4.3, the boundary conditions were similar to the boundary conditions which were mentioned in section 2.3.2. The boundary conditions can be concluded as an inlet temperature and velocity at the inlet portion, open boundary at the outlet portion, heat flux from the bottom of the heater and adiabatic walls at the remainder of the surface (see Figure 4.3).

4.2.3 Mesh Sensitivity Analysis

A tetrahedral element was used to describe the numerical model as mentioned in section 2.3.3. In order to perform mesh sensitivity analysis, calculations of the maximum temperature and local Nusselt number on was performed for different numbers of domain elements, as shown in Figure 4.4. The number of elements used was 1847400 and the variation was less than 0.001, as shown in Figure 4.5.

4.3 Results and Discussion

In this experimental study, three aluminum foam heat sink models (A, B, and C) were subjected to a uniform heat flux ranging from 13.8 to 8.5W/cm^2 [2, 3, and 53]. The water flow covered the Forchheimer regime (non-Darcy regime). In addition, a numerical model was developed using the finite element technique and the numerical results were compared to the experimental results.

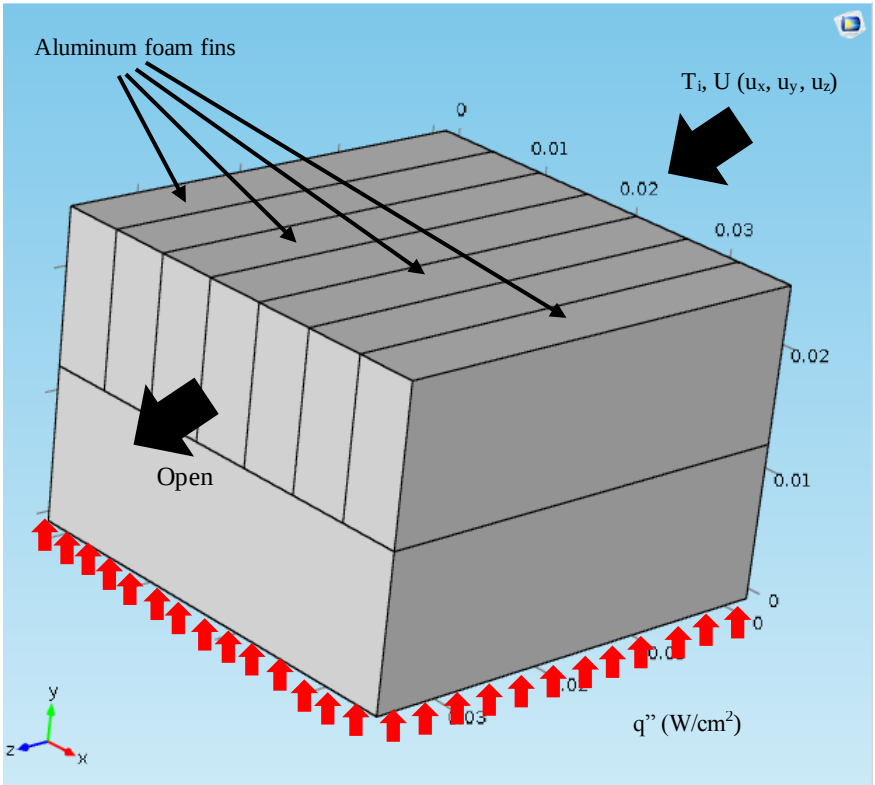

Figure 4.3: Boundary conditions

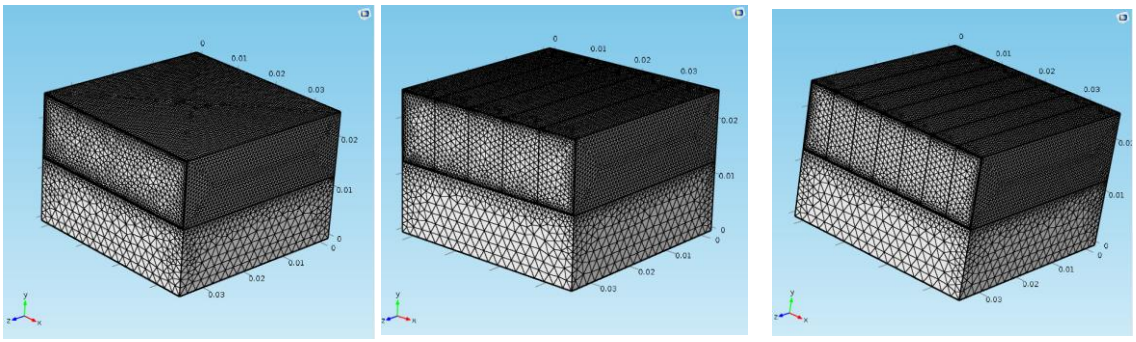

(a) Model A (b) Model B (c) Model C

Figure 4.4: Finite element models

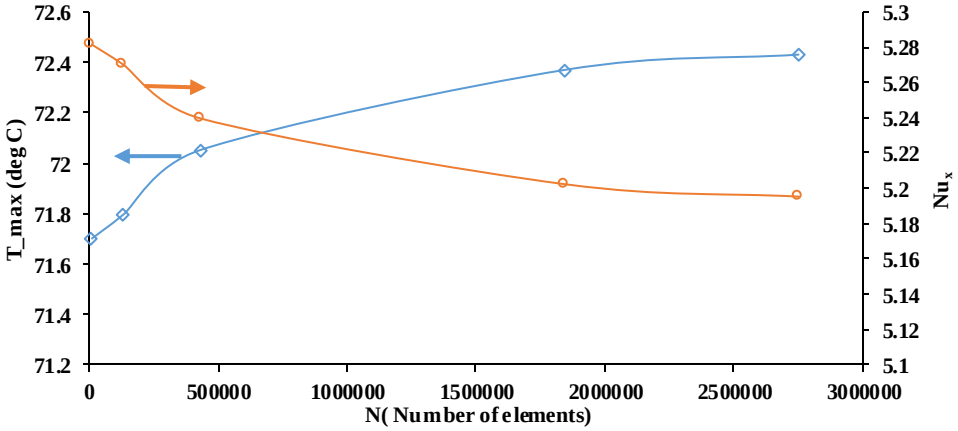

Figure 4.5: Mesh independent

4.3.1 Local Dimensionless Temperature Distributions Over the Surface

Figure 4.6(a, b) illustrates the surface temperature distributions along the dimensionless flow direction axis (x/D_e) at q"= 13.8 and 10.6 W/cm^2, respectively, and Re= 1353 for models (A), (B) and (C). As we can see, the surface temperature showed an increase in the flow direction. This trend was observed in previous experimental studies [69, 74]. The results revealed that model (A) achieved a lower temperature distribution when compared with models (B) and (C). The results also revealed that the dimensionless local surface temperatures of models (A) and (B) were almost identical at the beginning of the channel (x/D_e= 0-0.3) and began to diverge from each other along with the axial flow direction distant.

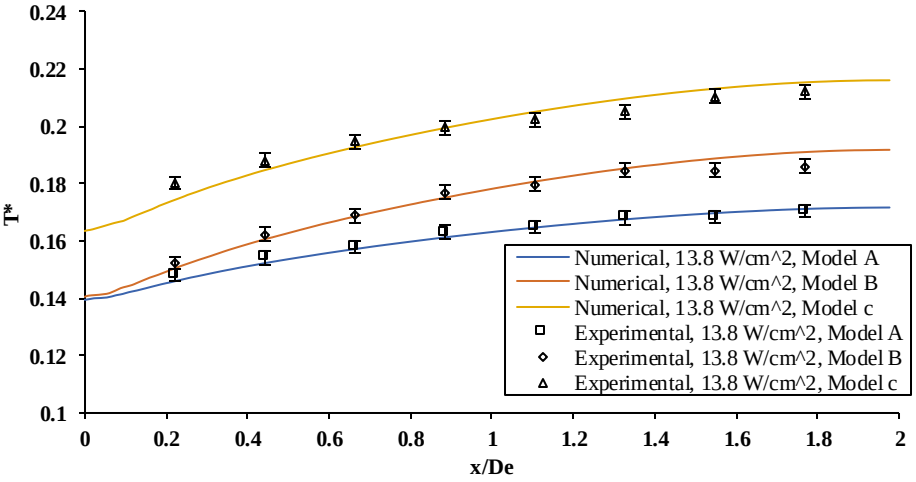

(a) Temperature distributions at q"=13.8W/cm^2

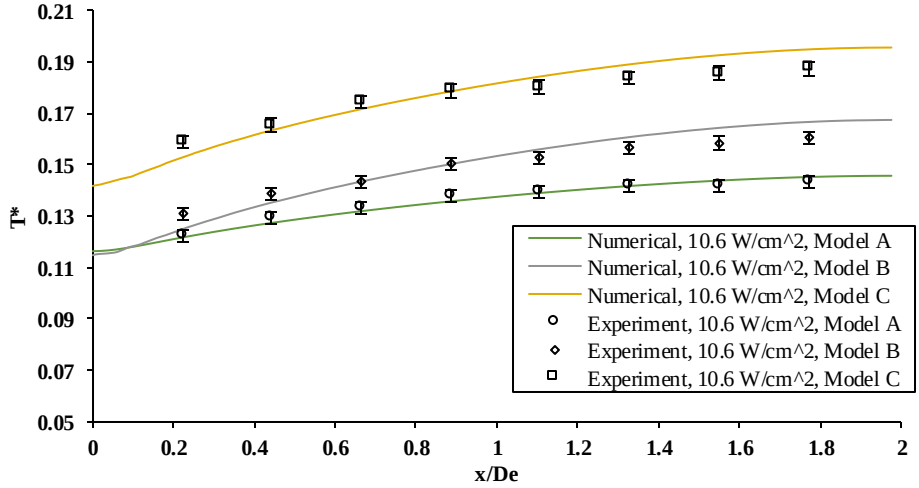

(b) Temperature distributions at q"=10.6W/cm^2

Figure 4.6: Surface temperature distributions at Re= 1353

The same trend can be observed in Figure 4.7(a, b) which illustrates the temperature distributions at Re=902 and q"= 13.8 and 8.5 W/cm^2, respectively. Moreover, Figure 4.8 shows the temperature distributions at Re= 541 and q"=13.8W/cm^2. We can also see that the surface temperature increases along with decreases in the Reynolds number and increases in the heat flux.

In order to complement the experimental results, a numerical model was developed using the finite element technique. Figures 4.6, 4.7 and 4.8 show the experimental and numerical surface temperature results for different heat flux and Reynolds numbers (Re=1353, 902 and 541). The numerical results are in good agreement with the experimental results, with a maximum relative error of 2%.

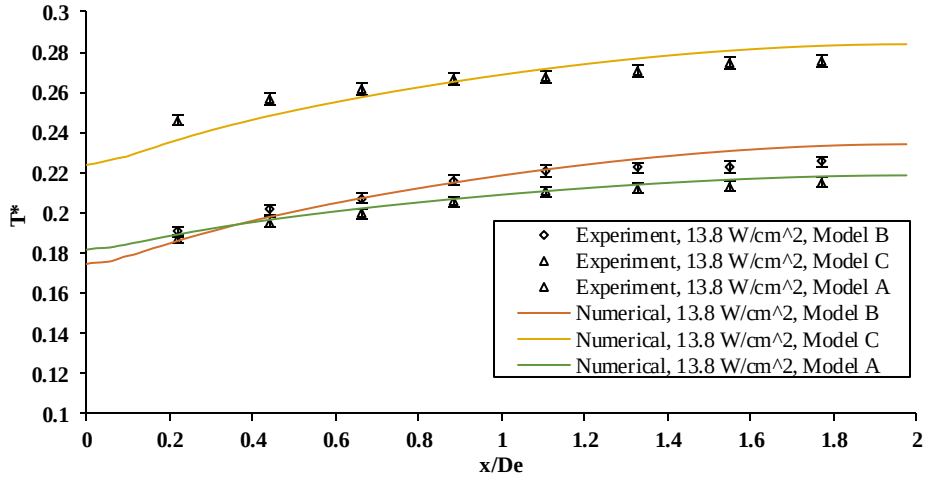

(a) Temperature distributions at q"=13.8W/cm^2

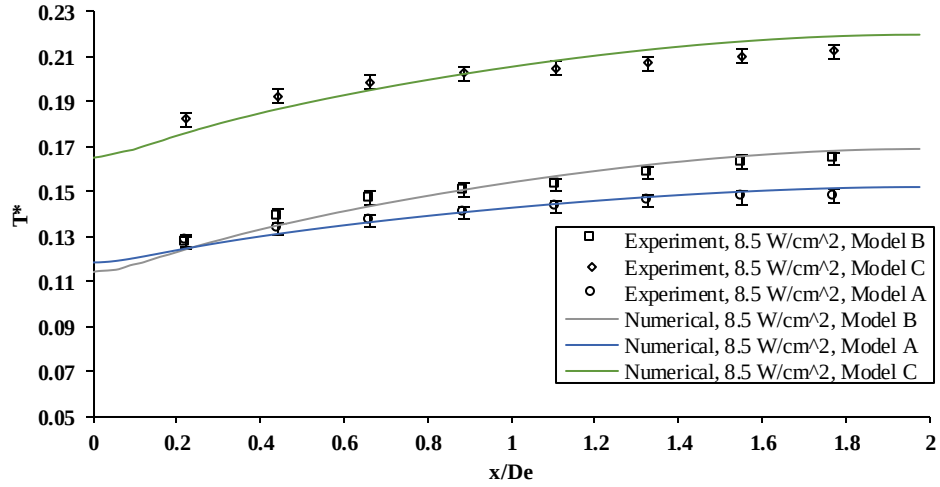

(b) Temperature distributions at q"=8.5W/cm^2

Figure 4.7: Surface temperature distributions at Re= 902

In addition, Figures 4.9 and 4.10 show the temperature contours of each model at q"=13.8 W/cm^2 and Re= 1353 and 902, respectively. The results revealed that the temperature of the heated surface (electronic surface) increases along with the flow direction axis. In addition, the use of channels in the aluminum foam (models B and C) creates a non- uniform temperature distribution along the line which is perpendicular to the flow direction. As shown in Figure 4.11, the temperature distribution along the line perpendicular to the flow direction of model (A) is perfectly uniform and lower than that of models (B) and (C) which suffer from non- uniform temperature.

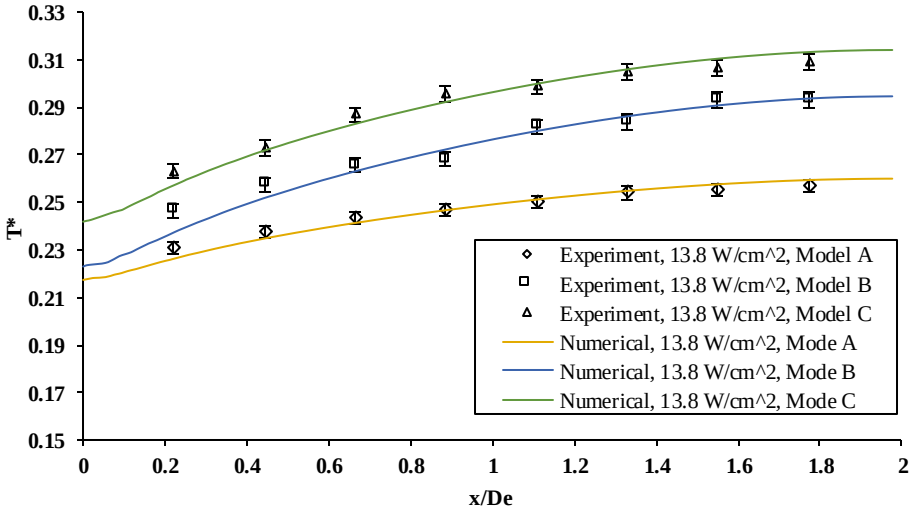

Figure 4.8: Surface temperature distributions at Re= 541

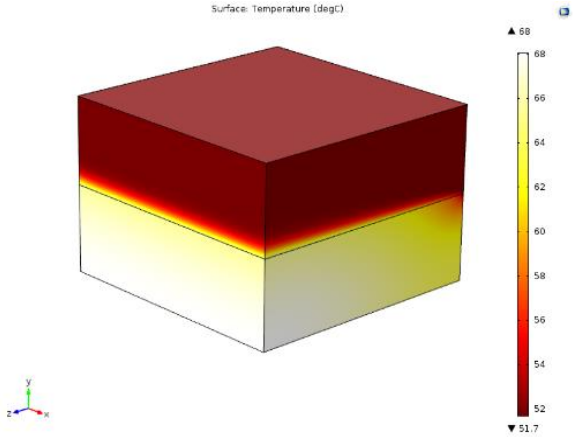

(a) Model (A)

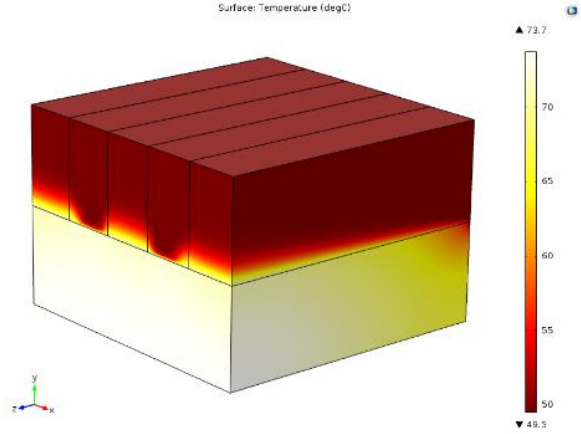

(b) Model (B)

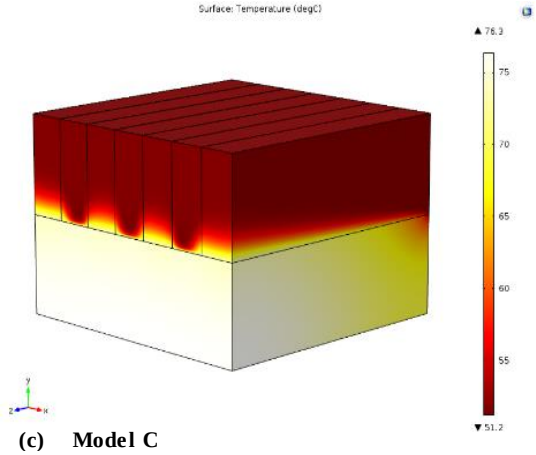

(c) Model C

Figure 4.9: Temperature contours at q"=13.8 W/cm2 and Re=1353

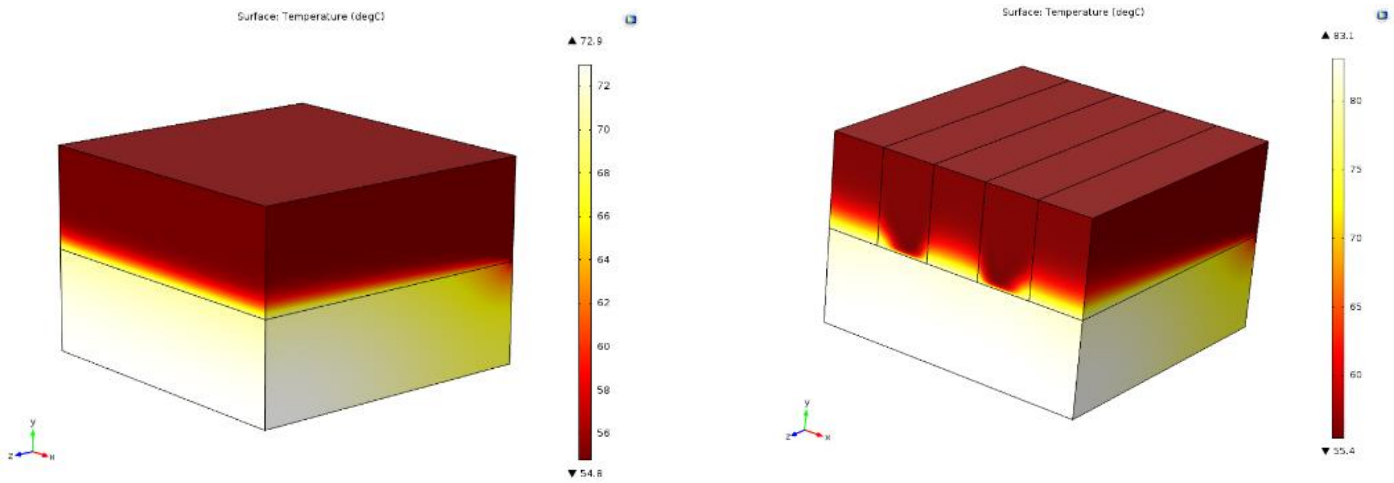

(a) Model (A)

(b) Model (B)

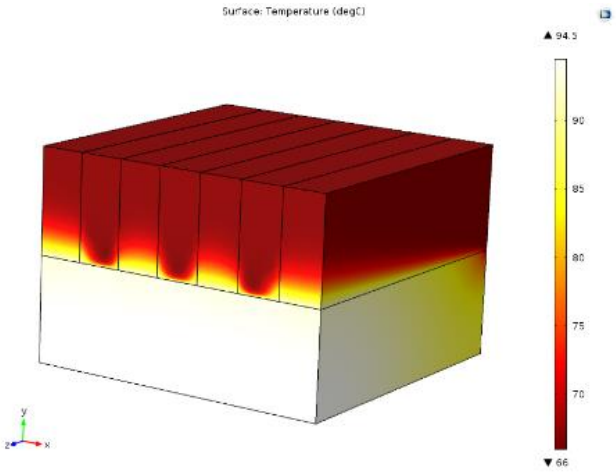

(c) Model C

Figure 4.10: Temperature contours at q"=13.8 W/cm² and Re=902

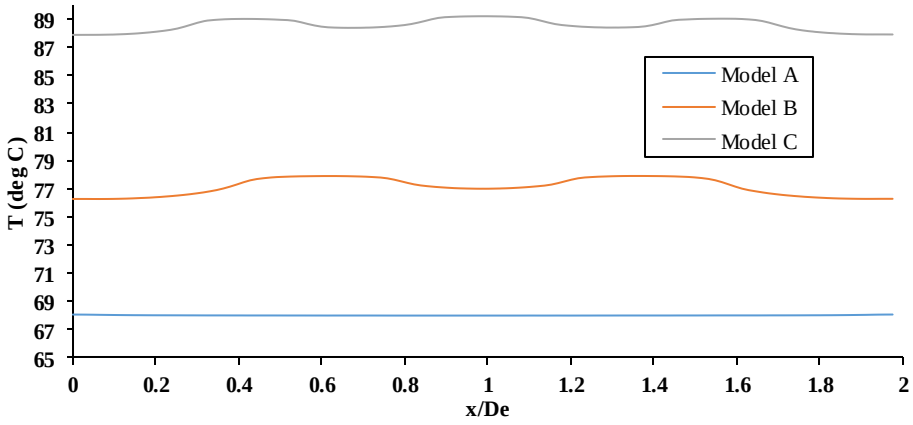

Figure 4.11: Temperature distribution at q"=13.8 W/cm² and Re=902

4.3.2 Local and Average Nusselt Number Distributions

Figures 4.12 and 4.13 show the calculated local Nusselt number variation with the dimensionless flow direction axis at Re= 1353 and 902, respectively. As we can see, the local Nusselt number is high in the entry region and begins to decrease until a constant value is reached when the flow and temperatures become thermally fully developed. This means that, in the entry regions, the local Nusselt number is inversely proportional to the boundary layer thickness. The results revealed that the Nusselt number was higher for model (A) compared to models (B) and (C). The numerical results were in good agreement with the experimental results with a maximum relative error of 3%.

In order to determine the heat transfer performance of aluminum foam models used as a heat sink, the average Nusselt number was obtained using the following equation:

$$Nu_{,avg} = \frac{1}{L}\int_0^L Nu_x \, dx \tag{4.7}$$

Where L represents the channel length and Nu_x represents the local Nusselt number. Figure 4.14 shows the relationship between the average Nusselt number of models (A), (B) and (C) and the Reynolds number. This figure clearly illustrates that the average Nusselt number increases with increases in the Reynolds number for different models. The results also revealed that the average Nusselt number was higher for model (A) compared to models (B) and (C).

The relationship between the average Nusselt number and the Reynolds number was obtained using the following equation:

$$Nu_{,avg} = C \cdot Re^m \tag{4.8}$$

Where C and m are constants listed in Table 4.1 and obtained using the present experimental data of steady water flow through different aluminum foam heat sink models for a given range of Reynolds numbers (Forchheimer regime).

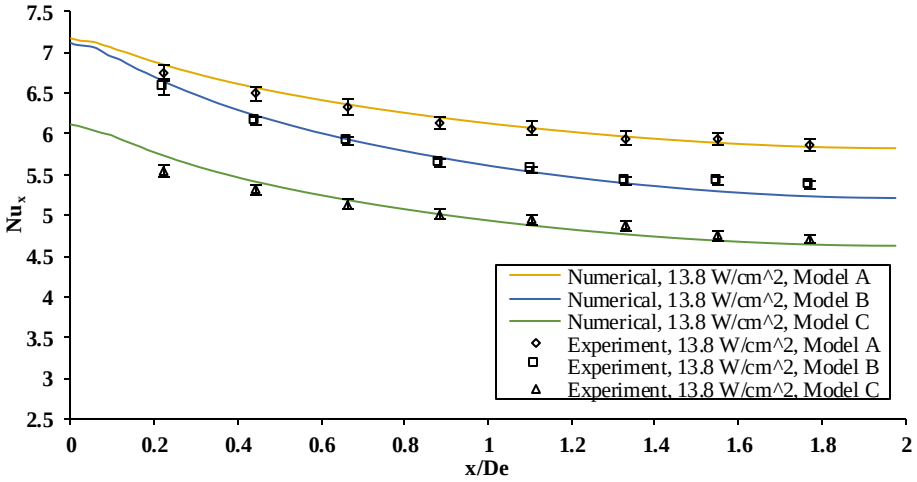

(a) Local Nusselt number distributions at q"=13.8 W/cm^2

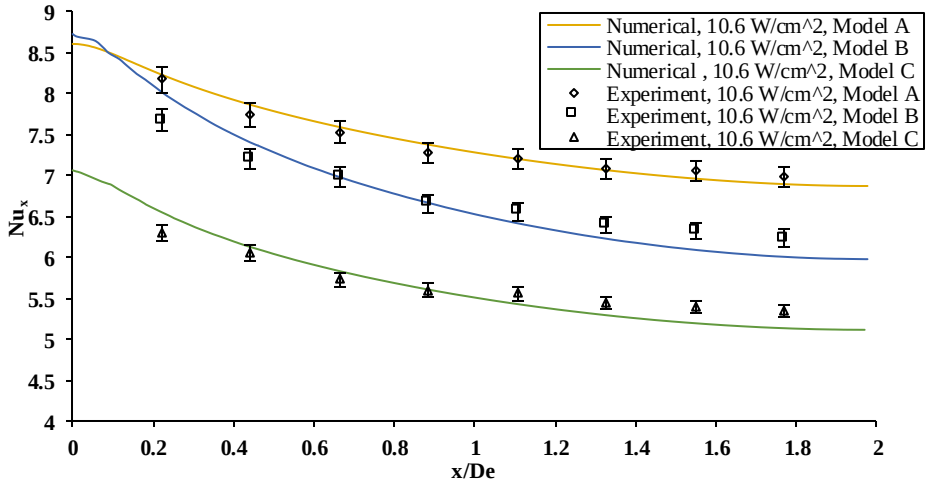

(b) Local Nusselt number distributions at q"=10.6 W/cm^2

Figure 4.12: Experimental and numerical results of Nusselt number at Re=1353

As shown in Figure 4.15, the ratio between the average Nusselt number of model (B) ($Nu_{avg,B}$) and model (A) ($Nu_{avg,A}$) is about 0.9 and the ratio between the average Nusselt number of model (C) ($Nu_{avg,C}$) and model (A) ($Nu_{avg,A}$) is about 0.75. This means that model (B) reduced the heat transfer by 10% and model (C) reduced the heat transfer by 25%.

Introducing channels in the heat sink (models B and C) is supposed to increase the surface area to volume ratio, causing increases in the heat transfer rate. This is in direct contrast with the results obtained in the experiment which revealed that models (B) and (C) reduced the heat transfer rate by 10% and 25%, respectively. In order to find an explanation of this phenomenon, the velocity contours obtained from the finite element.

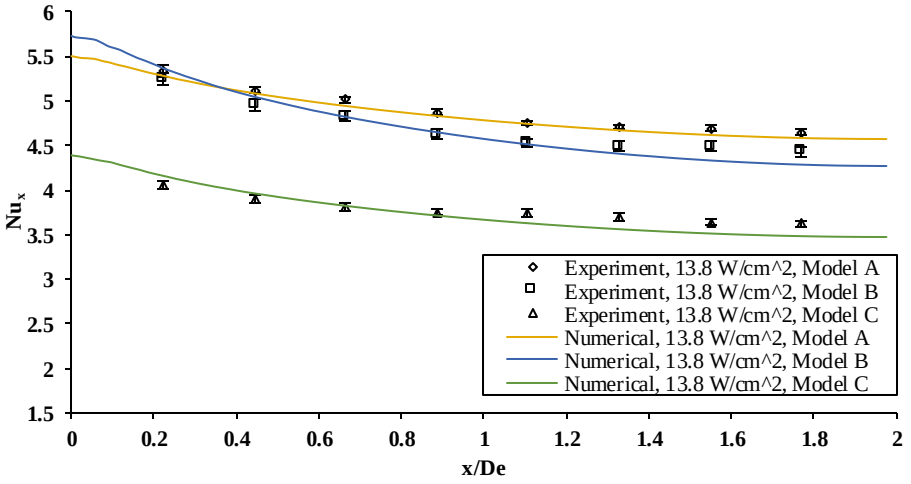

(a) Nusselt number distributions at q"=13.8 W/cm^2

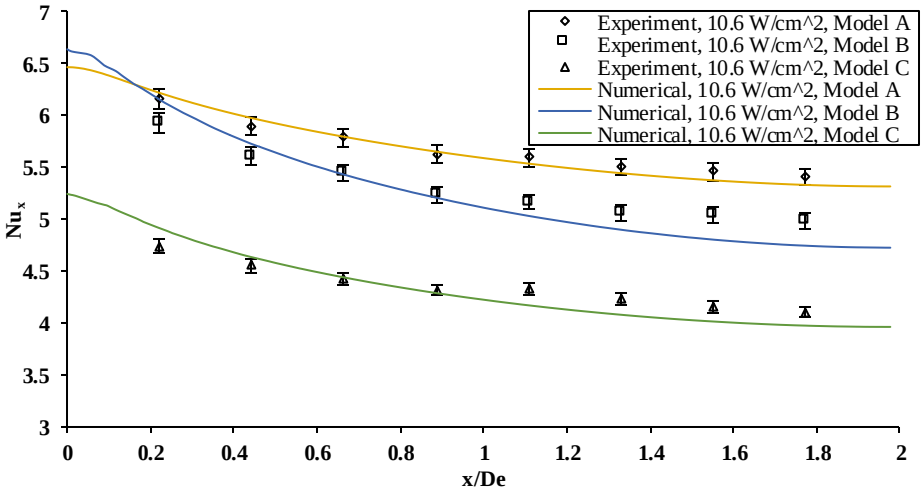

(b) Nusselt number distributions at q"=10.6 W/cm^2

Figure 4.13: Experimental and numerical results of Nusselt number at Re=902

Table 4.1: Average Nusselt Number constants

Heat Sink Models	C	m
Model (A)	0.342	0.41
Model (B)	0.121	0.54
Model (C)	0.1	0.56

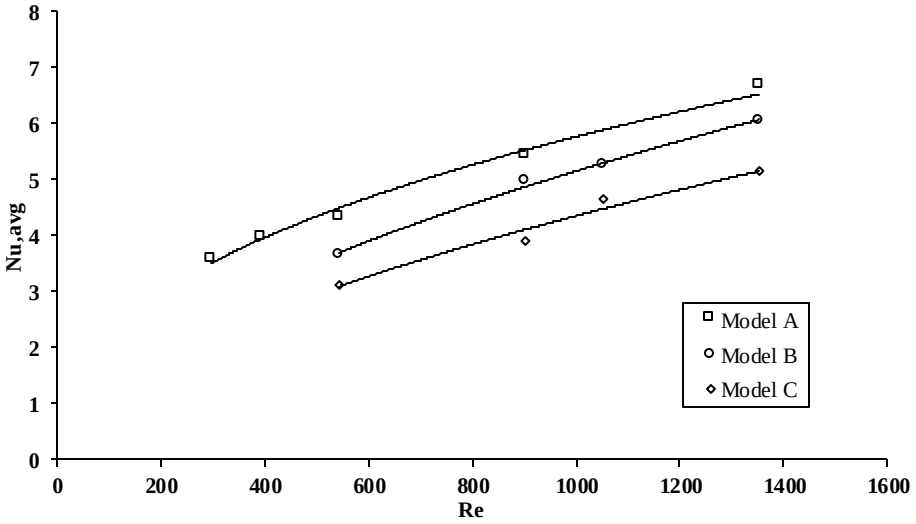

Figure 4.14: Average Nusselt number verses Reynolds number

Figures 4.16 and 4.17 show the velocity contours for models (A), (B) and (C) at q"=13.8 W/cm^2 and Re=1353 and 902, respectively. The results revealed that model (A) has a uniform velocity throughout the aluminum foam heat sink. On the other hand, the velocity contours of models (B) and (C) are different due to the acceleration of the flow inside the channels and a reduction of the water flow rate inside the aluminum foam portion (aluminum foam fin) because of high flow resistance caused by the aluminum foam.

Figure 4.18 shows the velocity profile at Re=1353 in order to provide a better picture of the velocity profiles of the models. The figure illustrates that model (A) achieved a perfect uniform flat velocity profile around 0.07 m/s. The figure also illustrates that models (B) and (C) achieved large parabolic velocity profiles through the channels and lower flat velocity profiles in aluminum foam portion. The same trend was observed in Figure 4.19 at Re=902.

This means that due to the high flow resistance caused by the aluminum foam, around 70% of water flow goes into the empty channel and around 30% of the flow goes into the aluminum foam portion, which causes decreases in the positive effect of the aluminum foam on the heat transfer rate. The velocity profiles of models (B) and (C) also revealed that a larger percentage of the water flow entered the aluminum foam portions of model (B).That is why model (B) achieved a higher heat transfer rate than model (C).

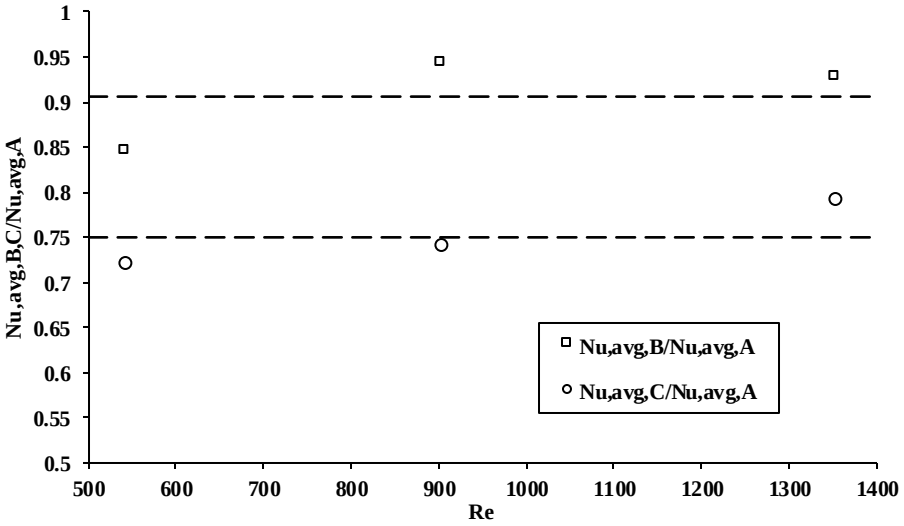

Figure 4.15: Average Nusselt number ratio of model (B) and (C) compared with model (A)

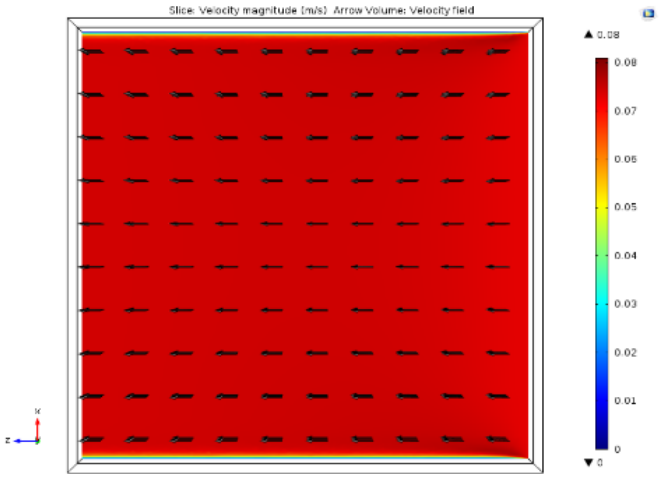

(a) Model (A)

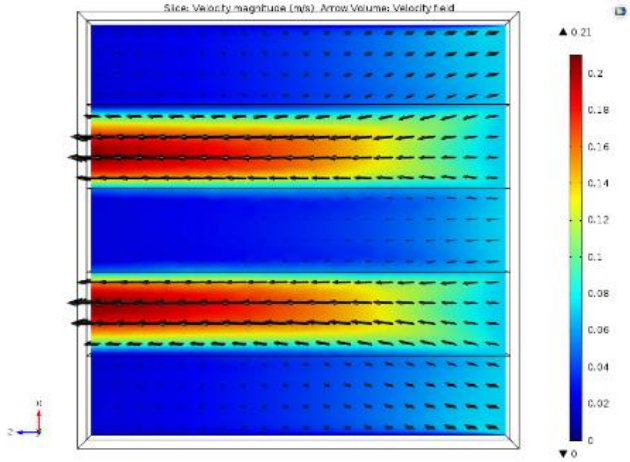

(b) Model (B)

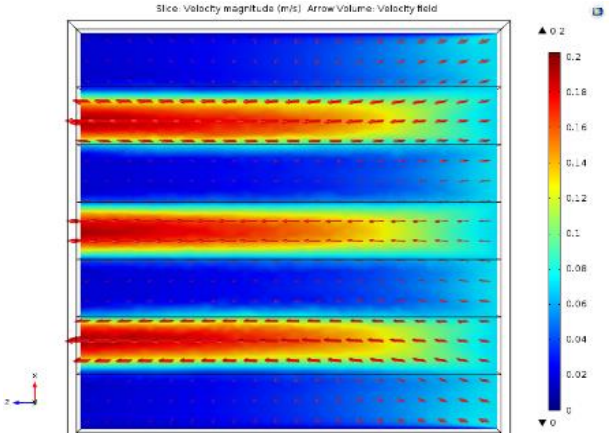

(c) Model C

Figure 4.16: Velocity contours at q"=13.8 W/cm^2, Re=1353

(a) Model (A)

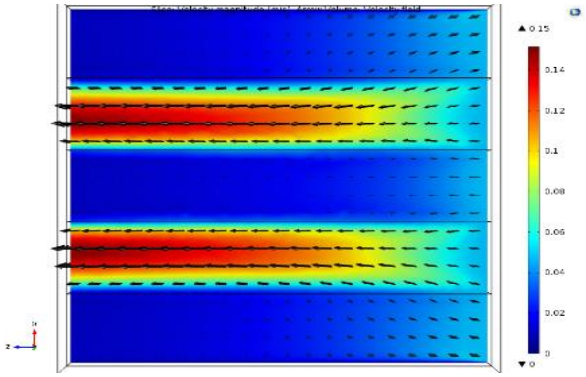

(b) Model (B)

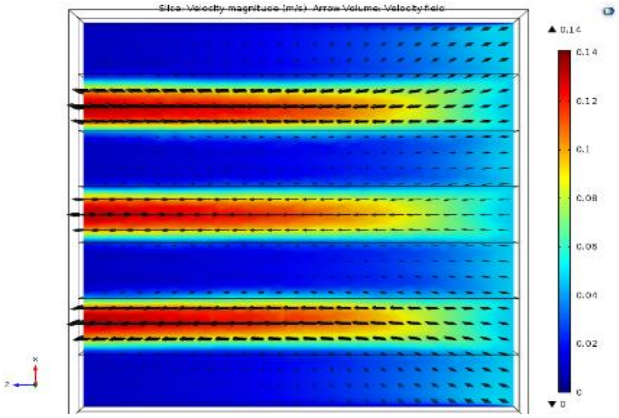

(c) Model (C)

Figure 4.17: Velocity contours at q"=13.8 W/cm^2, Re=902

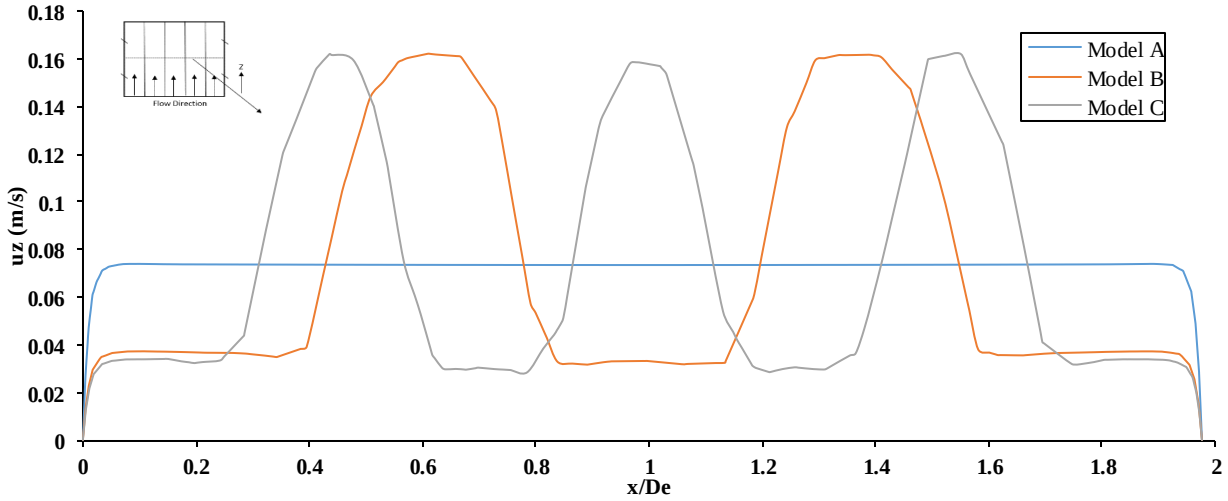

Figure 4.18: Velocity profile at Re= 1353

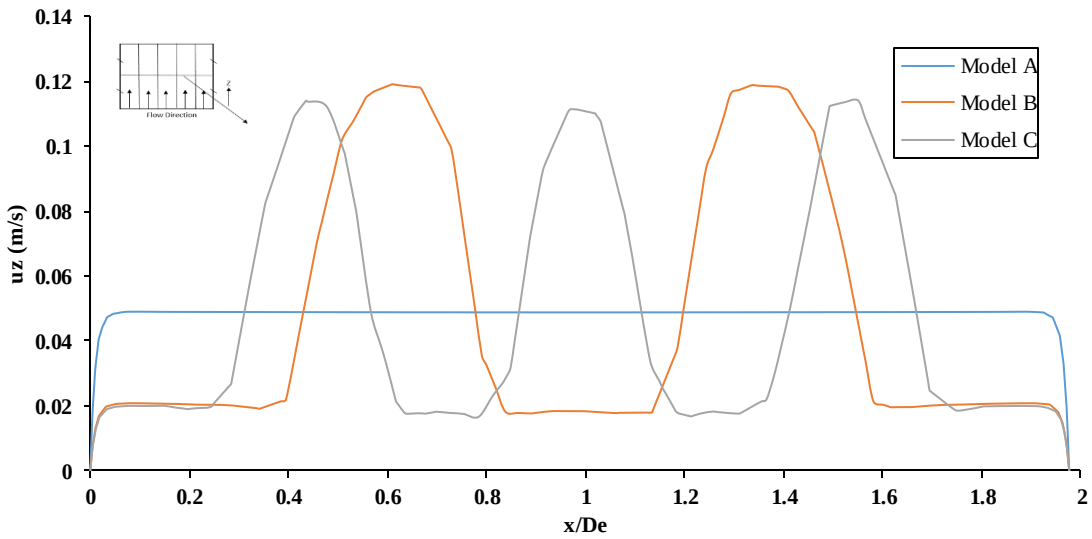

Figure 4.19: Velocity profile at Re=902

On the other hand, the results showed that the percentage of the flow which goes into the aluminum foam portion decreases along with the flow direction. This phenomenon occurs because the fluid particles turn from the aluminum foam portion (high flow resistance) to the empty channel. In order to take a closer look at this phenomenon, a particle tracing study was conducted using the finite element method. The results are displayed in Figure 4.20. As we can see, a portion of the fluid particles (red point) turn from the aluminum fin to the empty channel.

4.3.3 Thermal Performance of the Aluminum Foam Heat Sink Models

In order to evaluate the thermal performance of the aluminum foam heat sink models, the pressure drop across the aluminum foam was measured. Figure 4.21(a) illustrates the pressure drop verses the Reynolds number for models A, B and C. As we can see in this figure, the pressure drop increases along with increases in the Reynolds number and model (A) achieved a higher pressure drop than models (B) and (C) . There was good agreement between the numerical and experimental pressure drop results.

The Fanning friction factor (f) is commonly used to provide information regarding the required pressure drop of the heat exchanger. This is done to ensure that the pressure drop across the foam is non-dimensional. The friction factor of aluminum foam is obtained using the following equation:

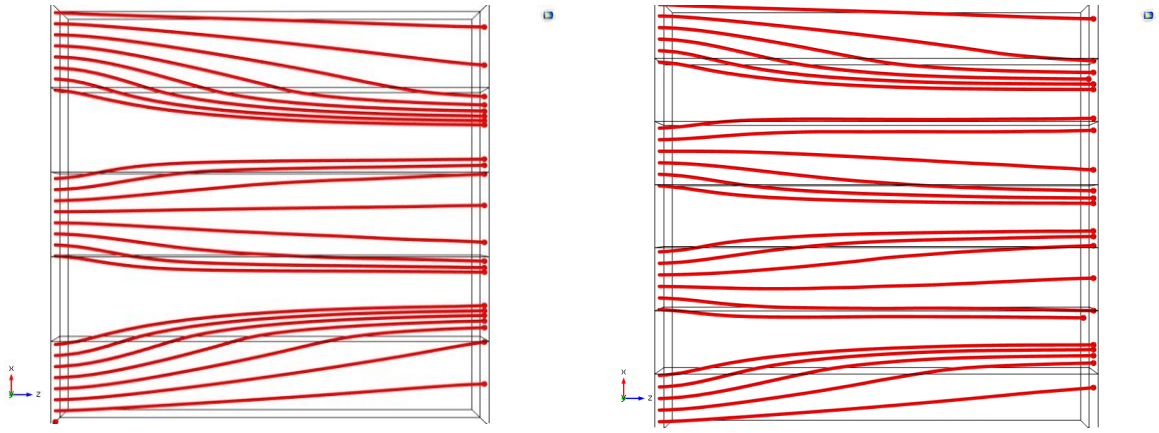

(a) Model (B) (b) Model (C)

Figure 4.20: Fluid flow particle tracing at Re=1353

$$f = \frac{\Delta p}{4\left(\frac{L}{De}\right)\left(\frac{\rho_f U^2}{2}\right)} \tag{4.9}$$

Where L represents the channel length, D_e represents the hydraulic diameter of the channel, ρ_f represents the water density, and U represents the velocity of the fluid. Figure 4.21(b) illustrates the friction factor of the foam verses the Reynolds number.

As we can see from the analysis of the heat transfer characteristics of water flow through the aluminum foam models, the average Nusselt number for all three models increased along with increases in the Reynolds number. This increase is accompanied by an increase in the required pumping power which is due to an increase in the pressure drop across the aluminum foam. In order to combine the heat transfer rate with the pressure drop, the thermal efficiency index is calculated using the following equation:

$$I_{efficiency} = \frac{Nu_{,avg} \cdot L}{f \cdot H} \tag{4.10}$$

Where f represents the Fanning friction factor of the aluminum foam, L represents the channel length, H represents the channel height, and $Nu_{,avg}$ represents the average Nusselt number. The thermal efficiency index combines the heat transfer with the pressure drop across the aluminum foam in order to find the optimal design condition that achieves higher heat transfer with lower pumping power. Figure 4.22 shows the thermal efficiency index verses the Reynolds number. As we can see in this figure, Model (B) achieved a higher thermal efficiency index over the Reynolds number range compared with models (A) and (C) based on the heat transfer rate and required

pumping power. Model (B) achieved a thermal efficiency index of 6.1 at Re=1353, which represents the optimal design condition.

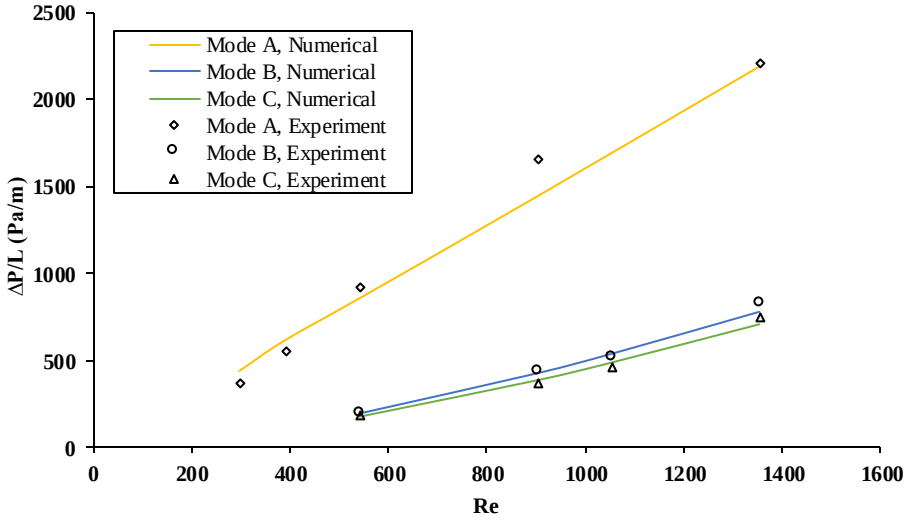

(a) Pressure drop verses Reynold number

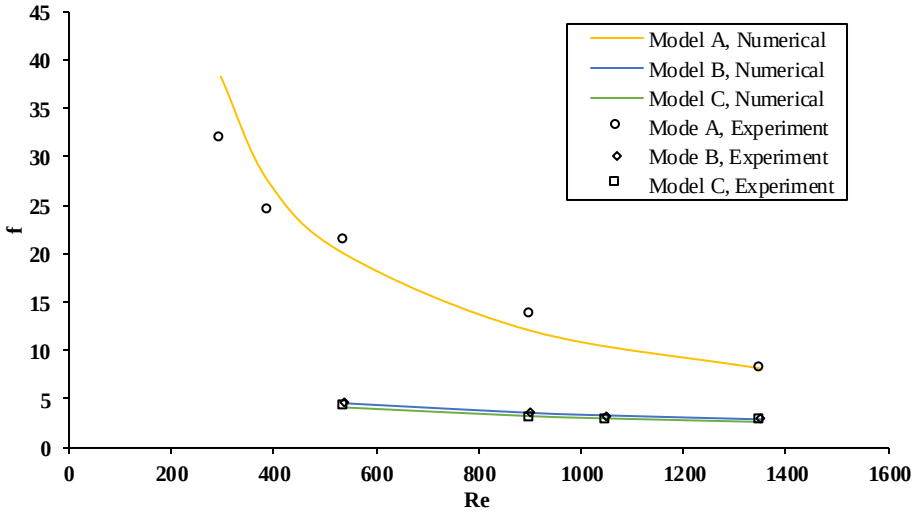

(b) Fanning friction factor verses Reynolds number

Figure 4.21: Pressure drop and Fanning friction factor

4.4 Conclusions

This chapter presented an experimental and numerical study of three different aluminum foam heat sink models in the cooling of electronics. The aluminum foam models were model (A) (without channels), model (B) with two channels and model (C) with three channels. The aluminum foam was subjected to a water flow covering the non-Darcy flow regime. The following conclusions were drawn based on the findings of the study:

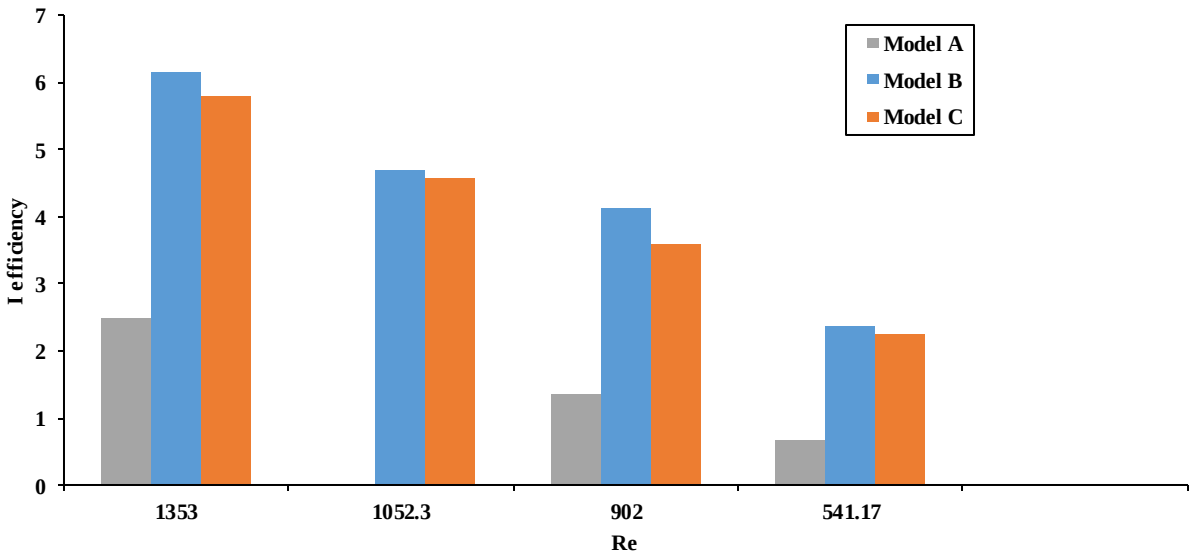

Figure 4.22: Thermal efficiency index verses Reynold number

- The local temperature distributions for models A, B and C increase along with increases in the dimensionless flow direction axis, decreasing the Reynolds number and increasing the heat flux.
- Model (A) achieved a lower local temperature than models (B) and (C)
- The numerical local surface temperature results were in good agreement with the experimental results, with a maximum relative error of 2%.
- At any given Reynolds number, the local Nusselt number is inversely proportional to the boundary layer thickness and reaches a constant value at the fully developed region.
- Model (A) achieved a higher local Nusselt number than model (B), and model (B) achieved a higher local Nusselt number than model (C).
- The numerical results of the local Nusselt number were in good agreement with the experimental results, with a maximum relative error of 3%.
- The average Nusselt number of models A, B and C increases along with increases in the Reynolds number.
- Models (B) and (C) reduced the average Nusselt number by 10% and 25%, respectively, compared to model (A)
- The pressure drop across the foam was measured. The results revealed that the pressure drop increases as the Reynolds number increases.

- The pressure drop across model (A) was higher than the pressure drop across models (B) and (C)
- The thermal efficiency index combines the heat transfer with the pressure drop across the aluminum foam models in order to find the optimal design condition that achieves higher heat transfer with lower pumping power. Model (B) achieved the optimal design condition with a thermal efficiency index of 6.1 at Re= 1353.

CHAPTER 5-ELECTRONIC COOLING USING γ-Al_2O_3 –WATER NANOFLUID FLOW IN ALUMINUM FOAM HEAT SINK

This chapter is based on the following submitted paper:

Bayomy, A. M., Saghir, M. Z., "Experimental Study of Using γ-Al_2O_3–Water Nanofluid Flow through Aluminum Foam Heat Sink: Comparison with Numerical Approach" Int. J. Heat Mass Transfer, vol. 107, pp. 181-203, 2017.

5.1 Introduction

One issue of great importance to the manufacturers of electronic components is the rapid removal of the heat generated by those components using cooling techniques. The lifetime and performance reliability of electronic components are inversely related to surface temperature. The continuous improvements in the design of electronic chips have resulted in an increase in the amount of heat generated per unit of volume.

The two parameters that play a key role in convention heat transfer augmentation are the surface area to volume ratio of the heat sink and the thermal conductivity of the coolant fluid (the coolant fluid's thermal properties). The surface area to volume ratio of heat sinks can be enhanced through the introduction of extended surfaces heat sinks [5-10], or by attaching fins to the heated surface [11].

Open cell porous structures with high thermal conductivity material, such as aluminum or copper metal foams, are now used as heat sinks for different applications. The heat transfer characteristics of metal foam are directly affected by the microstructure properties of the foam as mentioned earlier. These include porosity, relative density, pore density, pore size, ligament diameter, and permeability [54-59].

Some studies have compared the heat transfer performance of metal foams (porous structure) with conventional heat exchangers [60, 61, and 66]. The results revealed that metal foam transfers heat an order of magnitude better than conventional heat exchangers. The majority of the studies concerning the heat characteristics of metal foam and other porous media used air as a working coolant [62-65, 67-69]. A small number of studies used water as a working coolant fluid through metal foams [73-76]. The results of the literature review indicate that the use of porous structures with high thermal conductivity results in a higher heat transfer rate than conventional electronic cooling methods. In addition, the thermal properties of the coolant that is passed through

the porous heat sink play a significant role in enhancing heat transfer. This leads us to the second parameter that plays a key role in conventional heat transfer augmentation: the thermal properties of the coolant fluid.

It is well known that, at room temperature, the thermal conductivity of solid metals is higher than conventional coolant fluids such as air or water. For example, the thermal conductivity of copper is 700 times higher than the thermal conductivity of water. As a result, the thermal conductivity of conventional fluids that contain suspended solid metallic particles is expected to be better than conventional fluids. Maxwell [44] was the first person to disperse millimeter or micrometer sized particles in liquids. He observed that dispersing relatively large metallic particles caused the particles to settle down rapidly, therefore achieving low thermal properties at low particle concentrations. In addition, Maxwell's concept depends on the dispersal of a large number of particles (usually > 10vol%), resulting in high pressure drop and pumping power. Modern technology later allowed for the production of nano-sized metallic particles (less than 100 nm).

Choi [45] was the first to describe a new category of heat transfer fluids: nanofluids. He observed that nanofluids have superior thermal properties when compared to their host fluids or traditional heat transfer coolant fluids. Choi also presented the possibility of increasing the convection heat transfer coefficient by 100% of the nanofluids instead of increasing the pumping power. The goal of using nanofluids is to achieve the highest possible thermal properties at lower nanoparticle concentrations by using a uniform dispersion and stable suspension of nanoparticles in the host fluid. Eastman et al. [94] were the first to experimentally show that copper-ethylene glycol nanofluids lead to a 40% enhancement in thermal conductivity at a nanoparticle concentration of 0.3vol%. They observed that the thermal conductivity of copper nanofluids exceeded the values predicted by the macroscopic theory models [44, 95]. Choi et al. [96] also observed a 150% enhancement in the thermal conductivity of nanotube-oil suspension of particle loading of 1vol%.

Hong et al. [97] observed an enhancement in the thermal conductivity of Fe-ethylene glycol nanofluid. Chopkar et al. [98] observed a 200% enhancement in the thermal conductivity of $Al_{70}Cu_{30}$-ethylene glycol nanofluid at a concentration of 2vol% and a strong non-linear relationship between particle concentration and the thermal conductivity of the nanofluid. Many other studies have demonstrated the enhanced thermal conductivity of nanofluids [99-101], the

strongly temperature dependent thermal conductivity of nanofluids [102, 103], and the higher critical heat flux of nanofluids [104, 105] when compared with the host fluid.

Various studies have focused on obtaining the effective mechanisms for enhanced thermal properties of nanofluids, such as the Brownian motion, temperature, nanoparticle size and nanoparticle concentration. Three theoretical dynamic models [106-108] were developed and all three demonstrated that the Brownian motion of nanoparticles is as a key mechanism in the enhancement of the thermal properties of nanofluids. The influence of nanoparticle concentration, temperature, and size on the effective thermal conductivity of nanofluids were covered in all three models. Prasher et al. [109] demonstrated that the nano-convection caused by the Brownian motion is a primary factor in the enhancement of the thermal properties of nanofluids. Koo and Kleinstreuer [110] showed that the effect of the Brownian motion is much more important than the thermophoretic motion. Although thermal conductivity plays a significant role in the enhancement of the convective heat transfer coefficient of nanofluids, a number of other variables such as density, specific heat and viscosity also play key roles in convective heat transfer.

Various experimental and numerical studies have investigated the forced convective heat transfer of nanofluids [111, 112, and 113]. Xuan and Li [114] found that a 2vol% of copper (Cu) nanoparticles in water increases the heat transfer coefficient by 40%. Ho et al. [115] conducted experimental measurements of the thermo-physical properties of aluminum oxide-water nanofluid. Yang et al [116] found that the addition of 1wt% copper oxide nanoparticles in water lead to optimal heat removal in a heated pipe with micro- grooves. Jabari et al. [117] conducted an experimental study of the heat transfer enhancement of Al_2O_3-water nanofluid using an impingement of a round jet on a circular disk. They observed a 50% enhancement in the heat transfer coefficient at a nanoparticle concentration of 0.0597wt%. In their study, Yousefi et al. [118] observed that at low volume fractions (0.02% and 0.05%), there is a significant enhancement in both the local and average heat transfer coefficients (21.7% and 13.91%, respectively).

Two experimental investigations were conducted using TiO_2-water nanofluids in a jet impingement in a mini-channel heat sink for personal the processor unit cooling of a computer [119, 120]. The results revealed that the average heat transfer coefficient of nanofluids is higher than that of pure water. Various studies have also been conducted on the enhanced convective heat transfer of nanofluids [121-128]. Saghir et al. [129] performed a numerical simulation of Al_2O_3-water nanofluid in a square cavity. The numerical study was performed using both the single phase

and multi-phase (Eular-Eular) techniques. There was good agreement between the numerical results and the experimental data presented by Ho et al. [115]. They also observed that the single phase technique predicted the heat transfer with better accuracy than the multi-phase technique.

After looking at the information above, it could be concluded that using nanofluids instead of conventional heat transfer fluids would lead to higher convective heat transfer coefficients, higher thermal properties of the working fluid, and a small penalty of increasing the pressure drop [130]. The convective heat transfer of nanofluids through metal foam is a promising technique for compact cooling issues such as electronic cooling because it combines the higher heat transfer rate of metal foam due to high flow diffusion, high surface area to volume ratio and high thermal conductivity with the superior thermal properties of nanofluids.

Few experimental and numerical studies have been conducted in this area [131-134]. Hajipour and Molaei [135] conducted an experimental and numerical study of heat transfer enhancement due to the presence of the nanofluids in a vertical channel filled with a porous material. In their study, Behabadi et al. [136] found that the presence of Al_2O_3-water nanofluid in metal foam enhanced the heat transfer. Nazari et al. [137] conducted an experimental study of the convective heat transfer of aluminum oxide–water nanofluid through a pipe filled with metal foam. They observed a significant enhancement in the heat transfer.

To the best knowledge of the author, studies of the convective heat transfer of nanofluids through metal foams are very scarce and incomplete; therefore, this chapter presents an experimental and numerical study of ERG aluminum metal foam as a heat sink in the application of electronics cooling. The aluminum foam was subjected to a γ-Al_2O_3-water nanofluid laminar flow. The investigation was performed using a Reynolds number range between 210-631 (Forchheimer flow regime) and a heat flux range between 8.5 to 13.8 W/cm^2 [2, 3, and 53]. The dimensionless local temperature distributions along the heater surface (electronic surface) were measured and the local Nusselt number distributions along the surface were calculated. The optimum volume fraction of γ-Al_2O_3 nanoparticles was obtained. In addition, an empirical correlation of the average Nusselt number of the pulsating flow was developed as a function of the nanofluid's Reynolds number, Prandtl number and nanoparticle volume fractions.

5.2 Experimental Apparatus and Procedures

The previous experimental setup was used to examine the convective heat transfer characteristics of aluminum oxide γ-Al_2O_3-water nanofluid through an ERG aluminum foam heat sink in the cooling of electronics. The experiments were performed using a Reynolds number range between 210 and 631, which covers the non-Darcy laminar flow regime (Forchheimer flow regime) [138], and a heat flux range between 13.8 and 8.5W/cm^2.

5.2.1 Test Section and Experimental Facility

The experimental setup as well as the test section facilities were previously mentioned in section 2.2.1. All of the signals from the thermocouples and the flow meter were connected to a data acquisition system to monitor the experimental data in order to ensure that the experiment reached a steady state condition. The bonding between the ERG foam and heater surface was made by a carbon micro particle compound which causes extremely high thermal conductivity. The ERG aluminum foam heat sink is shown in Figure 5.1.

Figure 5.1: ERG aluminum foam heat sink

5.2.2 Uncertainty Analysis

Based on the uncertainties of the temperature and flow rate (mentioned in section 2.2.2), the uncertainties of (Nu_x), ($Nu_{,avg}$) and (Re) were obtained using the Taylor method [81]. The uncertainties of the local and average Nusselt number were used to evaluate the error bars for each data point in section 5.4. The maximum value of the uncertainty of the local and average Nusselt number were $\pm 1.8\%$ and $\pm 1.5\%$, respectively. In addition, the uncertainty of the Reynolds number was 0.44%.

5.2.3 Preparation and Specification of the Nanofluid

The stability and dispersion behaviour of nanofluids play a key role in the enhancement of the thermal properties. This depends on several factors such as particle size, particle concentration and the dispersion phases. The stable suspension of nanoparticles in conventional fluids is produced by two common methods: the two step and single step techniques. In the two step technique, the nano-powder is prepared in nano-scale size, mixed in the base fluid, and stabilized using a dispersion technique such as the high shear or ultrasound mixer.

Most of nanofluids prepared using the two step technique are a challenge because the individual nanoparticles quickly agglomerate due to the high attractive forces between them and settle down in the host fluid. Jaberi et al. [117] reported that although the agglomerated nanoparticles were ultrasonically dispersed in the host fluid, the nanoparticles quickly re-clustered and settled down. Therefore, the suspension of non-agglomerated or monodispersed nanoparticles is the key parameter in enhancing the thermal properties of nanofluids. In the single step technique, nanoparticles are formed and dispersed in the host fluid in a single process [46, 139]. In this technique, the drying and dispersion of nanoparticles is eliminated, reducing the chance of particle agglomeration.

In the present study, 5 Kg of γ-Al_2O_3-water nanofluid prepared by MKnano using the one step technique with a nanoparticle concentration of 20 wt% and average particle size (APS) of 50 nm, was used, as shown in Figure 5.2(a). The highly concentrated pre-prepared γ-Al_2O_3-water nanofluid was examined and stored for one week before making the diluted samples in order to ensure the stability of the nanofluid. There was no visible sign of nanoparticle sedimentation. When preparing the experimental samples, distilled water was used to dilute the highly concentrated nanofluid in order to achieve the required concentrations. Each sample was then mixed using a magnetic mixer in order to ensure the stability and uniformity of the nanoparticles for each sample, as shown in figure 5.2(b).

(a)

(b)

Figure 5.2: γ-Al_2O_3-water nanofluid preparation

Five different γ-Al_2O_3-water nanofluid concentrations were prepared (0.1, 0.2, 0.3, 0.4 and 0.6vol%), as shown in Figure 5.3. Each sample was stored at least 48hrs in order to ensure the stability of the suspension. The physical properties of the γ-Al_2O_3 nanoparticles are shown in Table 5.1.

Figure 5.3: prepared γ-Al_2O_3-water nanofluid in five different concentrations

Table 5.1: Physical properties of γ-Al_2O_3 nanoparticles

Particle size (APS)	50 nm
Density (ρ_p)	3600 Kg/m^3
Specific Heat (Cp_p)	0.765 KJ/Kg.K
Thermal Conductivity (k_p)	40 W/m.K
Expansion Coefficient (β_p)	8.46e-6 1/K

5.3 Numerical Model Description

Numerical results were obtained using the finite element method [78] and a single phase technique in order to allow for a comparison with the experimental data.

5.3.1 Governing Equations

Based on finite element modeling assumptions (mentioned in section 2.3.1), the Brinkman-Forchheimer equation and energy equation which describe the nanofluid fluid flow and heat transfer inside porous media are solved using the following formula:

$$\frac{\rho_{nf}}{\varepsilon}\left(\frac{\partial U}{\partial t}+(U.\nabla)\frac{U}{\varepsilon}\right)=\nabla.(-pI+\frac{\mu_{nf}}{\varepsilon}(\nabla U+(\nabla U)^T))-(\frac{\mu_{nf}}{K}+\beta_f|U|)U+F \quad (5.1)$$

$$\nabla.(\rho_{nf}U)=0 \quad (5.2)$$

$$(\rho c_p)_{eff}\frac{\partial T}{\partial t}+\left(\rho c_p\right)_{nf}U.\nabla T=\nabla.(k_{eff}.\nabla T) \quad (5.3)$$

Where ρ_{nf} represents nanofluid density, $\left(c_p\right)_{nf}$ represents nanofluid specific heat, ε represents the porosity of the ERG aluminum foam, p represents the pressure, U represents the velocity field vector, β_f represents the Forchheimer coefficient, T represents the temperature, μ_{nf} represents fluid dynamic viscosity, K represents the permeability of the ERG aluminum foam , k_{eff} represents the effective thermal conductivity of the ERG aluminum metal foam saturated by the nanofluid and $(\rho c_p)_{eff}=\varepsilon\cdot\left(\rho c_p\right)_{nf}+(1-\varepsilon)\cdot(\rho c_p)_s$.

The thermo-physical properties of the nanofluid were obtained from Ho et al. [115], who examined the thermo-physical properties of aluminum oxide-water nanofluid in a square cavity. In addition, correlations of the thermos-physical properties of aluminum oxide-water nanofluid as a function of the propertied of the host fluid and the volume fraction of the nanoparticles were

developed and compared with previous experimental and theoretical models [82-84]. The thermos-physical properties of γ-Al_2O_3-water nanofluid were calculated based on the following correlations:

$$\frac{\mu_{nf}}{\mu_{bf}} = 1 + 4.93 \cdot C_v + 222.4 \cdot C_v^2 \quad (5.4)$$

$$\rho_{nf} = C_v \cdot \rho_p + (1 - C_v) \cdot \rho_{bf} \quad (5.5)$$

$$\rho_{nf} \cdot c_{p_{nf}} = C_v \cdot \rho_p \cdot c_{p_p} + (1 - C_v) \cdot \rho_{bf} \cdot c_{p_{bf}} \quad (5.6)$$

$$\frac{k_{nf}}{k_{bf}} = 1 + 2.944 \cdot C_v + 19.672 \cdot C_v^2 \quad (5.7)$$

Where C_v represents the volume fraction of nanoparticles in the host fluid. The thermo-physical properties of γ-Al_2O_3-water nanofluid at 20°C (at inlet portion) and nanoparticle volume fractions of 0, 0.1, 0.2, 0.3, 0.4 and 0.6vol% are shown in table 5.2. It is important to note that the any variations in these properties with the temperature were taken into consideration in the numerical model.

Table 5.2: Thermo-physical properties of γ-Al_2O_3-water nanofluid for different nanoparticle concentrations

C_v (%)	μ_{nf} (kg/m.s)	ρ_{nf} (Kg/m^3)	Cp_{nf} (J/Kg.K)	k_{nf} (W/m.K)	Pr (Prandtl number)
0	0.001002	998.2	4182	0.613	6.8358303
0.1	0.001007	1000.802	4169.708655	0.614817	6.8306128
0.2	0.001013	1003.404	4157.481053	0.616658	6.8280628
0.3	0.001019	1006.005	4145.316698	0.618523	6.8281311
0.4	0.001025	1008.607	4133.215101	0.620412	6.8307691
0.6	0.00104	1013.811	4109.19825	0.624262	6.84356

5.3.2 Boundary Conditions

Boundary conditions can be concluded by inlet temperature and velocity (flat profile) at inlet portion, open boundary at outlet portion and heat flux at bottom as mentioned previously in section 2.3.3(see Figure 5.4).

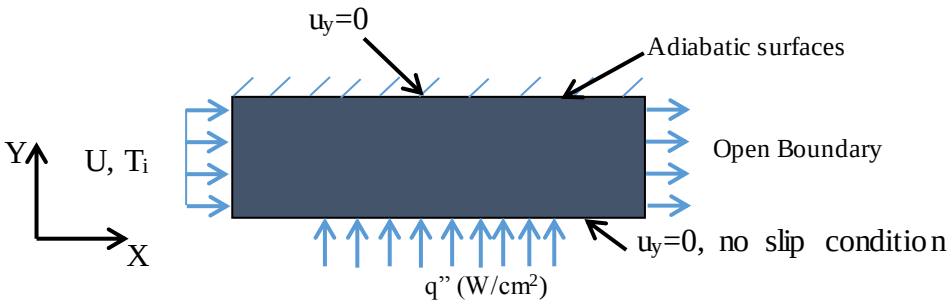

Figure 5.4: Boundary conditions

5.3.3 Mesh Sensitivity Analysis

A triangular element was employed to describe the numerical model. A mentioned in section 3.2.2, the maximum temperature and local Nusselt number on the heated surface were obtained for different numbers of domain elements, as shown in Figure 5.5(a). The number of elements used was 31901 at which the variation was less than 0.001. The shape of the mesh at triangular element 31901 is shown in Figure 5.5(b).

5.4 Results and Discussion

In this experimental study, an ERG aluminum foam heat sink was subjected to a uniform heat flux ranging from 13.8 to 8.5W/cm^2. The γ-Al_2O_3-water nanofluid flow covered the Forchheimer regime (Reynolds numbers ranged from 210 to 630). The nanoparticle concentrations ranged from 0.1vol% to 0.6vol%. In addition, a numerical model was developed and compared to the experimental results.

Figure 5.6 and 5.7 show the dimensionless surface temperature distributions at γ-Al_2O_3 particle volume fractions of 0, 0.1, 0.2, 0.3 and 0.4vol% through the aluminum foam for different Reynolds numbers and heat flux q"= 13.8, 10.6 and 8.5 W/cm^2, respectively. In addition, in order to obtain the effect of inserting the aluminum foam, the dimensionless surface temperature distribution of pure water flow through an empty channel is presented.

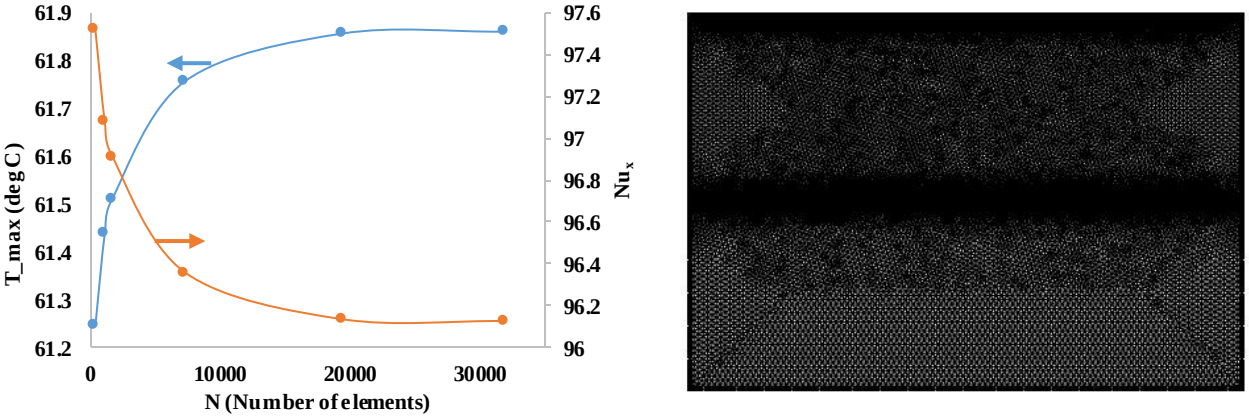

(a) Mesh independent

(b) Finite element model

Figure 5.5: Mesh sensitivity and finite element model

As we can see, at a given γ-Al_2O_3 particle volume fraction, the surface temperature shows an increase in the flow direction until it reaches a constant slope in the thermally fully developed region. The results also showed that the surface temperature decreases as the Reynolds numbers increase. The results also revealed that the average surface temperature is higher for the empty channel compared with the aluminum foam filled channel. This means that using an ERG aluminum foam filled channel reduces the average surface temperature due to a large surface area to volume ratio and positive effect in the fluid mixing provided by the foam.

The results also revealed that the average surface temperature decreases with increases in the γ-Al_2O_3 particle volume fractions until C_v=0.2% is reached. At that time, there was a sudden sharp decrease in the average surface temperature, followed by a small positive effect on the average surface temperature at nanoparticle volume fractions from 0.3% to 0.4%.

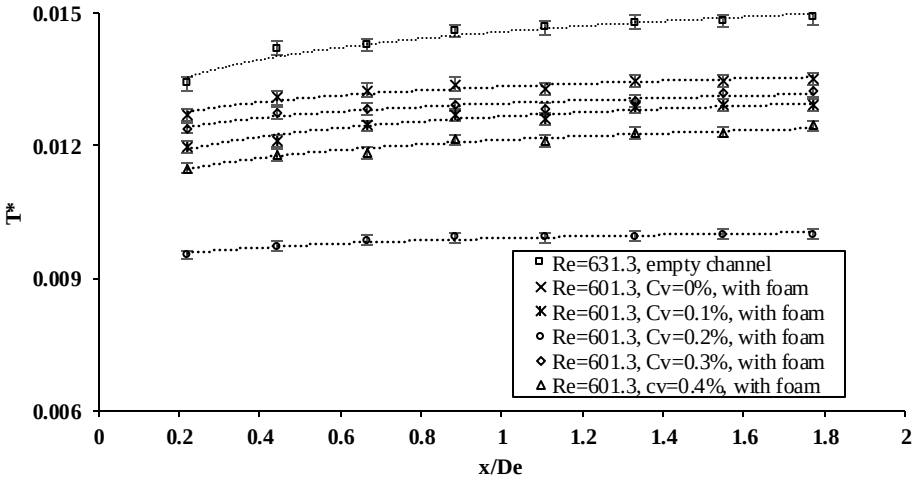

(a) Dimensionless surface temperature distribution at q"=13.8 W/cm^2, Re=601.3

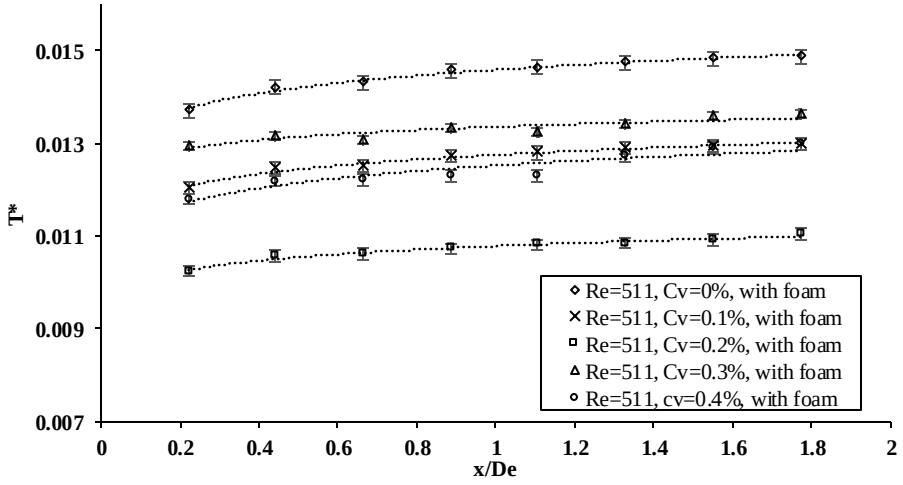

(b) Dimensionless temperature surface distribution at q"=13.8 W/cm^2, Re=511

Figure 5.6: Dimensionless surface temperature at q"=13.8W/cm^2

Figures 5.8 and 5.9 show the local Nusselt number distributions for different γ-Al_2O_3 particle volume fractions and Reynolds numbers of 601 and 511, respectively. The local Nusselt number was calculated based on the local surface temperature and inlet bulk temperature of the nanofluid. As we can see, at given nanoparticle loading, the local Nusselt number is high at the beginning of the channel and starts to decrease until it reaches an almost constant value when the flow becomes thermally fully developed. The results revealed that the highest local Nusselt number is achieved at a γ-Al_2O_3 particle loading of 0.2vol%. This means that the optimum nanoparticle loading, at which the highest heat transfer rate is achieved, was at 0.2vol% in this study. This phenomenon was previously observed by Jaberi et al. [117] who used a nanofluid

round jet on a circular disk, Yousefi et al. [118] who used a nanofluid planar jet on a V-shaped plate, and Yang et al. [116] who used nanofluids in a heated pipe with micro-grooves.

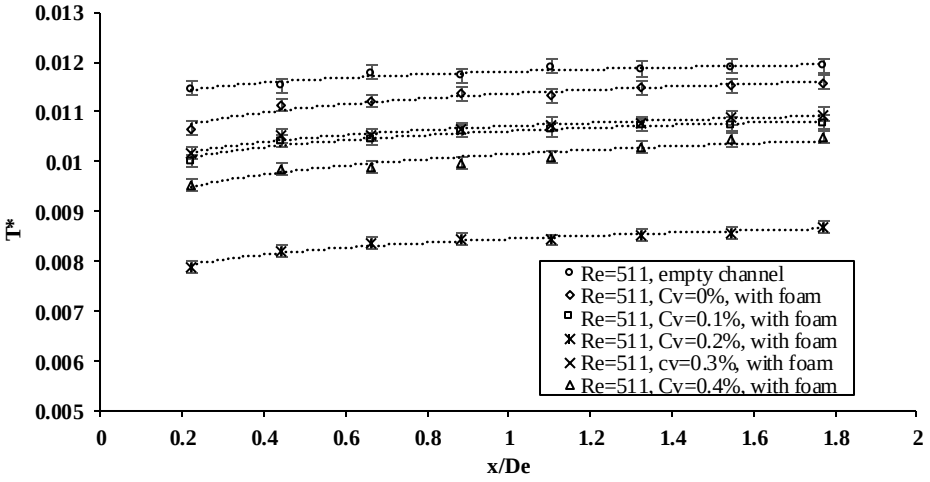

(a) Dimensionless temperature distribution over the surface at q"=10.6 W/cm^2, Re=511

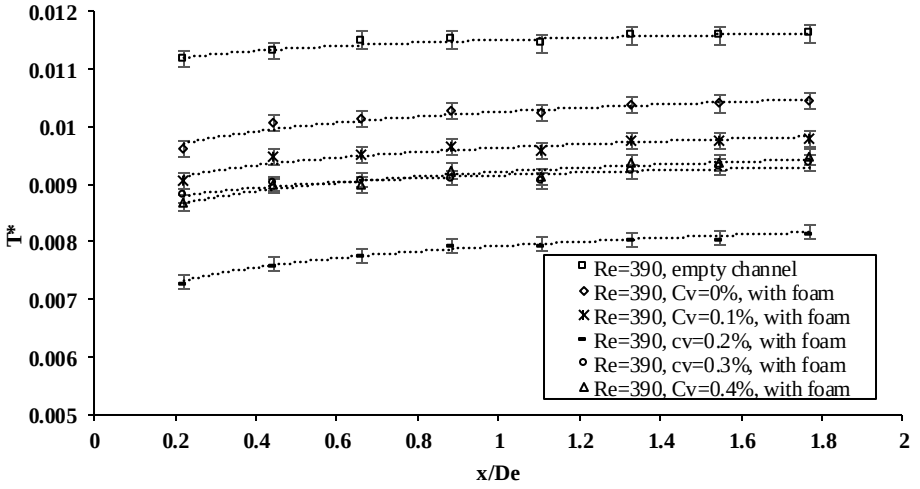

(b) Dimensionless temperature distribution over the surface at q"=8.5 W/cm^2, Re=390

Figure 5.7: Dimensionless surface temperature at q"=10.6W/cm^2 and 8.5 W/cm^2

As we can see from Figure 5.10, there is a sharp increase in the local Nusselt number at a nanoparticle volume fraction of 0.2vol% for various Reynolds numbers as well as axial positions (x/D_e). The average enhancement percentage of 0.2vol% γ-Al_2O_3-water nanofluid was 31% compared to pure water. On the other hand, for the nanofluid containing higher volume fractions of 0.3vol% to 0.6vol%, there was a small positive effect on the local Nusselt number (by 5% as an average enhancement) compared with pure water. In addition, the enhancement percentages in the local Nusselt number of 0.2vol% γ-Al_2O_3-water nanofluid increases gradually with increases in the Reynolds number at a given axial position, as shown in Figure 5.10.

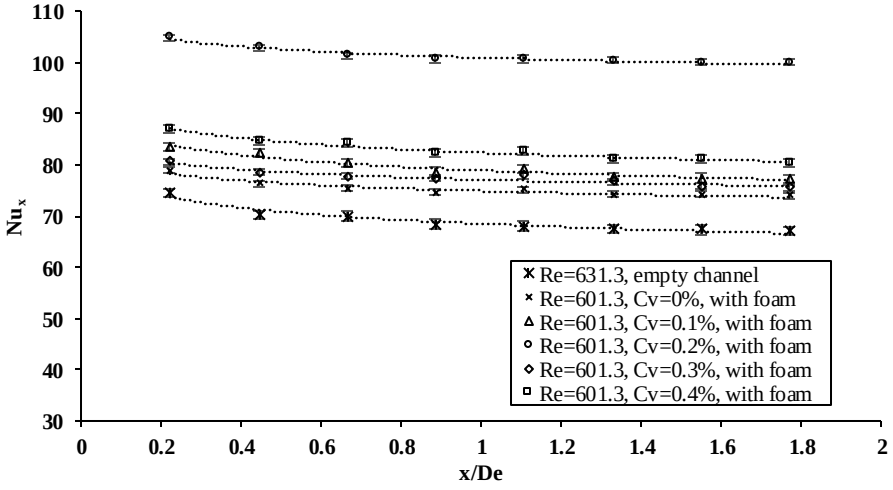

(a) Local Nusselt number distribution at q"=13.8 W/cm^2

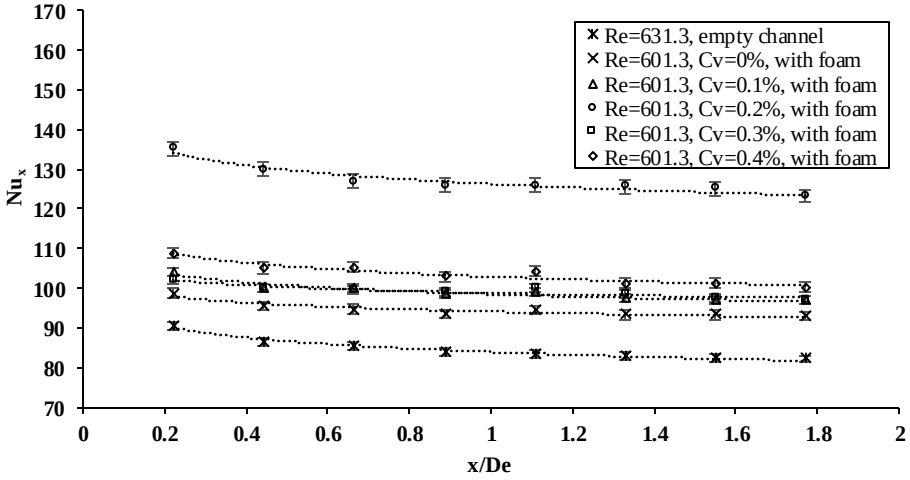

(b) Local Nusselt number distributions at q"=10.6 W/cm^2

Figure 5.8: Local Nusselt number distributions at Re=601.3

Upon closer observation of the distributions of the local Nusselt number, it was found that at given Reynolds number, the enhancement percentage in the local Nusselt number of 0.2vol% γ-Al_2O_3-water nanofluid decreases along with the axial distant (x/D_e), as shown in Figure 5.11. As we can see from this Figure, at Re=601.3, the enhancement percentage of 0.2vol% nanofluid at x/D_e =0.22 is 45% and starts to decrease along with the axial distant until it reaches 39% at x/D_e=1.77. The same observation was made at Re= 511 where the enhancement percentage is 39 % at x/D_e=0.22 and starts to decrease until it reaches 36% at x/D_e=1.77. The same trend was observed for entire range of Reynold numbers.

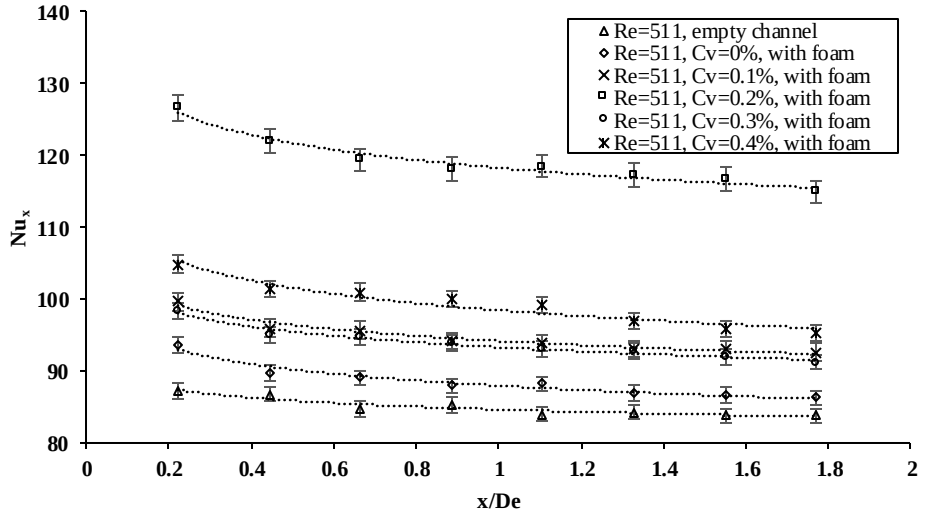

Figure 5.9: Local Nusselt number distributions at q"=10.6W/cm², Re=511

The results indicate that the enhancement percentage in the local Nusselt number of the optimum concentration of the γ-Al_2O_3-water nanofluid ranged from 45% to 20% (depending on the Reynolds number) at the entrance of the channel, and decreased to a range between 40% and 15% at the end of the channel. This means that the percentage of enhancement in the local Nusselt number, as a result of an optimal concentration of the nanofluid, is higher in the entry region compared to the fully developed region.

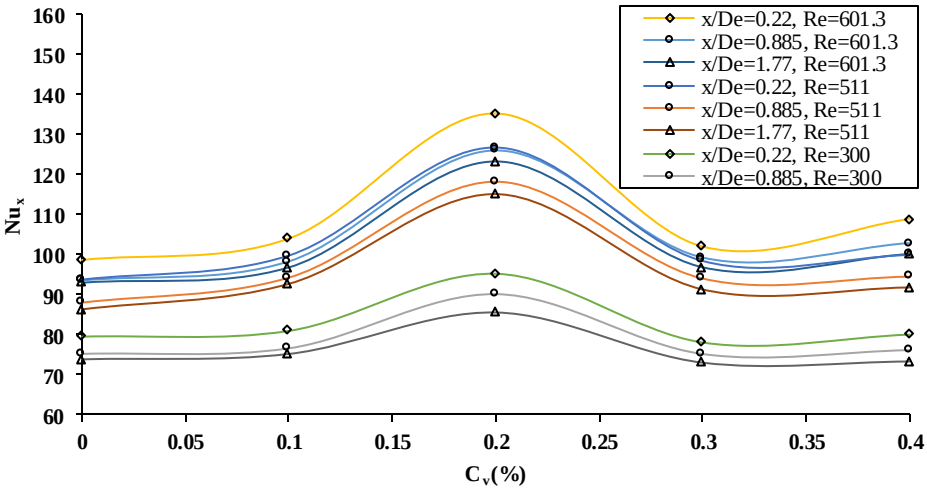

Figure 5.10: Local Nusselt number at different axial locations and Reynolds numbers

In order to complement the experimental results, a numerical model was developed using the finite element technique [77]. Figures 5.12 to 5.16 show the experimental and numerical results for the surface temperature and local Nusselt number of different heat flux and Reynolds numbers

at particle loading of 0, 0.1, 0.2, 0.3, and 0.6 vol%, respectively. The results revealed that surface temperature increases with increases in the heat flux.

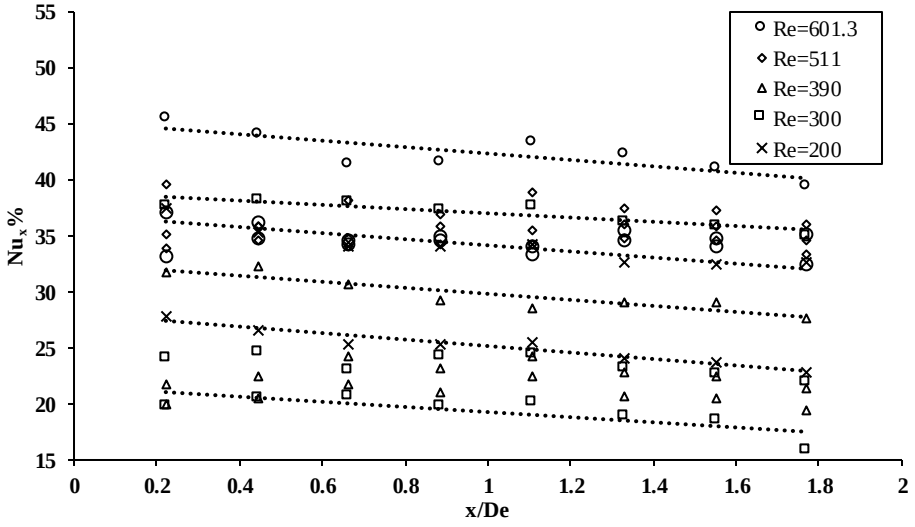

Figure 5.11: Enhancement percentages of local Nusselt number at C_v=0.2% compared with pure water

On the other hand, the results revealed that the local Nusselt number increases along with decreases in the heat flux for a given Reynolds number and nanoparticle volume fraction. The numerical results of the surface temperatures and local Nusselt numbers were both in good agreement with the experimental results with a maximum relative error of 2% and 3%, respectively.

Figure 5.17 (a) shows the velocity contours at a particle loading of 0.2vol% and Re=601.3. This figure illustrates the hydrodynamic boundary layer growth at the boundary (no slip condition). Figure 5.17(b) shows the magnification of the boundary layer growth shape.

Figure 5.18 shows the numerical variation of the local Nusselt number versus the nanoparticle volume fraction (C_v%) at x/D_e = 0.22 and 1.77 (which represent the beginning and the end of the channel), in comparison with the experimental data. The results revealed a sharp peak in the local Nusselt number at a particle loading of 0.2vol% and a small positive effect for nanofluids with higher particle concentrations. The numerical results were also in good agreement with the experimental results.

The temperature contours at q"=13.8 W/cm^2 and particle loadings of 0, 0.1, 0.2, 0.3, 0.4 and 0.6vol% are shown in Figure 5.19. As we can see from this figure, the surface temperature

increases along with the axial distant, and the 0.2vol% γ-Al_2O_3-water nanofluid achieved lower surface temperatures than the other volume fractions.

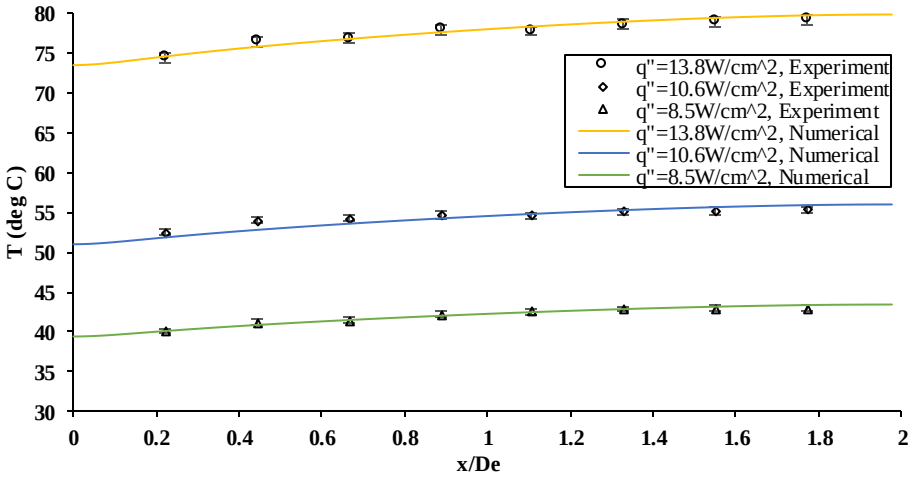

(a) Surface temperature distribution at C_v= 0%

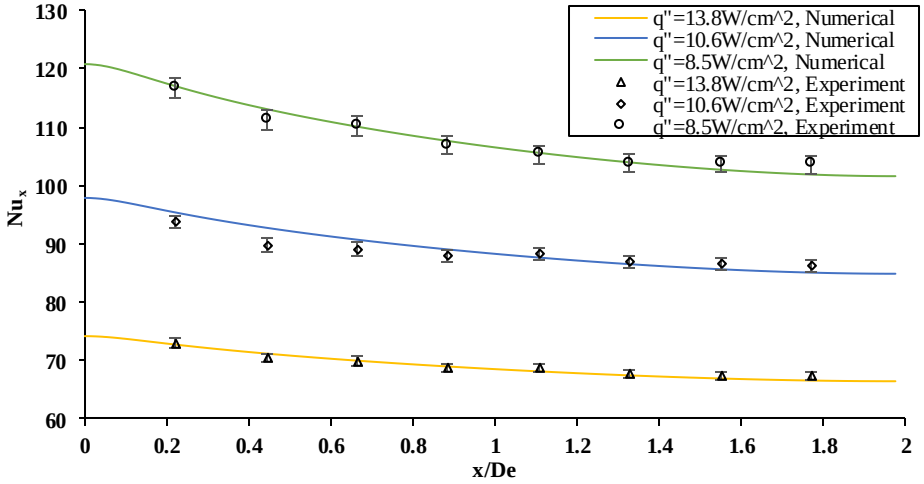

(b) Local Nusselt number distribution at C_v= 0%

Figure 5.12: Experimental and numerical surface temperature and local Nusselt number at C_v= 0% and Re= 511

In order to evaluate the heat transfer performance of the ERG aluminum foam heat sink subjected to γ-Al_2O_3-water nanofluid, the average Nusselt number was obtained. Figure 5.20(a) shows the variation in the average Nusselt number with respect to the Reynolds and Prandtl numbers of the ERG aluminum foam filled channel compared with the empty channel when subjected to the water flow. The figure illustrates that the average Nusselt number increases along with increases in the Reynolds number for both the empty and foam filled channels. The results

also revealed a 20% enhancement in the average Nusselt number when using the aluminum foam filled channel.

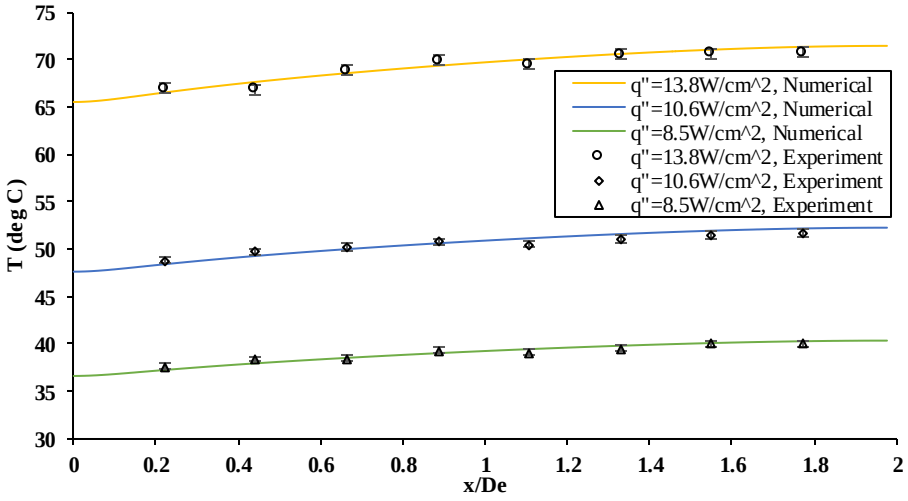

(a) Surface temperature distributions at C_v= 0.1%

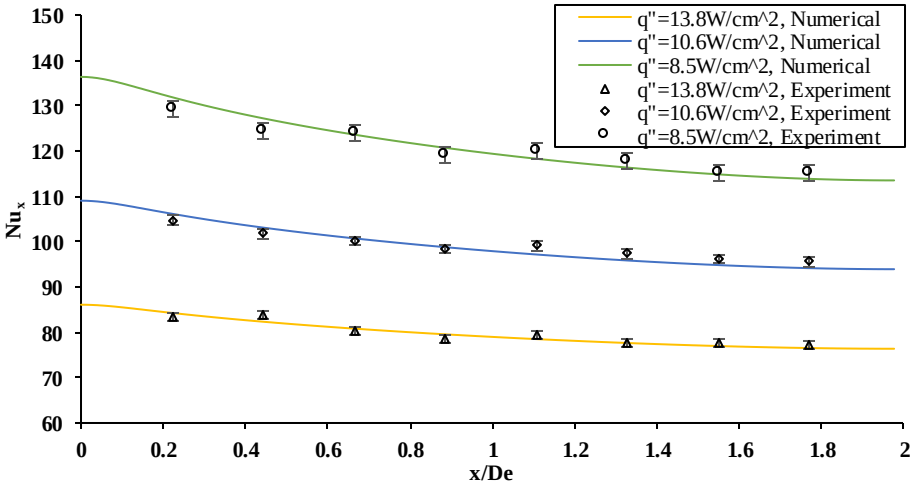

(b) Local Nusselt number distribution at C_v= 0.1%

Figure 5.13: Experimental and numerical surface temperature and local Nusselt number at C_v= 0.1% and Re=601.3

Figure 5.20(b) shows the average Nusselt number versus the Reynolds and Prandtl numbers for various nanoparticle volume fractions, allowing us to further investigate the effect of the presence of γ-Al_2O_3 nanoparticles in the base fluid (water). The results revealed an increase in the average Nusselt number of both the pure water and nanofluid (at various nanoparticle concentrations) through the aluminum foam channel with increasing Reynolds numbers. The presence of 0.2vol% of γ-Al_2O_3 nanoparticles yielded a higher average Nusselt number compared to pure water and other nanoparticle concentrations. The results also revealed a small positive

effect of γ-Al_2O_3-water nanofluid volume fractions of 0.1vol%, 0.3vol%, 0.4vol% and 0.6vol% compared to pure water.

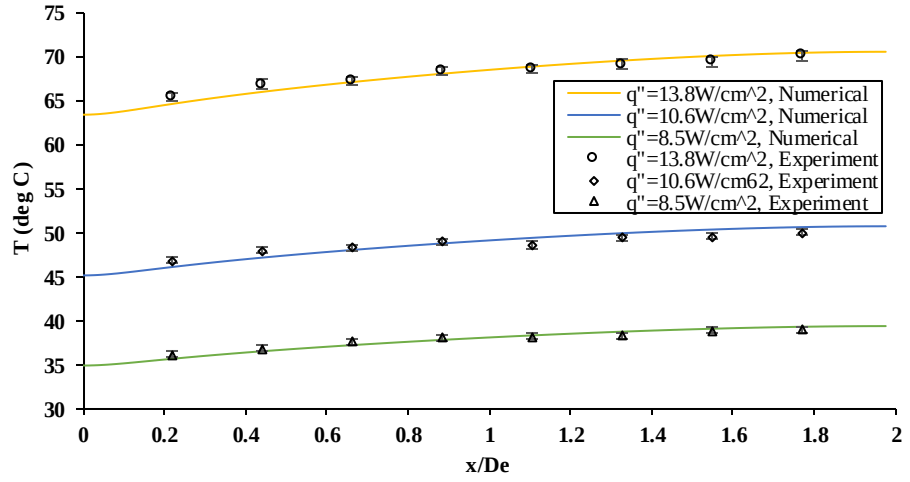

(a) Surface temperature distributions at C_v= 0.2%

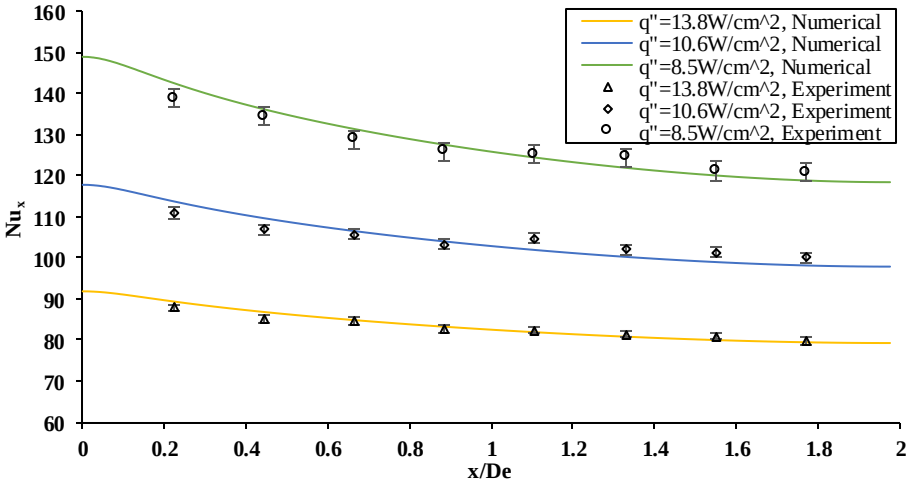

(b) Local Nusselt number distributions at C_v= 0.2%

Figure 5.14: Experimental and numerical surface temperature and local Nusselt number at C_v= 0.2%and Re=390

Figure 5.21 shows the average Nusselt number versus γ-Al_2O_3 particle volume fraction (C_v%) for different Reynolds numbers. As we can see in this figure, there is a sharp increase in the average Nusselt number at a nanoparticle volume fraction of 0.2vol%, followed by a decrease at 0.3vol% with a small positive effect on the average Nusselt number compared with pure water, and then a slight increase until C_v=0.6vol% is reached. The results revealed that the positive effects achieved as a result of the presence of nanoparticles in the water gradually increase along with increases in the Reynolds number. As we can see in Figures 5.20 and 5.21, the enhancement

percentages for the average Nusselt number of pure water and a nanoparticle volume fraction of 0.2vol% were 37% and 28% at Reynolds numbers of 601.3 and 210, respectively.

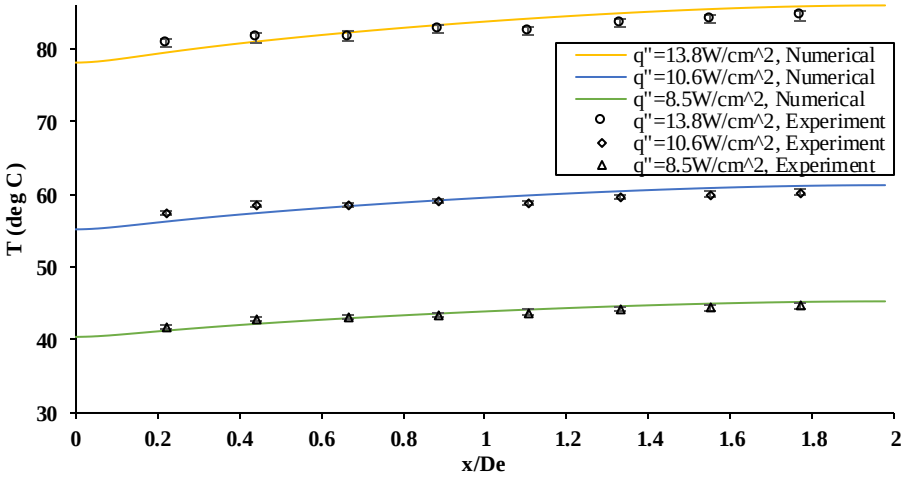

(a) Surface temperature distributions at C_v= 0.3%

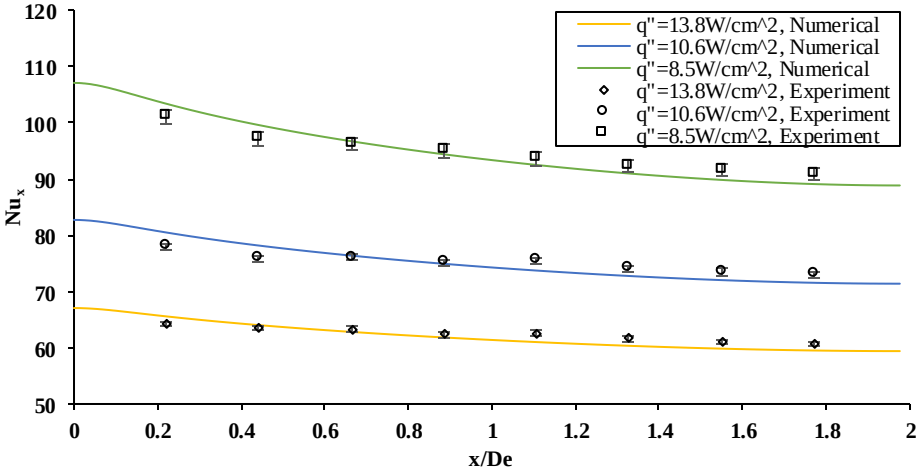

(b) Local Nusselt number distributions at C_v= 0.3%

Figure 5.15: Experimental and numerical surface temperature and local Nusselt number at C_v= 0.3% and Re=300

The average enhancement percentages of the average Nusselt numbers achieved using γ-Al_2O_3-water nanofluid compared with pure water is illustrated in Table 5.3.

Table 5.3: Effect of γ-Al_2O_3-water nanofluid at various volume fractions on the average Nusselt number

C_v(%)	0.1	0.2	0.3	0.4	0.6
Enhancement %	6.6%	31%	7.6%	8.5%	9.2%

Based on the experimental and numerical results obtained in this study, it is clear that the optimum concentration of the γ-Al_2O_3-water nanofluid is 0.2vol% and that the nanofluid contains larger particle concentration yields for lower Nusselt numbers.

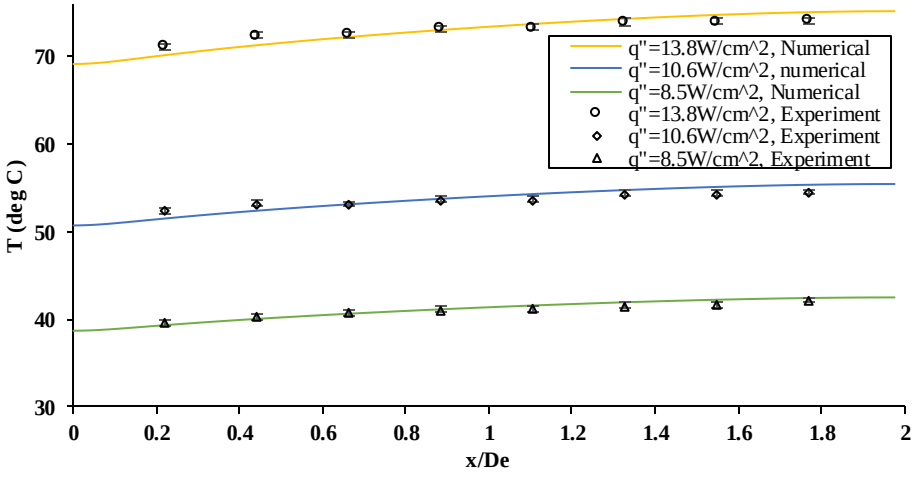

(a) Surface temperature distributions at C_v= 0.6%

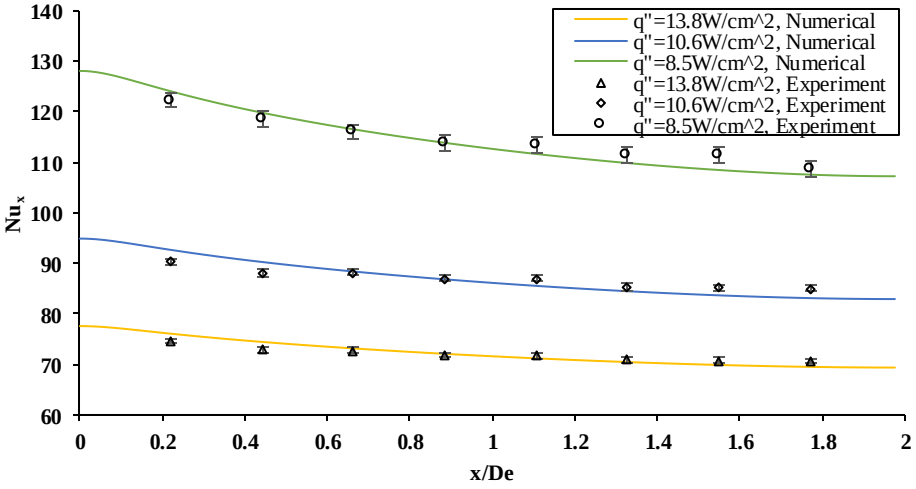

(b) Local Nusselt number distributions at C_v= 0.6%

Figure 5.16: Experimental and numerical surface temperature and local Nusselt number at C_v= 0.6% and Re=601.3

The increases in the thermal conductivity and thermal properties of nanofluids can be explained by two main mechanisms: the structure-based or static mechanism and the dynamic mechanism. The structure-based mechanism is based on the nano-layers acting as a thermal bridge between the solid particles and bulk fluid, the interfacial thermal resistance, and the fractal structure of agglomerates. The dynamic mechanism is based on the Brownian motion of the nanoparticles. Since nanofluids are dynamic systems, the motion of nanoparticles and the

interactions between the dancing nanoparticles or between dancing nanoparticles and liquid molecules must be considered.

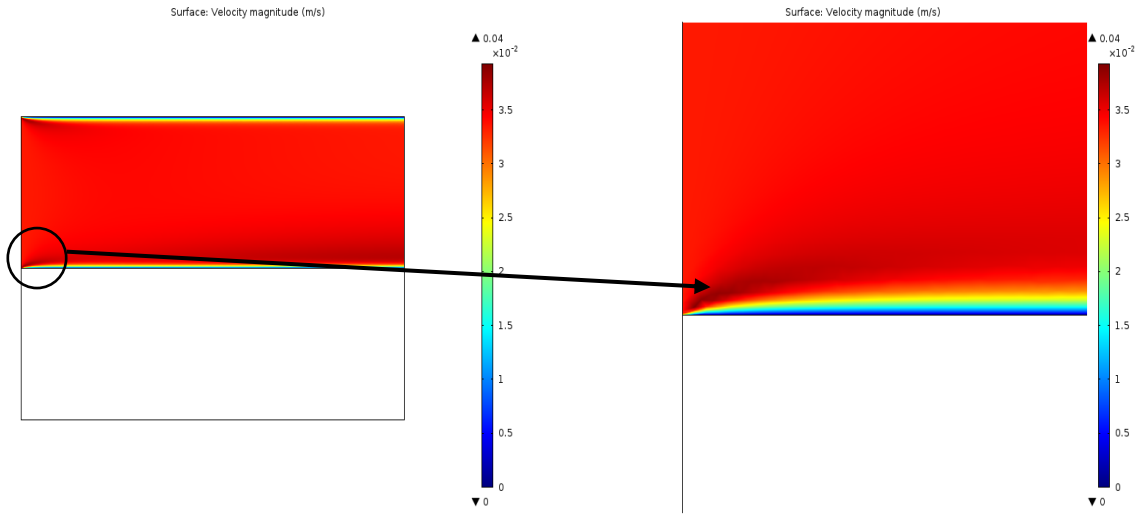

(a) Velocity contour at Re=601.3 **(b) Boundary layer shape**

Figure 5.17: Velocity contoyr and boundary layer shape

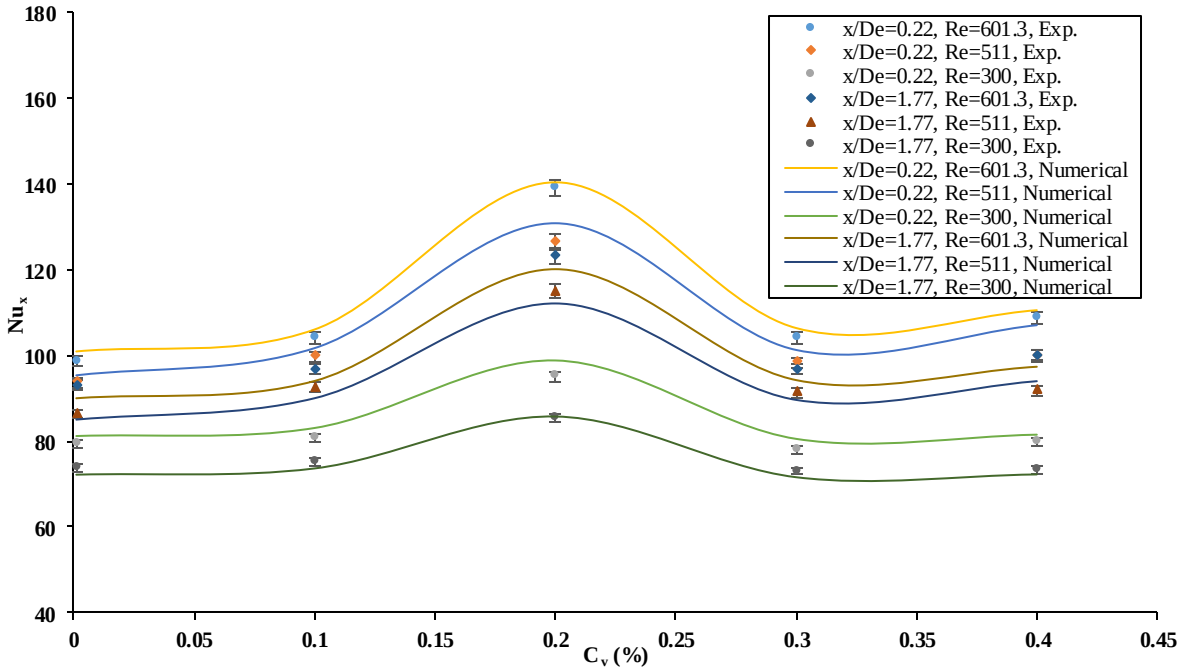

Figure 5.18: Experimental and numerical local Nusselt number verses particle loading (C_v(%)) at x/D_e= 0.22 and 1.77 and different Reynolds numbers

When increasing the volume fraction of γ-Al_2O_3 nanoparticle from 0.1vol% to 0.2vol%, it seems that the dynamic mechanism (e.g., Brownian motion) plays an important role in increasing the thermal conductivity of the nanofluid, however, the dynamic thermal conductivity of

nanofluids decreases with increasing nanoparticle concentrations [143]. For γ-Al_2O_3-water nanofluids containing higher volume fractions (0.3, 0.4, 0.6vol%), we can expect that the effect of the dynamic mechanism will be reduced and that the static mechanism will become dominant and play a key role in enhancing the static thermal conductivity of the nanofluid.

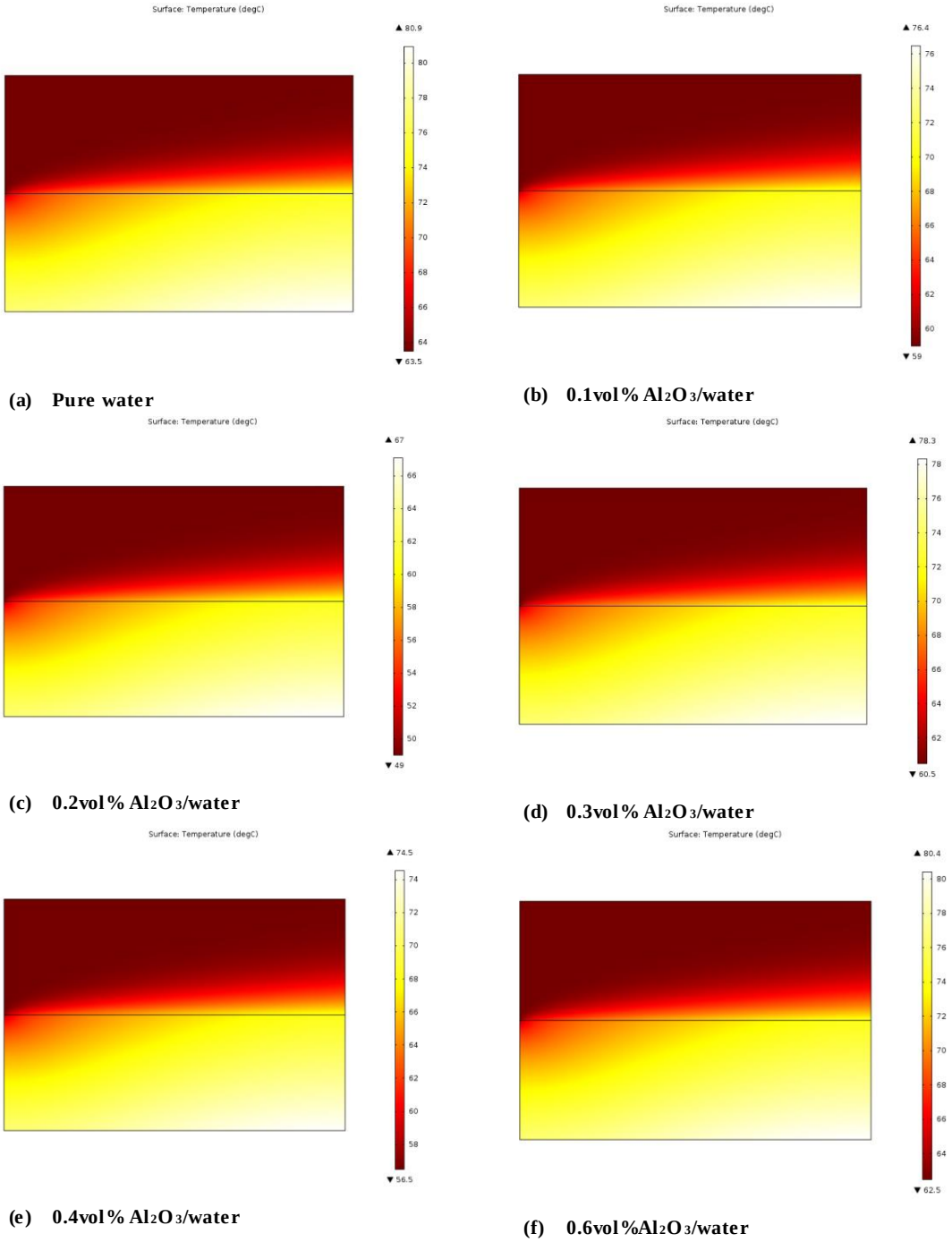

(a) Pure water

(b) 0.1vol% Al_2O_3/water

(c) 0.2vol% Al_2O_3/water

(d) 0.3vol% Al_2O_3/water

(e) 0.4vol% Al_2O_3/water

(f) 0.6vol%Al_2O_3/water

Figure 5.19: Temperature contours at different γ-Al2O3/water concentrations

This is why we discovered a small positive effect on the average Nusselt number for higher nanoparticle concentrations (0.3vol% to 0.6vol %) based on the enhancement that occurs in the static thermal conductivity of nanofluids. The empirical correlation of the average Nusselt number of γ-Al_2O_3-water nanofluid flow through an aluminum foam sink was obtained using the following formula:

$$Nu_{,avg} = C \cdot (Re \cdot Pr)^{\frac{1}{3}} \tag{4.14}$$

Where:

$$C = 40 \cdot C_v^2 + 5.2 \qquad 0 \leq C_v(\%) \leq 0.2, \tag{4.15}$$

$$C = 0.6 \cdot C_v + 5.4 \qquad 0.2 < C_v(\%) \leq 0.6 \tag{4.16}$$

Where $Nu_{,avg}$, Re, Pr and C_v represent the average Nusselt number, Reynolds number, Prandtl number and nanoparticle volume fraction (%), respectively.

It is important to note that these empirical correlations were developed based on the experimental results, Reynolds number range, and experimental nanoparticle volume fraction range. The deviation between the experimental data and the empirical correlations developed in this study was 2.5%. As we can see from the results of these correlations, at low concentrations where the dynamic mechanism is the effective mechanism, the coefficient (C) reveals a non-linear relationship with the nanoparticle volume fraction. This non-linear relationship between the thermal properties of nanofluids and particle loading was previously seen at low nanoparticle concentrations [36, 38, 39, and 40].

The results of this study indicate that the use of a γ-Al_2O_3-water nanofluid over the Forchheimer laminar regime at the optimum nanoparticle concentration of 0.2 vol% through an ERG aluminum foam heat sink increased the heat transfer rate by 31% compared to pure water through the foam and 50% compared to pure water through an empty channel.

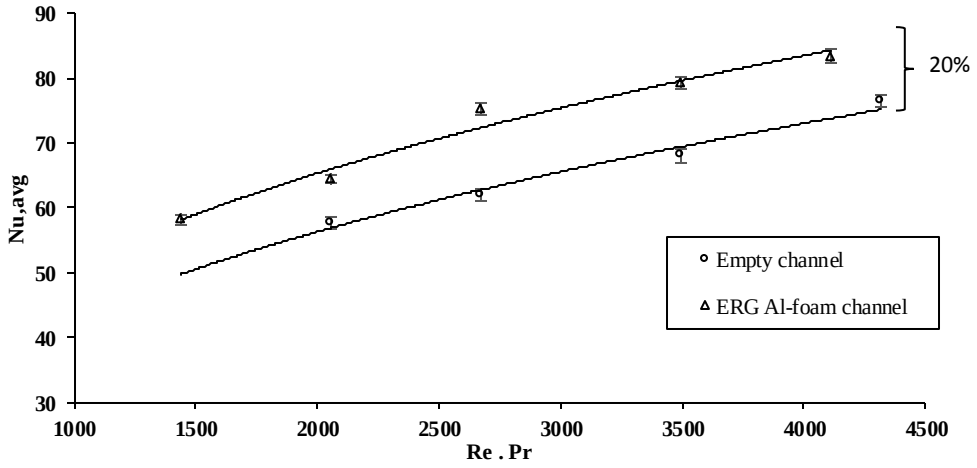

(a) Average Nusselt number variation with Reynolds and Parndtle number for empty and foam filled channel

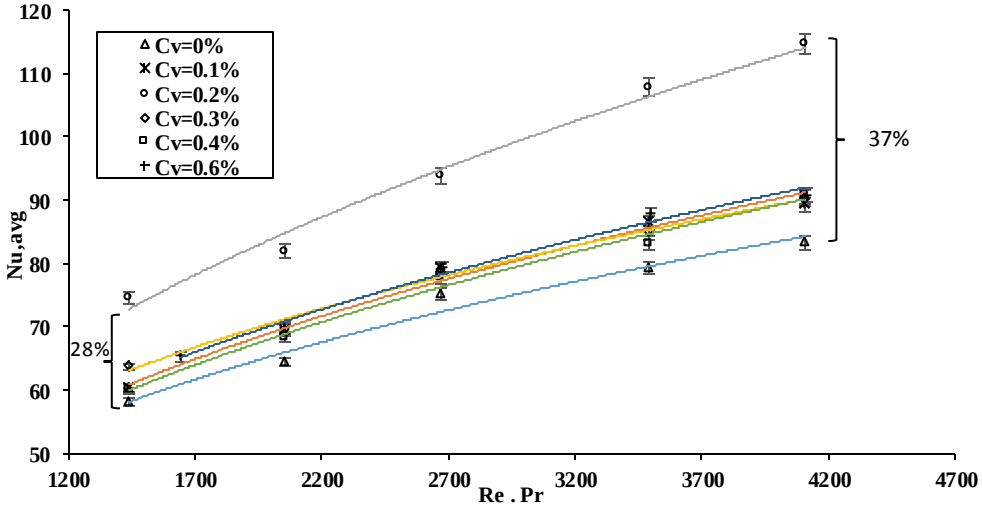

(b) Average Nusselt number for different γ-Al_2O_3-water concentrations

Figure 5.20: Average Nusselt number variation with Reynolds and Parndtle

This finding is of great importance to the area of electronic cooling since the reliability and operating speed of transistors depend on the electronic surface temperature. In addition, individual electronic components have no moving parts, and thus, nothing to wear out with time. They are therefore more reliable and can operate safely for many years. This would be the case if components operated at room temperature, however, electronic components have been known to fail under prolonged use at high temperatures.

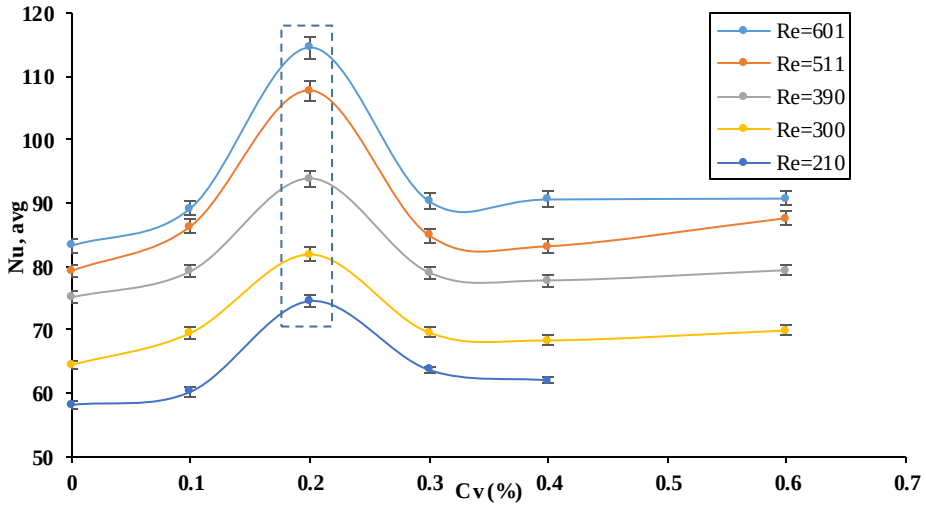

Figure 5.21: Variation of the average Nusselt number verses nanoparticle volume fractions (C_v(%))

5.5 Conclusions

This chapter presented an experimental and numerical study in employing the interaction between an ERG aluminum foam heat sink and a γ-Al_2O_3-water nanofluid. The aluminum foam was subjected to a γ-Al_2O_3-water nanofluid flow covering the non-Darcy flow regime. The volume fractions of γ-Al_2O_3 nanoparticles varied between 0.1vol% and 0.6vol%. The following conclusions were drawn based on the findings of the study:

- The surface temperature distributions increase along with increases in the dimensionless flow direction axis, decreasing the Reynolds number and increasing the heat flux for various nanoparticle concentrations.
- The local Nusselt number is high at the beginning of the channel and starts to decrease until an almost constant value is reached when the flow becomes thermally fully developed.
- The presence of an ERG aluminum foam filled channel enhanced the heat transfer by 20% when compared to an empty channel.
- The results revealed that the highest local Nusselt number is achieved at a γ-Al_2O_3 particle loading of 0.2vol%. This means that the optimal nanoparticle loading, at which the highest heat transfer rate is achieved, was at 0.2vol%.
- The enhancement percentages in the local Nusselt number of 0.2vol% γ-Al_2O_3-water nanofluid was 45-20% at the beginning of the channel and 40-15% at the end of the channel.

- The numerical results of both surface temperature and local Nusselt number were in good agreement with the experimental data with a maximum relative error of 2% and 3%, respectively.
- The enhancement percentages in the average Nusselt number of 0.2vol% nanofluid compared with the pure water were 37% and 28% at Reynolds numbers of 601.3 and 210, respectively.
- Empirical correlations of the average Nusselt number were developed based on the experimental data, range of Reynolds numbers, and the range of experimental nanoparticle volume fractions.

CHAPTER 6-CONCLUSIONS AND FUTURE WORK

6.1 Conclusions

This research project involved an experimental and numerical study using of an ERG aluminum foam heat sink as a porous structured heat sink in the cooling of electronics. The aluminum foam was subjected to a forced flow covering the non-Darcy laminar flow regime. The ERG aluminum foam heat sink was subjected to a uniform heat flux ranging from 13.8 to 8.5W/cm^2.

After studying the thermal and hydro-dynamic development and heat transfer characteristics of the aluminum foam heat sink in Chapter 2, three main features were added to the aluminum foam heat sink in order to overcome electronic cooling challenges such as the achievement of uniform surface temperatures below a certain level in order to enhance the performance reliability and lifetime of silicon semi-conductor devices.

These features included: 1) the use of a pulsating or oscillating water flow at frequency range of 0.04 to 0.1Hz in order to achieve a uniform surface temperature distribution and higher heat transfer rate compared to the steady flow (Chapter 3), 2) the inclusion of channels in the aluminum foam in order to increase the surface area to volume ratio (Chapter 4) and 3) the use of γ-Al_2O_3-water nanofluid as a fluid coolant through the aluminum foam (the volume fractions of γ-Al_2O_3 nanoparticles varied between 0.1vol% and 0.6vol%) in order to achieve higher thermal properties of the working coolant fluid (Chapter 5).

The heat transfer characteristics and thermal performance were measured for each feature and comparisons with the other features were conducted. It is important to note that the thermal performance of the heat sink is defined by the thermal efficiency index which combines the heat transfer rate and the pressure drop caused by the heat sink. Table 6.1 shows the summary of all of the empirical equations developed in this study. The following conclusions were drawn based on the findings of the study:

- The thermal entry length of the fluid flow through porous media is longer for higher Reynolds numbers and decreases as the Reynolds numbers decrease
- A correlation of the thermal entry length of the fluid flow through porous media was obtained (see Table 6.1)

- The temperature distributions for steady flow through the porous media increase along with increases in the dimensionless flow direction axis, decreasing the Reynolds number and increasing the heat flux.
- At any given Reynolds number, the local Nusselt number is inversely proportional to the boundary layer thickness and reaches a constant value in the fully developed region.
- The local Nusselt number in the fully developed region of the fluid flow through the porous foam is highly dependent on the Reynolds number.
- Based on the experimental results and the given range of Reynolds numbers, an empirical equation of the average Nusselt number of the fluid flow through aluminum foam was developed (see Table 6.1).
- The temperature distributions of the pulsating water flow show a convex profile with the maximum temperature at the center of the test section.
- The local Nusselt number of the pulsating flow is higher at both channel entrances and begins to decrease until it reaches a minimum point at the center of the test section.
- The pulsating flow enhanced the local Nusselt number by 7-16% at the entrance and 20-31% at the end of the channel, the average Nusselt number by 14% and the uniformity of the surface temperature distributions by 73% compared with the steady flow.
- An empirical equation for the average Nusselt number of the pulsating flow as a function of pulsating flow amplitude and kinetic Reynolds number was developed (see Table 6.1).
- Model (A) (without channel) achieved a lower local temperature than models (B) (with two channels) and (C) (with three channels).
- Model (A) achieved a higher local Nusselt number than model (B), and model (B) achieved a higher local Nusselt number than model (C).
- Models (B) and (C) reduced the average Nusselt number by 10% and 25%, respectively, compared to model (A).
- Model (B) achieved the optimal design condition with highest thermal efficiency index of 6.1 at Re= 1353 compared with models (A) and (C).

- Empirical equations of the average Nusselt number for models (A), (B), and (C) were developed (see Table 6.1).
- The presence of an ERG aluminum foam filled channel enhanced the heat transfer by 20% when compared to an empty channel.
- 0.2vol% γ-Al_2O_3-water nanofluid was the optimal concentration which achieves the highest heat transfer rate compared with pure water.
- The 0.2vol% γ-Al_2O_3-water nanofluid enhanced the local Nusselt number by 45-20% at the beginning of the channel and 40-15% at the end of the channel, and the average Nusselt number by 37% and 28% at Reynolds numbers of 601.3 and 210, respectively.
- The 0.3vol% to 0.6vol% γ-Al_2O_3-water nanofluid concentrations achieved lower heat transfer enhancement percentages compared with that of 0.2vol% γ-Al_2O_3-water nanofluid.
- An empirical correlation of the average Nusselt number as a function of the Reynolds number, Prandtl number and nanoparticle volume fractions was developed.
- The numerical results were in good agreement with the experimental data for the local Nusselt number and local temperature with a maximum relative error of 3% and 2%, respectively, in all studies.

6.2 Contributions

Based on the results and conclusions presented above, the contributions of the current study are as follows:

- ❖ A study of the thermal behaviour and heat transfer characteristics of the porous structured heat sinks subjected to a water steady flow.
- ❖ A study of the heat transfer characteristics of pulsating water flow through porous structured heat sink.
- ❖ A study of the effect of a pulsating flow on the surface temperature uniformity and heat transfer rate.
- ❖ A study of different designs of the porous structured heat sink (e.g. with two and three channels) subjected to a steady flow.

- A comparison of the thermal performance of different features and designs.
- A study of the heat transfer characteristics of nanofluids flow through porous structured heat sink.
- A comparison of different nanofluid particle loadings
- The determination of the optimal nanoparticle concentration which achieves the highest heat transfer rate.
- The development of empirical correlations of the average Nusselt number for each feature or design as a function of appropriate parameters.

Table 6.1: Summary of the empirical correlation developed in the study

Equation	Description
$\left[\frac{L_{laminar,thermal}}{D_e}\right]_{Porous\ media} = 0.0004.Re.Pr$	$L_{laminar,thermal}$ is the thermal entry length of the fluid flow through the porous media, D_e is the hydraulic dimeter of the channel, **Re** is Reynolds number based on hydraulic diameter, **Pr** is Prandtl number, The thermo-physical properties is evaluated at the inlet temperature of the fluid, $297 \leq Re \leq 1353$
$Nu_{,avg} = C \cdot Re^m$	$Nu_{,avg}$ is the average Nusselt number, **C=0.41 and m=0.38** based on fluid bulk temperature, **C=0.342 and m=0.41** based on fluid inlet temperature, $297 \leq Re \leq 1353$
$Nu_{,avg} = C \cdot Re^m$	**C=0.342 and m=0.41** for model (A), without channel, **C=0.121 and m=0.54** for model (B), with two channels, **C=0.1 and m=0.56** for model (c), with three channel, $297 \leq Re \leq 1353$
$Nu_{,avg} = 0.2 \cdot A_o^{0.46} \cdot e^{0.000025 Re_w}$	$Nu_{,avg}$ is the average Nusselt number of pulsating flow through the porous media, A_o and Re_w represent the pulsating flow amplitude and the kinetic Reynolds number, respectively, $297 \leq A_o \leq 1353$, $5162 \leq Re_w \leq 12905$
$Nu_{,avg} = C \cdot (Re \cdot Pr)^{\frac{1}{3}}$	$Nu_{,avg}$ is the average Nusselt numbet of γ-Al_2O_3-water nanofluid through the porous media, The thermo-physical properties is evaluated at the inlet temperature of the fluid, $210 \leq Re \leq 631$, $C = 40 \cdot C_v^2 + 5.2 \quad 0 \leq C_v(\%) \leq 0.2$, $C = 0.6 \cdot C_v + 5.4 \quad 0.2 < C_v(\%) \leq 0.6$, C_v is nanoparticle volume fraction (%)

6.3 Future work

The literature review revealed that, the previous research involving porous structured heat sinks (such as aluminum foam) are incomplete, especially when they involve liquid cooling (steady or pulsating). There is also very little research involving, the interaction of porous structured heat sink and nanofluids. The current research study involved an intensive examination of heat development through metal foam in order to further scientific understanding of the thermal behaviour of metal foam. Three features were then added and examined. The following are areas which were not addressed by this study and are suggested for future research:

- Combining the effects of a pulsating flow (to enhance the temperature uniformity) and γ-Al_2O_3-water nanofluid at 0.2vol% (optimal concentration) through aluminum foam heat sink.
- Combining the effects of a pulsating flow (to enhance the temperature uniformity) and γ-Al_2O_3-water nanofluid at 0.2vol% (optimal concentration) through aluminum foam with two channels (model (B)) (achieved the optimal design condition in the current research study).
- The introduction of plate finned aluminum heat sink with aluminum foam inserted between the fins and subjected to a steady water flow.
- Combining the effects of the plate finned aluminum heat sink with aluminum foam inserted between the fins and a pulsating γ-Al_2O_3-water nanofluid flow.
- The introduction of aluminum foam with different pore densities (e.g. 10 and 20 PPI) and determination the optimal pore density.
- Employing different types of nanofluids such as CuO-water nanofluid.

REFERENCES

[1] Cengel, Y. A., and Ghajar, A. J., "Heat and Mass Transfer: Fundamentals & Applications 3rd edition" McGraw-Hill, 2010.

[2] Lee, J., "Convection performance of nanofluids for electronics cooling" PhD thesis, Stanford University, 2009.

[3] Gochman, S., Ronen, R., Anati, I., Berkovits, A., Kurts, T., Naveh, A., Saeed, A., Sperber, Z., and Valentine, R., "The Intel Pentium M processor: microarchitecture and performance" Int. Technol. J., vol. 7, pp. 21-36, 2003.

[4] Reliability Prediction of Electronic Equipment. U.S. Department of Defense, MIL-HDBK-2178B, NTIS, Springfield, VA, 1974.

[5] Buller, M., and Kilburn, R., "Calculation of surface heat transfer coefficient for electronic module packages" ASME Winter Annual Meeting, vol. 20, pp. 15-29, 1981.

[6] Sparrow, E., Niethammer, J., and Chaboki, A., "Heat transfer and pressure drop characteristics of array of rectangular modules in electronic equipment" Int. J. Heat and Mass Transfer, vol. 25, pp. 961-973, 1982.

[7] Sparrow, E., Vemuri, S., and kadle, D., "Enhanced local heat transfer, pressure drop, flow visualization for arrays of block-like electronic components" Int. J. Heat and Mass Transfer, vol. 26, pp. 689-699, 1983.

[8] Sparrow, E., Yanezmoreno, A., and Otis, D., "Convective heat transfer response to height differences in an array of block-like electronic components" Int. J. Heat and Mass Transfer, vol. 27, pp. 469-473, 1984.

[9] Jubran, B., Swiety, S. and Hamdan, M., "Convective heat transfer and pressure drop characteristics of various array configurations to simulate the cooling of electronic modules" Int. J. heat and Mass Transfer, vol. 39, pp. 3519-3529, 1996.

[10] Igarashi, T., Nakamura, H., and Fukuoka, T., "Pressure drop and heat transfer of arrays of in-line circular blocks on the wall of parallel channel" Int. J. Heat and Mass Transfer, vol.47, pp. 4547-4557, 2004.

[11] Iwasaki, H., and Ishizuka, M., "Forced convection air cooling characteristics of plate fins for notebook personal computers" Int. Society Conference on Thermal Phenomena, vol. 2, pp. 6-21, 2000.

[12] ERG, Introduction to Duocel Application. Available from: http://www.ergaerospace.com/Material-Applications-guide.html (accessed 12.07.16).

[13] Joen, C., Jaeger, P. D., Huisseune, H., Van Herzeele, S., Vorst, N., Paepe, M. D., "Thermo hydraulic study of a single row heat exchanger consisting of metal foam covered round tubes" Int. J. Heat Mass Transfer, vol. 53, pp. 3262–3274, 2010.

[14] Metafoam, Metafoam Technical Fact Sheet, 2010. Available from: http:// www.metafoam.com/products.htm (accessed 06.08.10).

[15] FrostyTech, Cryo Tech and New Cooling Technologies You Have Never Seen, 2010. Available from: http://www.frostytech.com/ articleview.cfm?articleid=2424&page=8 (accessed 06.08.10).

[16] Zhao, C., "Review on thermal transport in high porosity cellular metal foams with open cells" Int. J. Heat Mass Transfer, vol. 55, pp. 3618-3632, 2012.

[17] Kaviany, M., "Principles of Heat Transfer in Porous Media" second ed. Springer-Verlag, New York, 1995.

[18] Darcy, H., "Les Fontaines Publiques de la Ville de Dijon" Victor Dalmont, Paris, 1856.

[19] Forchheimer, P., "Wasserbewegung durch Boden" Zeitschrift des Vereines Deutscher Ingenieure, vol. 45, pp. 1736–174, 1901.

[20] Ward, J. C., "Turbulent flow in porous media" ASCE J. Hydraul. Div., vol. 90, pp. 1–12, 1964.

[21] Brinkman, H. C., "A calculation of the viscous force exerted by a flowing fluid on a dense swarm of particles" Appl. Sci. Res. A 1, pp. 27–34, 1947.

[22] Brinkman, H. C., "On the permeability of media consisting of closely packed porous particles. Appl. Sci. Res. A 1, pp. 81–86, 1947.

[23] Martys, N., Bentz, D. P. and Garboczi, E. J., "Computer simulation study of the effective viscosity in Brinkman equation" Phys. Fluids, vol. 6, pp. 1434–1439, 1994.

[24] Liu, S. and Masliyah, J. H., "Dispersion in porous media. Handbook of Porous Media" (ed. K. Vafai) 2nd ed., Taylor and Francis, Boca Raton, FL, pp. 81–140, 2005.

[25] Saez, A. E., Perfetti, J. C. and Rusinek, I., "Prediction of effective diffusivities in porous media using spatially periodic models" Transport Porous Media, vol. 11, pp. 187–199, 1991.

[26] Ochoa-Tapia, J. A. and Whitaker, S., "Momentum transfer at the boundary between a porous medium and a homogeneous fluid: Theoretical development" Int. J. Heat Mass Transfer vol. 38, pp. 2635–2646, 1995.

[27] Valdes-Parada, F. J., Ochoa-Tapia, J. A. and Alvarez-Ramirez, J., "On the effective viscosity for the Darcy-Brinkman equation" Physica, vol. 385, pp. 69–79, 2007.

[28] Durlofsky, L. and Brady, J. F., 'Analysis of the Brinkman equation as a model for flow in porous media" Phys. Fluids, vol. 30, pp. 3329–3341, 1987.

[29] Rubinstein, J., "Effective equations for flow in random porous media with a large number of Scales" J. Fluid Mech., vol. 170, pp. 379–383, 1986.

[30] Vafai, K. and Tien, C.L., "Boundary and inertia effects on flow and heat transfer in porous media" Int. J. Heat Transfer, vol. 24, pp. 95–203, 1981.

[31] Vafai, K. and Tien, C. L. 1982 Boundary and inertial effects on convective mass transfer in porous media. Int. J. Heat Mass Transfer, vol. 25, pp. 1183–1190.

[32] Hsu, C. T. and Cheng, P., "Thermal dispersion in a porous medium" Int. J. Heat Mass Transfer, vol. 33, pp. 1587–1597, 1990.

[33] Nield, D. A., "Discussion of a discussion by F. Chen and C.F. Chen" ASME J. Heat Transfer Vol. 119, pp. 193–194, 1997.

[34] Payne, L. E. and Song, J. C., "Spatial decay estimates for the Brinkman and Darcy flows in a semi-infinit cylinder" Cont. Mech. Thermodyn., vol. 9, pp. 175–190, 1997.

[35] Payne, L. E. and Song, J. C., "Spatial decay for a model of double diffusive convection in Darcy and Brinkman flow" Z. Angew. Math. Phys., vol. 51, pp. 867–889, 2000.

[36] Payne, L. E. and Song, J. C., "Spatial decay bounds for the Forchheimer equation" Int. J. Engng. Sci., vol. 40, pp. 943–956, 2002.

[37] Payne, L. E. and Straughan, B. "Analysis of the boundary condition at the interface between a viscous fluid and a porous medium and related modelling questions" J. Math. Pures Appl., vol. 77, pp. 317–354, 1998.

[38] Payne, L. E. and Straughan, B. "Convergence and continuous dependence for the Brinkman-Focrchheimer equations" Stud. Appl. Math.,vol. 102, pp. 419–439,1999.

[39] Payne, L., Song, J. and Straughan, B."Continuous dependence and convergence results for Brinkman and Forchheimer models with variable viscosity"Proc. Roy. Soc. Londaon, vol.455, pp. 2173–2190, 1999.

[40] Payne, L. E., Rodriigues, J. F. and Straughan, B., "Effect of anisotropic permeability on Darcy's law" Math. Meth. Appl. Sci., vol. 24, pp. 427–438.

[41] Song, J. 2002 Spatial decay estimate in time-dependent double-diffusive Darcy plane flow. J. Math. Anal. Appl 267, 76–88, 2001.

[42] Auriault, J. L., "On the domain of validity of Brinkman's equation" Transp. Porous Media, vol. 79, pp. 215–223, 2009.

[43] Zhao, C., Lu, W., and Tassou, S., "Thermal analysis on metal-foam filled heat exchangers. Part II: Tube heat exchangers" Int. J. Heat Mass Transfer, vol. 49, pp.2762–2770, 2006.

[44] Maxwell, J. C., "Treatise on Electricity and Magnetism" Clarendon Press, Oxford, 1873.

[45] Choi, S. "Enhancing thermal conductivity of fluids with nanoparticles" in Developments and Applications of Non-Newtonian Flows, D. A. Singer and H. P. Wang, Eds., ASME, New York, Vol.105, pp. 66-99, 1995.

[46] Lee, S., Choi, S., Li, S., and Eastman, J., "Measuring thermal conductivity of fluids containing oxide nanoparticles" J. Heat. Transfer, vol. 121, pp. 280-289, 1999.

[47] Yu, W., France, D. M., Choi, S. U., and Routbort, J. L. "Review and Assessment of Nanofluid Technology for Transportation and Other Applications" Argonne National Laboratory (ANL), 2007.

[48] Eastman, J. A., Choi, S. U. S., Li, S., Thompson, L. J., and Lee, S., "Enhanced thermal conductivity through the development of nanofluids" Proc. Symposium Nanophase and Nanocomposite Materials II, Materials Research Society, Boston, MA, vol. 457, pp. 3–11, 1997.

[49] Zhu, H., Lin, Y., and Yin, Y., "A novel one-step chemical method for preparation of copper nanofluids" J. Colloid Interface Sci., vol. 277, pp.100–103, 2004.

[50] Yu, W., and Choi, S. U. S., The role of interfacial layers in the enhanced thermal conductivity of nanofluids: a renovated Hamilton-Crosser model" J. Nanopart Res., Vol. 6: pp. 355–361, 2004.

[51] Xue, Q. Z., "Model for effective thermal conductivity of nanofluids" Phys. Lett. A, vol. 307, pp. 313–317, 2003.

[52] Yu, W., and Choi, S. U. S, "An effective thermal conductivity model of nanofluids with a cubic arrangement of spherical particles" J. Nanosci. Nanotechnol., vol. 5, pp. 80–586, 2005.

[53] Trivedi A. "Thermo-mechanical solutions in electronic packaging: component to system level" MS thesis, The University of Texas at Arlington, August 2008.

[54] Hwang, J., Hwang, G., Yeh, R., and Chao, C., "Measurement of interstitial convective heat transfer and frictional drag for flow across metal foams" J. Heat Transfer, vol. 124, pp. 120-129, 2002.

[55] Lu, W., Zhao, C., and Tassou, S., "Thermal analysis on metal foam filled heat exchangers Part I: Metal-foam filled pipes" Int. J. Heat Mass Transfer, vol. 49, pp. 2751-2761, 2006.

[56] Seyf, H., and Layeghi, M., "Numerical analysis of convective heat transfer from an elliptic pin fin heat sink with and without metal foam insert" J. Heat Transfer, vol. 132, 2010.

[57] Mancin, S., Zilio, C., A. Diani, A., and Rossetto, L., "Experimental air heat transfer and pressure drop through copper foams" Exp. Therm. Fluid Sci., vol. 36, pp. 224-232, 2012.

[58] Mancin, S., Zilio, C., Rossetto, L., and Cavallini, A., "Heat transfer performance of aluminum foams" J. Heat Transfer, vol. 133, 2011.

[59] Boomsma, K., and Poulikakos, D., "On the Effective Thermal Conductivity of a Three-Dimensionally Structured Fluid-Saturated Metal Foam" International Journal of Heat and Mass Transfer, Vol. 44, No. 4, 2001, pp. 827–836.

[60] Zhao, C., Lu, W., and Tassou, S., "Thermal analysis on metal-foam filled heat exchangers. Part II: Tube heat exchangers" Int. J. Heat Mass Transfer, vol. 49, pp.2762–2770, 2006.

[61] Klett, J., Stinton, D., Ott, R., Walls, C., Smith, R., and Conway, B., "Heat exchangers/radiators utilizing graphite foams" Oak Ridge National Laboratory, US Department of Energy, 2001.

[62] Bhattacharya, A., and Mahajan, R., "Finned metal foam heat sinks for electronics cooling in forced convection" J. Elect. Packag., vol. 124, pp. 155-163, 2002.

[63] Ding, X., Lu, L., Chen, C., He, Z., and Ou, D., "Heat transfer enhancement by using four kinds of porous structures in a heat exchanger" Appl. Mech. Mater., vol. 52–54, pp. 1632-1637, 2011.

[64] Bai, M., and Chung, J., "Analytical and numerical prediction of heat transfer and pressure drop in open-cell metal foams" Int. J. Therm. Sci., vol. 50, pp. 869-880, 2011.

[65] Tzeng, S. C., Jeng, T. M., and Wang, Y. C., "Experimental study of forced convection in asymmetrically heated sintered porous channel with/without periodic baffles" Int. J. Heat and Mass Transfer, vol. 49, pp. 78-88, 2006.

[66] Kim, S. Y., Paek, J. W., and Kang, B. H., "Thermal Performance of aluminum foam heat sinks by forced air cooling" IEEE transactions on components and packaging technologies, vol. 26, pp. 262-267, 2003.

[67] Sung, H., Kim, S., and Hyun, J., "Forced convection from an isolated heat source in a channel with a porous medium" Int. J. Heat and Fluid Flow, vol. 16, pp. 527–535, 1995.

[68] Rachedi, R., and Chikh, S., "Enhancement of electronic cooling by insertion of foam materials" J. Heat and Mass Transfer, vol. 37, pp. 371-378, 2001.

[69] Fu, H., Leong, K., Huang, X., and Liu, C., "An experimental study of heat transfer of a porous channel subjected to oscillating flow" ASME J. Heat Transf., vol. 123, pp. 162-170, 2001.

[70] Hooman, K., and Ejlali, A., "Entropy generation for forced convection in a porous saturated circular tube with uniform wall temperature" Int. Commun. Heat Mass Transfer, vol. 34, pp. 408–419, 2007.

[71] Hooman, K., and Haji-Sheikh, A., " Analysis of heat transfer and entropy generation for thermally developing Brinkman–Brinkman forced convection problem in a rectangular duct with isoflux walls" Int. J. Heat Mass Transfer, vol. 50, pp. 4180–4194, 2007.

[72] Nield, D., Kuznetsov, A., and Xiong, M., "Thermally developing forced convection in a porous medium: Parallel-plate channel or circular tube with walls at constant heat flux" J. Porous Media, vol. 6, pp. 203–212, 2003.

[73] Boomsma, K., Poulikakos, D., and Zwick, F., "Metal foams as compact high performance heat exchangers" J. Mech. Mater., vol. 35, pp. 1161-1176, 2003.

[74] Noh, J., Lee, K., and Lee, C., "Pressure loss and forced convective heat transfer in an annulus filled with aluminum foam" Int. Commun. Heat Mass Transfer, vol. 33, pp. 434–444, 2006.

[75] Hetsroni, G., Gurevich, M., and Rozenblit, R., Metal foam heat sink for transmission window, Int. J. Heat Mass Transfer, vol. 48, pp. 3793–3803, 2005.

[76] Dukhan, N., Bağci, ö., özdemir, M., "Thermal development in open cell metal foam: an experiment with constant heat flux" Int. J. Heat and Mass Transfer, vol. 85, pp. 852-859, 2015

[77] COMSOL Multiphysics, retrieved from http://www.comsol.com/comsol-multiphysics, March, 2015.

[78] Bayomy, A. M., Saghir, M. Z., and Yousefi, T., "Electronic Cooling Using Water Flow in Aluminum Metal Foam Heat Sink: Experimental and Numerical Approach" Int. J. Thermal Science, vol. 109, pp. 182-200, 2016.

[79] Calmidi, V. V., and Mahajan, R. L., "Forced Convection in High Porosity Metal Foams" Journal of Heat Transfer, Vol. 122, No. 3, 2000, pp. 557–565.

[80] Calmidi, V. V., "Transport Phenomena in High Porosity Fibrous Metal Foams" Ph.D. Dissertation, Dept. of Mechanical Engineering, Univ. of Colorado, CO, July 1998.

[81] Taylor, J., "An Introduction to Error Analysis-Study of Uncertainty in Physical Measurements, Oxford University Press, 1995.

[82] Hsu, C. T., Cheng, P., and Wong, K. W., "Modifed Zehner Schlunder models for stagnant thermal conductivity of porous media" Int. J. Heat Mass Transfer, vol. 37, pp. 2751-2759, 1994.

[83] Calmidi, V., and Mahajan, R., "The effective thermal conductivity of high porosity fibrous metal foams" J. Heat Transfer, vol. 121, pp. 466-471, 1999.

[84] Bhattacharya, A., Calmidi, V. V., and Mahajan, R. L., "Thermophysical properties of high porosity metal foams" Int. J. Heat Mass Transfer, vol. 45, pp. 1017-1031, 2002.

[85] Dai, Z., Nawaz, K., Park, Y., Bock, J., Jacobi, A., "Correcting and extending the Boomsma–Poulikakos effective thermal conductivity model for three-dimensional, fluid-saturated metal foams" Int. Comm. in Heat Mass Transfer, vol. 37(6), pp. 575–580, 2010.

[86] Yang, X.H., Bai, J.X., Yan, H.B., Kuang, J.J., Lu, T.J., and Kim T., "An analytical unit cell model for the effective thermal conductivity of high porosity open-cell metal foams" Trans. in Porous Media, vol. 102(3), pp. 403-426, 2014.

[87] Leong, K. and Jin, L. " An experimental study of heat transfer in oscillating flow throught a channel filled with an aluminum foam" Int. J. Heat Mass Transfer, vol. 48, pp. 243-253, 2005.

[88] Al-Sumaily, G, Thompsom, M., "Forced convection from a circular cylinder in pulsating flow with and without the presence of porous media" Int. J. of heat and mass transfer, vol. 61, pp.226-244, 2013.

[89] Leong, K., and Jin, L., "Heat transfer of oscillating and steady flows in a channel filled with porous media" Int. Commun. Heat Mass Transfer, vol. 31, pp. 63-72, 2004.

[90] Paek, J., Kang, B., and Hyun, J., "Transient cool-down of a porous medium in pulsating flow" Int. J. Heat Mass transfer, vol. 42, pp. 3523–3527, 1999.

[91] Cooper, W., Nee, V., and Yang K., "An experimental investigation of convective heat transfer from the heated floor of a rectangular duct to a low frequency, large tidal displacement oscillatinf flow" Int. J. Heat Mass transfer, vol. 37, pp. 581-592, 1994.

[92] Bayomy, A. M., Saghir, M. Z., "Heat Transfer Characteristics of Aluminum Metal Foam Subjected to a Pulsating/Steady Water Flow: Experimental and Numerical Approach" Int. J. Heat Mass Transfer, vol. 97, pp. 318-336, 2016.

[93] Comsol Manual ver. 5, Boston, USA, 2015

[94] Eastman, J. A., Choi, S. Li, S., Yu, W., and Thomson, L. J., "Anomalously increased effective thermal conductivities of ethylene glycol based nanofluids containing copper nanoparticles" Appl. Phys. Lett., vol. 78, pp. 718-720, 2001.

[95] Lu, S., and Lin H., "Effective conductivity of composites containing aligned spherical inclusions of finite conductivity" J. Appl. Phys., vol. 79, pp. 6761-6769, 1996.

[96] Choi, S., Zhang, Z. G., Yu, W., Lockwood, F. E., and Grulke, E. A., "Anomalous thermal conductivity enhancement in nano-tube suspensions" Appl. Phys. Lett., vol. 79, pp. 2252-2254, 2001.

[97] Hong, T. K., Yang, S. Y., and Choi, C. J., "Study of the enhanced thermal conductivity of Fe nanofluids" J. Appl. Phys., vol. 97, 2005.

[98] Chopkar, M, Das, P. K., and Manna, I, "Synthesis and characterization of nanofluid for advanced heat transfer applications" Scr. Mater., vol. 55, pp. 549–552, 2006.

[99] Devpura A., Phelan, P. E. and Prasher, R. S., "Size effect on the thermal conductivity of polymers laden with highly conductive filler particles" Microscale Thermophys. Eng., vol.5, pp. 177–189, 2001.

[100] Biercuk, B. J., Llaguno, M. C., Radosavljevic, M., Hyun, J. K., and Johnson, A. T., "Carbon nanotube composites for thermal management" Appl. Phys. Lett., vol. 80, pp. 2767–2772, 2002.

[101] Murshed, S. M. S., Leong, K. C., and Yang, C., "Enhanced thermal conductivity of TiO2 – water based nanofluids" Int. J. Therm. Sci., vol. 44: 367-373, 2005.

[102] Das, S. K., Putra, N., Thiesen, P., and Roetzel, W., "Temperature dependence of thermal conductivity enhancement for nanofluids" ASME J. of Heat Transfer, vol. 125(4), pp. 567-574, 2003.

[103] Patel, H. E., Das, S. K., Sundararajan, T., Nair, A. S., George, B., and Pradeep, T., "Thermal conductivities of naked and monolayer protected metal nanoparticle base nanofluids: manifestation of anomalous enhancement and chemical effects" Applied Physics Letters, vol. 83(14), pp. 2931-2933, 2003.

[104] You, S. M., Kim, J. H., and Kim, K. H., "Effect of nanoparticles on critical heat flux of water in pool boiling heat transfer" Applied Physics Letters, vol. 83(16), pp. 3374-3376, 2003.

[105] Vassallo, P., Kumar, R., and Damico, S., "Pool boiling heat transfer experiments in silica-water nanofluids" Int. J. of Heat Mass Transfer, vol. 47(2), pp. 407-411, 2004.

[106] Bhattacharya, P., Saha, S. K., Yadav, A., Phelan, P. E., and Prasher, R. S., "Brownian dynamics simulation to determine the effective thermal conductivity of nanofluids" J. of App. Phys., vol. 95, pp. 6492–6494, 2004.

[107] Jang, S. P., and Choi, S. U. S., "Role of Brownian motion in the enhanced thermal conductivity of nanofluids" Appl. Phys. Lett., vol. 84, pp. 4316–4318, 2004.

[108] Hemanth, K. D., Patel, H. E., Rajeev, K. V. R., Sundararajan, T., Pradeep, T., and Das, S. K., "Model for heat conduction in nanofluids" Phys. Rev. Lett., vol. 93,144301, 2004.

[109] Prasher, R., Bhattacharya, P., and Phelan, P. E., "Thermal conductivity of nanoscale colloidal solutions (nanofluids)" Phys. Rev. Lett., vol. 94, 025901, 2005.

[110] Koo, J., and Kleinstreuer C., "Impact analysis of nanoparticle motion mechanisms on the thermal conductivity of nanofluids" Int. Commun. Heat Mass Transfer, vol. 32(9), pp. 1111–1118, 2005.

[111] Faulkner, D. J., Rector, D. R., Davidson, J. J., and Shekarriz, R., "Enhanced heat transfer through the use of nanofluids in forced convection, Paper IMECE2004-62147, presented at the 2004 ASME International Mechanical Engineering Congress and RD&D Expo, Anaheim, CA, Nov. 13–19.

[112] Wen, D., and Y. Ding, Y., "Experimental investigation into convective heat transfer of nanofluids at the entrance region under laminar flow conditions" Int. J. Heat Mass Transfer, vol. 47, pp. 5181–5188, 2004.

[113] Xuan, Y., and Q. Li, Q, "Investigation on convective heat transfer and flow features of nanofluids" J. Heat Transfer, vol. 125, pp.151–155, 2003.

[114] Yang, Y. T., and Lai, F. H., "Numerical investigation of cooling performance with the use of Al_2O_3/water nanofluids in a radial flow system" Int. Thermal Sciences, vol. 50(1), pp. 61-72, 2011.

[115] Ho, C. J., Liu, W. K., Chang, Y. S., and Lin, C. C., "Natural convection heat transfer of alumina-water nanofluid in vertical square enclosure: An experimental study" Int. J. Thermal Sciences, vol. 49, pp. 1345-1353, 2010.

[116] Yang, X. F., Liu, Z., and Zhao, J., "Heat transfer performance of a horizontal micro-grooved heat pipe using CuO nanofluid" J. of Micromechanics and microengineering, vol. 18, pp. 1-6, 2008.

[117] Jaberi, B., Yousefi. T., farahbakhsh, B., and Saghir, M. Z., "Experimental investigation on heat transfer enhancement due to $Al_2 O_3$ -water nanofluid using impingement of round jet on circular disk" Int. J. Thermal Science vol. 74, pp. 199-207, 2013.

[118] Yousefi, T., Shojaeizadeh, E., Mirbagheri, H.R., Farahbaksh, B. and Saghir, M. Z., "An experimental investigation on the impingement of a planar jet of Al2O3–water nanofluid on a V-shaped plate" vol. 50, pp. 114-126, 2013.

[119] Naphon, P., and Wongwises, S., "Experimental study of jet nanofluids impingement system for cooling computer processing unit" J. Electron. Cooling Therm. Control, vol. 1, pp. 38–44, 2011.

[120] Naphon, P., and Nakharintr, L., "Nanofluid jet impingement heat transfer characteristics in the rectangular mini-fin heat sink" J. Eng. Phys.Thermophys., vol. 85(6), pp. 1324–1331, 2012.

[121] Xuan, Y. and Li, Q., "Heat transfer enhancement of nanofluids" Int. J. Heat Fluid Flow, vol. 21, pp. 58–64, 2000.

[122] Zamamian, A., Oskouir, S., Doosthoseini, A., Joneidi, A. and Pazouki, M., "Experimental investigation of forced convection heat transfer coefficient of Al_2O_3/EG and CuO/EG in double pipe and plate heat exchangers under turbulent flow" Experimental Thermal and Fluid Science, vol. 35, pp. 495-502, 2011.

[123]Sunder, L., Naik, M., Sharma, K., Singh, M. and Ressy, T., "Experimental investigation of forced convection heat transfer and friction factor in a tube with Fe_3O_4nanofluid" Experimental Thermal and Fluid Science, vol. 37, pp. 65-71, 2012

[124] Maiga, S., Palm, S. J., Nguyen, C. T., Roy, G., and Galanis, N., "Heat transfer enhancement by using nanofluids in forced convection flows" Int. J. Heat Fluid Flow, vol. 26, pp. 530–546, 2005.

[125] Palm, S. J., Roy, G., and Nguyen, C. T., "Heat transfer enhancement in radial flow cooling system-using nanofluid" ICHMT Inter. Symp. Advance Comp. Heat Transfer, Norway, 2004.

[126] Roy, G., Nguyen, C. T., and Lajoie, P. R., "Numerical investigation of laminar flow and heat transfer in a radial flow cooling system with the use of nanofluids" Superlattices and Microstructures, vol. 35, pp. 497–511, 2004.

[127] Koo, J., and Kleinstreuer, C., "Laminar nanofluid flow in microheat-sinks" Int. J. Heat Mass Transfer, vol. 48, pp. 2652-2661, 2005.

[128] Chein, R., and Chuang, J., Experimental microchannel heat sink performance studies using nanofluids" Int. J. Thermal Science, vol. 46, pp. 57–66, 2007.

[129] Saghir, M. Z., Ahadi, A., Yousefi, T., Farahbakhsh, B., "Two-phase and single phase models of flow of nanofluid in a square cavity: Comparison with experimental results" vol. 100, pp. 372-380, 2016.

[130] Kayhani, M. H., Nazari, M., Soltanzadeh, H., Heyhat, M. M., and Kowsary, F., Experimental analysis of turbulent convective heat transfer and pressure drop of Al_2O_3/water nanofluid in horizontal tube" Micro Nano Lett. IET, vol. 7, pp. 223-227, 2012.

[131] Maghrebi, M. J., Nazari, M., and Armaghani, T., "Forced convection heat transfer of nanofluids in a porous channel" Transp. Porous Media, vol. 93, pp. 401-413, 2012.

[132] Hosseini, M., Mohammadian, E., Shirvani, M., Mirzababaei, S., and Aski, F. S., "Thermal analysis of rotating system with porous plate using nanofluid" Powder Technology, vol. 254, pp. 563 – 571, 2014.

[133] Matin, M. H., and Pop, I., "Forced convection heat and mass transfer flow of a nanofluid through a porous channel with a first order chemical reaction on the wall" Int. Commun. Heat Mass Transfer, vol. 46, pp. 134-141, 2013.

[134] Das, K., "Slip flow and convective heat of nanofluids over a permeable stretching surface". Computers& Fluids, vol. 64, pp. 34-42, 2012.

[135] Hajipour, M., and Dehkordi, A. M., "Analysis of nanofluid heat transfer in parallel-plate vertical channels partially filled with porous medium" Int. J. Thermal Science, vol. 55, pp. 103-113, 2012.

[136] Behabadi, M. A., Pakdaman, M. F., and Ghazvini, M., "Experimental investigation on the convective heat transfer of nanofluid flow inside vertical helically coiled tubes under uniform wall temperature condition" Int. Commun. Heat Mass Transfer, vol. 39, vol. 556-564, 2012.

[137] Nazari, M., Ashouri M., Kayhani, M. H., and Tamayol, A., " Experimental styudy of convective heat transfer of nanofluid through a pipe with metal foam" Int. J. Thermal Science, vol. 88, pp. 33-39, 2015.

[138] Dukhan, N., Bağcı, O., and Ozdemir, M., "Metal foam hydrodynamics: flow regimes from pre-Darcy to turbulent" Int. J. Heat Mass Transfer, vol. 77, pp. 114–123, 2014.

[139] Yu, W., France, D. M., Choi, S. U., and Routbort, J. L. "Review and Assessment of Nanofluid Technology for Transportation and Other Applications, Argonne National Laboratory (ANL), 2007.

[140] Wang, X., Xu, X., and Choi, S. U. S., "Thermal conductivity of nanoparticle fluid mixture" J. Thermophysics and Heat Transfer, vol. 13, pp. 474-480, 1999.

[141] A.Einstein, A., "Eineneuebestimmungdermolekuldimensionen.Annalender Physik" vol. 19, pp. 289-306, 1906.

[142] Maïga, S. E. B., and C.T.Nguyen, C. T., "Heat transfer behaviours of nanofluids in a uniformly heated tube" Superlatticesand Microstructures, vol. 35, pp. 543-557, 2004.

[143] Sohel, A. M., Murshed, and Nieto de Castro, C. A., "Contribution of Brownian motion in thermal conductivity of nanofluids" World Congress on Engineering 2011, London, UK, vol. III, 2011.